Performance and Reliability of Liquid Encapsulated PV Modules

Manufacturing, Accelerated Ageing and Proposing Improvements for Liquid Encapsulated PV Modules

<u>Sebastian Weemaes</u>



Performance and Reliability of Liquid Encapsulated PV Modules

Manufacturing, Accelerated Ageing and Proposing Improvements for Liquid Encapsulated PV Modules

by

Sebastian Weemaes

to obtain the degree of Master of Science at the Delft University of Technology, to be defended publicly on Thursday July 3, 2025 at 2:00 PM.

Student number: 5169623

Project duration: November 12th, 2024 - July 3rd, 2025

Prof.dr.ir. O. Isabella, TU Delft, chair of the committee Thesis committee:

TU Delft, Thesis supervisor

TU Delft

Dr. M.R. Vogt, Dr. M. Cvetkovic, Dr. U. Bothra, TU Delft, daily supervisor

A. Poli, Biosphere Solar

Cover: Close up photo of a solar panel on a building by Benjamin Jopen

on unsplash (Unmodified)

TU Delft Report Style, with modifications by Daan Zwaneveld Style:

An electronic version of this thesis is available at http://repository.tudelft.nl/.





Abstract

With the enormous rise in installed photovoltaic (PV) modules over the past decade, it is to be expected that soon, a massive increase in decommissioned PV modules will arise. Current PV modules are difficult and energy-intensive to recycle, leading to some of the most valuable materials going to waste. To prevent this, new PV module structures have been proposed, with the most promising structure containing a layer of air between the module's front glass and the solar cell. Due to this replacement of the ethylene vinyl acetate (EVA) layer, the air-filled modules are easier to disassemble and recycle. However, it lowers the module efficiency due to a mismatch in the refractive index of the front glass and air.

To overcome the refractive index mismatch of air-filled modules, this study evaluates the performance and degradation behaviour of self-manufactured, liquid-filled PV modules, which are subjected to humidity freeze accelerated ageing and their results are compared to air-filled and EVA-laminated modules. To achieve this, suitable liquids are selected. Subsequently, several one-cell mini-modules are hand-manufactured, which are filled with air, the selected liquids, and laminated with EVA. The results are obtained by subjecting the modules to 30 cycles of humidity freeze testing and by measuring their electrical characteristics under standard testing conditions. Initial performance measurements show that all four tested liquids, including water (3.7%), polydimethylsiloxane (PDMS) (6.2%), mono propylene glycol (MPG) (5.1%), and glycerol (5.1%), offer substantial efficiency improvements over air-filled modules, with PDMS even slightly outperforming EVA (5.5%). A major point of failure is the PIB edge seal, especially at the liquid injection points, indicating a need for improved manufacturing techniques. The module failures also allowed for disassembly trials, which show that liquid-filled modules can be completely disassembled with ease, allowing for full material recovery. This highlights the reusability potential of liquid-filled designs due to the absence of more permanent encapsulant layers like EVA.

The humidity freeze accelerated ageing, subjects the modules to extremely low and high temperatures of -40 °C and 85 °C, whilst also subjecting them to 85% relative humidity. Intermediate visual and electroluminescence inspections revealed mechanical failure in air-filled modules due to edge seal flattening and cell breakage. Whilst after the full 30 humidity freeze cycles the relative degradation in module efficiency in both PDMS and glycerol encapsulated modules (both 5.2%) are comparable to that of an air-filled module (5.5%) but worse than that of EVA (3.9%), whilst the module encapsulated with MPG shows the lowest degradation (2.8%). These results highlight the potential of MPG as a stable encapsulant and underscore the importance of redesigning the liquid injection method for reliability of the polyisobutene edge seal.

Acknowledgements

First of all, I am very grateful for my supervisors, Malte Vogt and Urvashi Bothra. This thesis would not have been possible without their guidance, feedback and support throughout the project.

Furthermore, I want to thank Stefaan Heirman and Tim Velzeboer for making sure all equipment was always working and for contributing to brainstorming solutions of failing aspects.

I want to thank everyone from Biosphere Solar for the fun interactions, experiences, and not to forget the warm lunches. I am also thankful for using Biosphere Solar's workspace and equipment for the liquid injection part of my project. From Biosphere Solar, I specifically want to thank Alberto Poli for helping me out when the project did not go as planned.

Lastly, I would like to thank my family and friends for week in, week out helping me to take my mind off studying and having fun

Sebastian Weemaes Delft, June 2025

Contents

1	Intro		1
	1.1		2
	1.2		4
	1.3	, 0	6
	1.4		6
	1.5	Accelerated Ageing and Testing Methods	8
	1.6	Research Gap	8
	1.7		9
	1.8	,	9
2	Liqu		0
	2.1		0
	2.2	1	2
	2.3	Selected Liquids	3
		2.3.1 PDMS	3
		2.3.2 glycerol	3
		2.3.3 MPG	3
			5
			5
		·	5
	2.4		5
3	Mar	· · · · · · · · · · · · · · · · · · ·	7
	3.1	Solar Cells	7
	3.2	Soldering	7
	3.3	Lamination	8
		3.3.1 EVA	8
			9
	3.4		9
	3.5	Liquid Injection	
	0.0	3.5.1 Water	
		3.5.2 PDMS	
		3.5.3 Mono Propylene Glycol	
		3.5.4 Glycerol	
	2.0		
	3.6	Reusability of the Modules	
		3.6.1 Failed Modules	
		3.6.2 Liquid Encapsulant	_
		3.6.3 Solar Cells	
		3.6.4 PIB edge seal	
			3
	3.7	Conclusion	4
4	Mat	hodology 2	F
4			_
	4.1	Solar Simulator	_
	4.2		7
	4.3	3. 3	7
		4.3.1 Humidity Freeze	
	4.4	Cell Temperature Calculation	-
		4.4.1 Used Equations 2	R

Contents

		4.4.2	Required Heating Time	29
5	Mea	surem	ent Results and Discussion	31
	5.1	Air-Fill	led to Liquid-Filled Modules	31
		5.1.1	Air-Filled Modules	31
		5.1.2	Air- to Liquid-Filled Efficiency	32
		5.1.3	Current, Voltage and Fill Factor	34
		5.1.4	Discussion	36
	5.2	Degra	adation Every 6 Humidity Freeze Cycles	37
		5.2.1	Early Failures	37
		5.2.2	Efficiency	38
		5.2.3	Jsc	39
		5.2.4	Voc	39
		5.2.5	Fill Factor	39
	5.3		ımidity Freeze Cycles	40
		5.3.1	Efficiency	41
		5.3.2	Short-Circuit Current Density (Jsc)	41
		5.3.3	Open-Circuit Voltage (Voc)	41
		5.3.4	Fill Factor (FF)	41
		5.3.5	Overall Performance	42
	5.4		oluminescence and Visual Inspection	42
		5.4.1	Electroluminescence (EL)	42
			Visual Inspection	44
	5.5	concil	usion	45
6	Con	clusio	n	47
	6.1	Concl	usion	47
	6.2	Recor	mmendations	48
Re	ferer	nces		49
	Cod			55
В	Figu		Outhernation Tool	57
			Submersion Test	
	B.Z	All Ele	ectroluminescence Images	58

List of Figures

1.1	IRENA [4]	1
1.2	Projected cumulative waste from solar PV projects under IRENA's 1.5°C Scenario up till	2
1 2	2050 [7]	3
1.3		6
1.4	Simplified cross-section of a conventional PV module (left) and the NICE PV module (right)	
1.5	Performance ratio of TPedge building integrated PV application [53]	7
3.1		18
3.2		18
3.3	·	19
3.4	· • • • • • • • • • • • • • • • • • • •	20
3.5	, , ,	22
3.6		23
3.7		23
3.8	Separation process of the PIB and the glass	24
4.1	The solar simulator (left) and the reference module, ready for the calibration of the solar	
		26
4.2	Reference module (left) next to the PV module lying on top of a small piece of foam to match the cell heights	26
4.3		20 27
4.4		21 29
4.5		30
5.1	Efficiency values for each of the air-filled modules and the average efficiency value	32
5.2	Measured efficiencies for each of the air-filled and the liquid-filled versions of the modules 3	32
5.3	Relative change in module efficiency between the air-filled and liquid-filled modules 3	33
5.4	Average change in module efficiency between the air-filled and liquid-filled modules per liquid	33
5.5	·	35
5.6		35
5.7	·	36
5.8	visual inspection of module 9, initially encapsulated with PDMS, after six humidity freeze	00
0.0		37
59		38
		39
	, ,	40
	relative change in hii factor from a to do namidity freeze cycles	
	· · · · · · · · · · · · · · · · · · ·	40
J. 13	Electroluminescence images of sample 2 (EVA) before any accelerated ageing and after	
	Electroluminescence images of sample 2 (EVA) before any accelerated ageing and after 30 humidity freeze cycles	42
5.14	Electroluminescence images of sample 2 (EVA) before any accelerated ageing and after 30 humidity freeze cycles	42 43
5.14 5.15	Electroluminescence images of sample 2 (EVA) before any accelerated ageing and after 30 humidity freeze cycles	42 43 43
5.14 5.15 5.16	Electroluminescence images of sample 2 (EVA) before any accelerated ageing and after 30 humidity freeze cycles	42 43 43 44
5.14 5.15 5.16 5.17	Electroluminescence images of sample 2 (EVA) before any accelerated ageing and after 30 humidity freeze cycles	42 43 43
5.14 5.15 5.16 5.17 5.18	Electroluminescence images of sample 2 (EVA) before any accelerated ageing and after 30 humidity freeze cycles	42 43 43 44 45

List of Figures	vi

B.3	EL images of module 2, laminated with EVA	59
B.4	EL images of module 3, air-filled	59
B.5	EL images of module 4, air-filled	30
B.6	EL images of module 7, encapsulated with PDMS	30
B.7	EL images of module 10, encapsulated with glycol	31
B.8	EL images of module 13, encapsulated with glycerol	31

List of Tables

	Selected materials and their characteristics	
5.1	Relative performance in efficiency, short-circuit current density (Jsc), open-circuit voltage (Voc) and fill factor (FF) after 30 cycles of humidity freeze testing	41

Nomenclature

DH	
	damp heat.
EL	
	electroluminescence.
EOL	
- \/A	end-of-life.
EVA	ethylene vinyl acetate.
	Carylene varyi doctate.
FF	fill factor.
	illi factor.
GW	
	gigawatt.
HF	
	humidity freeze.
IBC	
	interdigitated back contact.
IEC	international electrotechnical commission.
IREN	
	international renewable energy agency.
Jsc	
	short-circuit current density.
kWh	
KVVII	kilowatt-hour.
LCO	levelized cost of electricity.
LID	levenzed cost of closuroity.
	light induced degradation.
MPG	i
	mono propylene glycol.

Nomenclature

NICE

new industrial cell encapsulation.

PDMS

polydimethylsiloxane.

PET

polyethylene terephtalate.

PIB

polyisobutene.

PID

potential induced degradation.

POE

polyolefin elastomer.

PV

photovoltaic.

SHJ

silicon heterojunction.

STC

standard test conditions.

TOPCON

tunnelling oxide passivated contact.

TPO

thermoplastic polyolefin.

 TW

terawatt.

UV

ultraviolet.

Voc

open-circuit voltage.

Introduction

Solar panels are rapidly becoming the preferred source of electricity worldwide, primarily due to their relatively low cost per kilowatt-hour (kWh) and minimal maintenance requirements. But the most significant reason is their low carbon footprint, essential for lowering emissions and ensuring that global warming remains below 1.5 °C as committed to in the 2015 Paris Agreement [1]. As of November 2024, the global installed photovoltaic (PV) capacity has surpassed the 2 terawatt (TW) mark [2]. Notably, just two years earlier, the global PV capacity reached 1 TW, highlighting the exponential growth in installations and, consequently, the increase in module production. In Figure 1.1, the substantial rise of globally installed solar capacity over the last 24 years, from just over 1 gigawatt (GW) to 2.1 TW, is plotted on a log scale [3, 4].

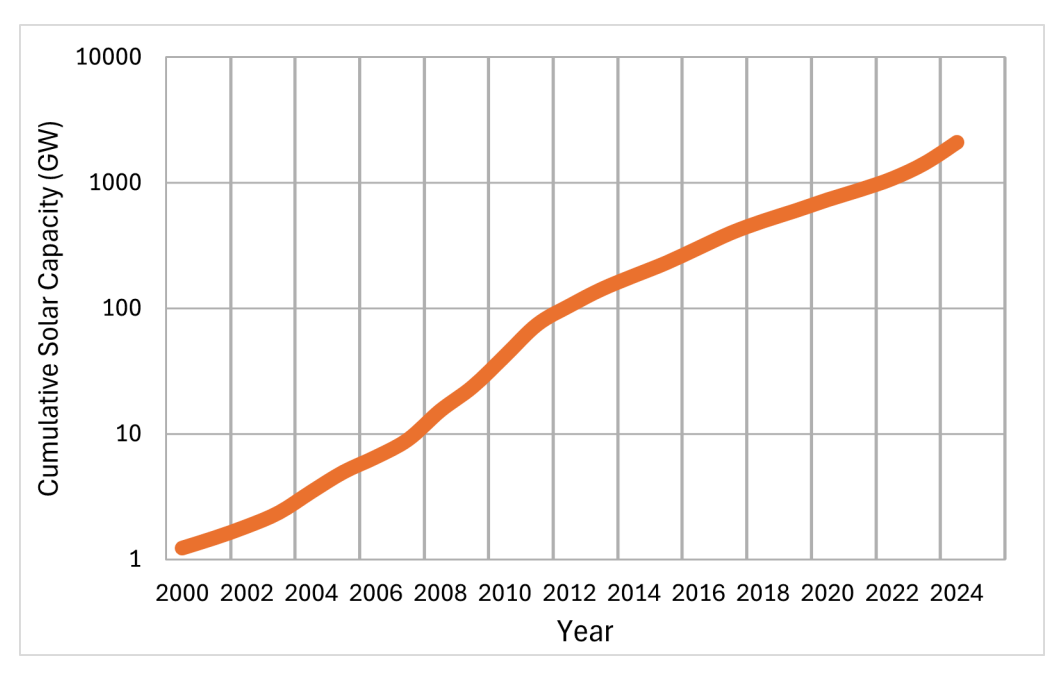


Figure 1.1: Worldwide cumulative installed solar capacity from 2000 to 2024, based on data from IRENA [4]

The current rate at which new PV capacity is installed is over 500 GW per year and it is likely to increase even further as more countries invest in renewable energy. Furthermore, PV installations can be expected to increase due to it being one of the cheapest forms of electricity generation when looking at the levelized cost of electricity (LCOE) [5]. These expected increases further amplify the challenge of waste management at the end-of-life (EOL) of PV modules. By assuming that the installation rate stays constant at 500 GW each year, a rough estimate can be made that the worldwide installed capacity will reach 5 TW by 2030 and 15 TW in 2050. These rough estimations pretty much align with the solar

PV capacity required for the 1.5°C scenario as predicted by the international renewable energy agency (IRENA) [6]. This expected increase in installed capacity means that over 86% of all PV modules that will be used by 2050 are yet to be manufactured and installed, allowing for advantageous adjustments regarding their efficiency and circularity.

PV modules are generally estimated to have a lifespan of at least 25 years, meaning that the earliest deployed PV modules are slowly starting to reach their EOL. Because the worldwide installed PV capacity has increased exponentially over the past 25 years, as shown in Figure 1.1, it can safely be assumed that the amount of decommissioned PV modules will increase exponentially in the upcoming years. The projected cumulative waste from the solar sector is shown in Figure 1.2. In their estimation, both the expected increase of PV modules reaching their EOL, and the extra increase in PV needed to adhere to the Paris agreement have been taken into account by IRENA. Without any significant changes in circularity, PV waste is projected to reach 4 million tonnes by 2030, nearly 50 million tonnes by 2040, and an astonishing 212 million tonnes by 2050 [7].

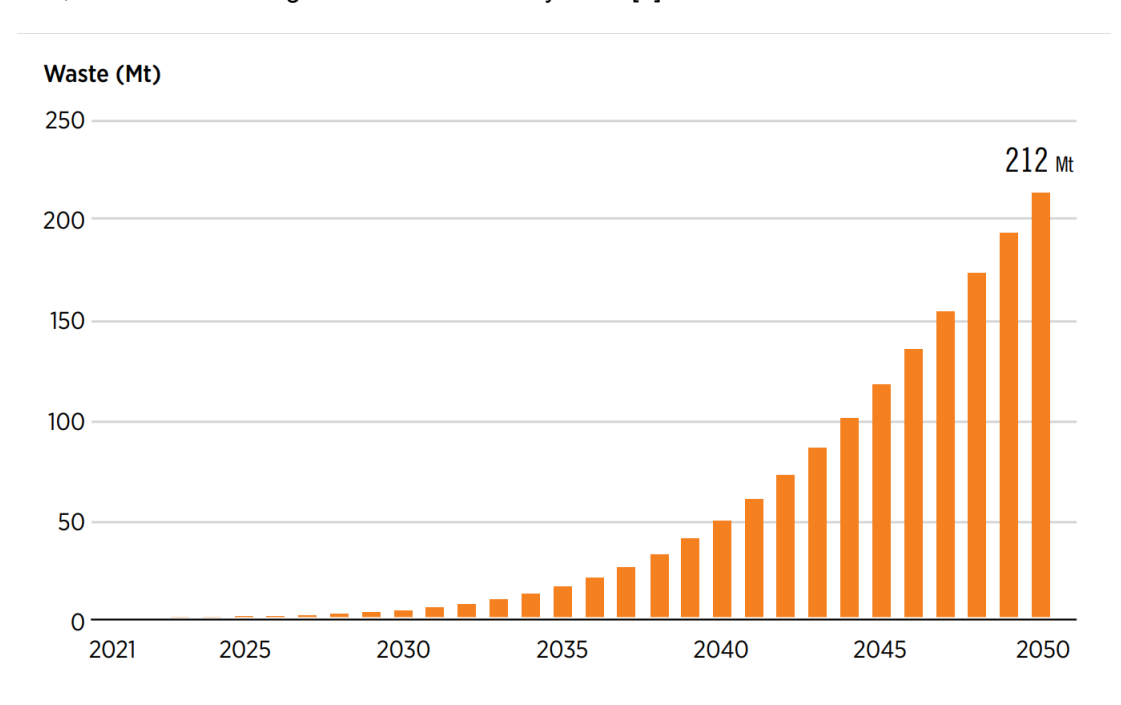


Figure 1.2: Projected cumulative waste from solar PV projects under IRENA's 1.5°C Scenario up till 2050 [7]

As of 2025, PV modules are rarely completely recycled. It is not an impossible feat, but it requires a complex process that is highly energy-intensive and not cost-effective. Only the readily detachable parts, such as the aluminium frame and junction box, are removed and completely recycled. Hereafter, the glass, encapsulant and solar cell are crushed to be used as low-level filler material. Establishing a closed-loop system is vital to being truly sustainable and eliminating waste. This entails that at the EOL all materials are re-used in new products. This would include recovering valuable materials such as silicon, copper, silver and glass. This approach reduces the total use of scarce resources, lowers manufacturing costs, and minimises the waste stream. By integrating re-usability in the design of PV modules, a sustainable lifecycle can be created, ensuring that renewable energy sources remain both environmentally friendly and economically viable.

1.1. Photovoltaic Module Architecture

Of the newly installed solar panels, 98% utilise silicon wafer solar cells [8]. Therefore, this report will consider their PV module structure as the standard structure. The key component of a PV module consists of the solar cells, which must be protected from its surroundings such as moisture and air whilst being allowed to be reached by as much light as possible. To achieve this, a protective encapsulant layer is added on both the top and bottom of the solar cell. Furthermore, it is important to add mechanical rigidity, which is achieved by adding two layers of glass to the PV module. This creates a

so-called glass-glass module, sometimes it is decided to use a polymer backsheet. A polymer backsheet is often used for mono-facial solar cells and is usually chosen to reduce weight and costs. To keep the optical losses at a minimum, all of the layers above the solar cells are required to have optimal reflection, transmittance and absorption properties. Finally, an aluminium frame is added to mount the solar panel, and a junction box with diodes is added to collect the current and to prevent power from going the wrong way. This structure is shown in Figure 1.3 and its components will be discussed in detail, from top to bottom [9].

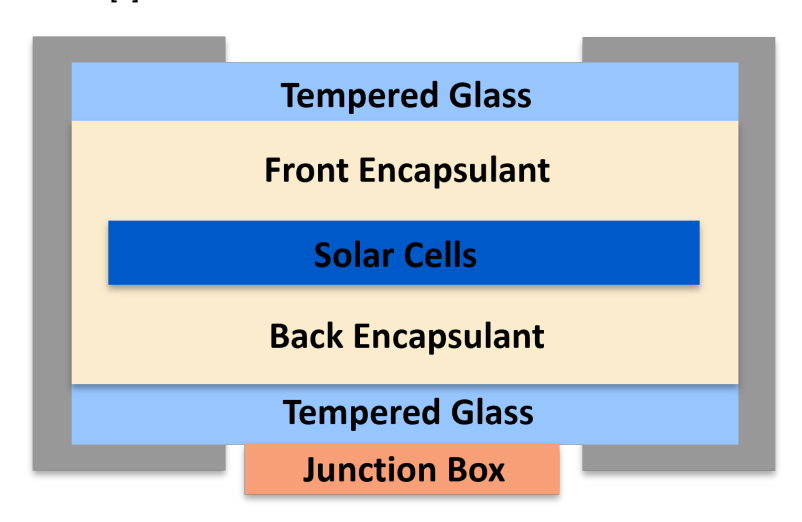


Figure 1.3: Simplified cross section of a silicon cell PV module

Front glass

Firstly, a layer of tempered low-iron soda-lime float glass is used on the top. This type of glass is used due to its water and impact resistance, stability under prolonged ultraviolet (UV) light exposure and low thermal conductivity. In most modules, the front glass is used to provide the mechanical strength and rigidity needed. The front glass can be textured or coated to ensure more light can reach the solar cell and thereby improve the overall module performance.

1st Encapsulant layer

The front glass is most commonly followed by an encapsulant layer, with the goal of keeping the cell and its electronics in place whilst also being stable at elevated temperatures and high doses of UV light exposure, finally it should have a high thermal conductivity to ensure the solar cell can cool down swiftly. EVA is the most widely used encapsulant material. EVA has been the main choice for quite some time and it is still a popular encapsulant to use. However, as of recently polyolefin elastomer (POE) and thermoplastic polyolefin (TPO) are increasing in popularity, mainly due to their higher resistance against moisture ingress, potential induced degradation (PID) and temperature changes [10, 11].

Solar Cell

The third and middle layer of a PV module is the solar cell, which is the part that generates the current through the photovoltaic effect [12]. The solar cell is the main part of the module. Depending on the voltage and current requirements, they can be strung together in series, parallel or a combination of both. There are numerous types of solar cells, each with its pros and cons. According to the international technology roadmap for PV, the four main solar cell technologies that will be used in 2034 are tunnelling oxide passivated contact (TOPCON), silicon heterojunction (SHJ), interdigitated back contact (IBC) and tandem solar cells [8]. For this thesis, IBC solar cells will be used, the choice of which is explained in detail in Chapter 3.1.

2nd Encapsulant Layer

Underneath the solar cell another encapsulant layer is added. This layer ensures that the solar cell is properly enclosed so that moisture can not deteriorate the cell by interacting with it. The 2nd encapsulant

layer will be of the same material as the 1st encapsulant layer because the same properties are desirable and because this ensures that the layers stick well to each other.

Back Glass

To finish the stack of layers, a backsheet is added to protect the module from the external environment and most importantly to give extra rigidity. For mono-facial PV modules, backsheets generally are multi-layered laminates providing excellent weatherability, good reflectance, flame resistance, high electrical insulation and good adhesion to the encapsulant [13]. Due to its good cost-performance ratio, the most often used backsheet material is polyethylene terephtalate (PET). However, for Bifacial PV modules, another glass layer is most beneficial due to its transmittance properties required for light to reach the back side of the solar cell.

Frame

All of the aforementioned layers are being held together and reinforced by a frame, which provides additional strength and rigidity to the PV module. The frame is typically made of aluminium due to its high strength combined with its relatively low weight. Furthermore, aluminium is highly resistant to corrosion, ensuring it won't degrade, even in damp environments [14]. Finally, the aluminium frame is essential for allowing the solar panel to be mounted onto rooftops and solar arrays.

Junction Box

Lastly, a junction box is attached to the back of the solar panel, allowing for a safe and controlled method of collecting and directing the generated electrical current. It serves as the bridge between the solar cells and the external grid. The junction box houses electrical connections and often includes bypass diodes. Bypass diodes are key components in ensuring stability and preventing damage to the solar cells caused by hotspots and partially shaded solar cells. Additionally, the junction box is designed to be weather-resistant, protecting internal wiring from moisture, dust, and other environmental factors.

1.2. Module Failures & Degradation

All appliances deteriorate over time until they ultimately break down, PV modules are no exception to this. During its lifetime, a module will be exposed to simultaneous environmental stresses such as sunlight, heat and cold, moisture, and mechanical loads. These factors often lead to various types of degradations, resulting in a gradual decrease of the energy yield and in extreme cases to complete failure. A PV modules degradation is estimated by the degradation rate, which entails the expected decrease in module efficiency every year. Sometimes a PV module comes with a warranty that states that after a given number of years, the module should still have at least 80% of the initial efficiency level. Due to this warranty threshold, reaching below 80% of the initial performance is considered as module failure. An elaborate study focusing on 288 modules that were connected to the grid in 1982, at the time of the study 35 years ago, determined that approximately 60% of these modules still performed above the 80% threshold [15]. The best-performing modules have a mean degradation rate of only -0.2% per year whilst the majority of the module's mean degradation rate is -0.69% per year [15]. Failure and degradation can occur in every part of the module, the most common degradation mechanisms have been summarised in studies [16–19] and each component will be individually discussed in detail.

Glass Lavers

First and foremost the glass can break, this is the most common failure mode of the glass layers and it accounts for up to a third of the failures occurring in the field [19, 20]. Glass breakage can arise for several reasons, for example due to improper handling during transport and installation or due to weather conditions such as hail or a storm. Another possibility is that the glass breaks during operation due to thermal hotspots, which can arise due to module shading, mismatched cells, diode failure or cell cracks [21]. Furthermore, a decrease in efficiency can occur due to the anti-reflection coating layers eroding and due to soiling building up over time [22].

Encapsulant Layers

An encapsulant layer has the main purpose of keeping the layers close together whilst allowing as much of the light to pass through it, as discussed in section 1.1. First of all, delamination can occur,

which means that either of the interfaces between the layers is no longer attached properly. This can be caused by poor lamination or by weather-induced degradation. Another common degradation in encapsulants, specifically EVA, is discolouration of the layer. Due to this discolouration, more light is absorbed in the encapsulant allowing for less light to reach the solar cell and therefore decreasing the power generation [23].

Another very important degradation mechanism is the material interaction between the encapsulant layer and the solar cell. For EVA it is the case that acetic acid is released from the encapsulant which can degrade the solar cell by inducing corrosion, metallisation, and it can accelerate PID [24, 25]. Other encapsulant materials will have their own downsides so it is important to find a balance between the up- and downsides of the materials.

Solar Cells

Four main degradation mechanisms occur in solar cells that will be discussed, these are cell cracking, thermal hotspots, light induced degradation (LID) and PID. Solar cells are generally fragile and brittle, so very little force is needed to break them [26]. A crack does not immediately mean a cell stops working, however, and depending on the orientation and size of the crack, it can drastically decrease the power output and therefore its efficiency [27].

Thermal Hotspots

Thermal hotspots are selective areas of the cell experiencing higher temperatures than the rest of the cell, which can induce several failure mechanisms. They occur due to large currents which can arise due to module shading, mismatched cells, diode failure or cell cracks [21]. Furthermore, degradation can be induced by the coating layers eroding and by soiling building up over time.

Light Induced Degradation

LID occurs in most solar cells and happens at the extremely early stages of its lifetime, such as in the first hours after installation [28]. Due to this, manufacturers already take the LID loss into account on their data sheets and adjust a PV module power output by the expected decrease in power [19].

Potential Induced Degradation

Another distinct driver of degradation in solar cells is PID. PID does not directly degrade the performance of the solar, instead it induces a gradual degradation over time [29]. PID arises when solar cells are exposed to large amounts of voltage, which happens relatively often due to solar cells being connected in series inside the module, and its degradation is accelerated in hot and humid environments [30, 31].

Frame

The frame is typically made of aluminium due to its low cost, weight, and high strength. It can however, still bend, break or come loose altogether [19]. While frame failure is not the most common cause of failure, when it does occur, it is a significant problem. This is because the frame provides structural integrity, protects internal components, and ensures proper mounting and alignment [18].

Junction Box

The junction box itself, but also the bypass diodes it contains can break down. Research from real-life PV power plants noted that the junction box has to be repaired or replaced quite often [19, 32]. It has been found that 85% of the junction box failures can be attributed to improper installation, therefore they occur in the first three months after on-grid [33]. The main reasons for junction box failure are detachment (from the back of the module), improperly sealed boxes, corrosion, and arcing due to bad or degraded wiring. Degradation and failure of the junction box can lead to significant performance losses and safety risks due to the high currents [18, 19]. Bypass diodes, located inside the junction box, also have several causes of failure, such as the wrong choice of diodes or high-voltage events. In a module with three bypass diodes, one shunted diode might already reduce the output power by a third [34].

1.3. Recycling of PV Modules

Current PV modules are challenging to recycle, an extensive analysis on the recycling of PV modules is performed by Isherwood [35]. Only the aluminium frame and junction box can easily be separated from the rest of the module. The main problem with recyclability comes down to the highly adhesive properties of the EVA layer. There are methods, such as thermal separation, to recover intact solar cells and relatively undamaged glass sheets. However thermal separation creates toxic gases which complicates the recycling process [36]. In the end, it comes down to the fact that every part of the module in contact with the EVA layer cannot be easily separated whilst staying intact. Therefore, it is easiest to crush the module, even though it destroys the solar cells and glass layers. After crushing the module, chemical and mechanical methods can be used to separate the different materials [37–39]. This crushing means that it is more difficult to reuse the materials, resulting in the glass being used as low-level filler material instead of being refurbished to be used for a new solar panel. This down-cycling, in combination with the fact that the IRENA estimates a total of 212 million tons of PV waste by 2050, would mean a huge waste of materials [7].

The problem with recyclability comes from the fact that for a long lifetime the EVA layers should hold the other components together for decades, without creating air bubbles or being separated. Whilst for recycling optimisation, all of the layers should be easily detachable from each other. The biggest advantage of EVA during a PV module's lifetime becomes the biggest disadvantage after decommissioning. Due to this discrepancy, substituting the EVA layer with a less sticky encapsulant might solve the recyclability problem, however that would entail a significantly shorter lifetime due to the formation of air bubbles and delamination. Whilst other encapsulant materials are being looked into, such as silicones, polyvinyl butyral and thermoplastic polyurethane, they all have their downsides [40]. This replacement material should have the same beneficial properties as EVA whilst also having properties that allow for an easy separation mechanism.

1.4. Gas & Liquid-Filled Modules

One way to prevent the problems caused by glueing the layers together is to search for different methods of holding the module together. A novel technique, first presented by Apollon Solar in 2004, is the new industrial cell encapsulation (NICE) technology [41, 42]. PV modules using the NICE encapsulation technology have been proven to be easier to disassemble and recycle [43]. The EVA layer is in essence replaced by a layer of air, contained with the help of an edge seal. This causes the NICE module structure to differ from the previously discussed structure. Both structures can be compared in Figure 1.4, where the previously discussed standard PV module structure [9] is shown in Figure 1.4a next to the structure that makes up the NICE module [44], as shown in Figure 1.4b.

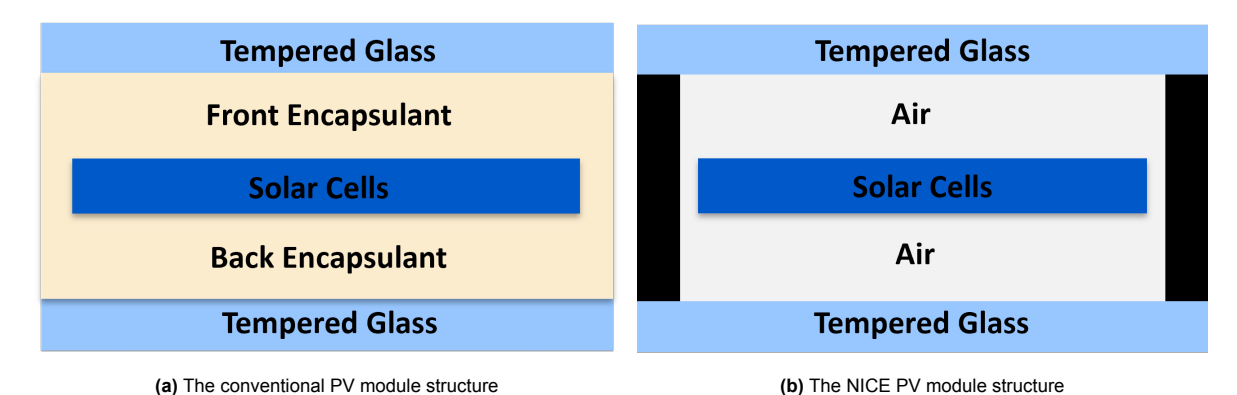


Figure 1.4: Simplified cross-section of a conventional PV module (left) and the NICE PV module (right)

The main differences lie in the cell-ribbon connection and the encapsulant layer. The encapsulant layer is removed and the remaining space in between the glass sheets is filled with air, which is contained by a polyisobutene (PIB) seal around the edges of the module. PIB is classified as: "a synthetic polymer based sealant with integrated desiccant for dehydrating the airspace in photovoltaic and thermal module constructions" [45]. The combination of the integrated desiccant and the low vapour transmission of

the PIB make it suitable for slowing moisture ingress [46]. The air inside of the module has a lower pressure than the ambient air in order to create under pressure. The resulting force from this pressure difference pushes the layers against each other, ensuring that the ribbons and cells stay connected and all components are kept in place. For this to work it is of utmost necessity that this lower pressure is always maintained, otherwise the PV module components would be fully detached due to the lack of adhesives and other connection methods. Luckily, the PIB edge seals are already widely used in the double-glazed window industry. Therefore, it has already been proven to live up to industry standards. Furthermore, PIB in combination with EVA is sometimes applied to glass-glass PV modules and it has been significantly researched. This addition of an edge seal in standard modules has been found to substantially slow moisture ingress [47-49]. Several problems with the NICE modules arise from the fact that they contain air. This layer of air can create oxidation and it causes the refractive indices on the path to the solar cells to be suboptimal. Thus increasing the reflection coefficient and lowering the amount of light reaching the solar cells. This correlates to a lower PV module efficiency. To optimise the refractive indices and to try to avoid drawbacks of air, such as corrosion, the use of inert gases, like nitrogen and argon, has been tested in NICE modules [43, 44, 50]. Another, relatively similar method of encapsulation is used in TPedge modules, developed by Fraunhofer ISE on behalf of the German Ministry for Economic Affairs and Energy. The TPedge modules are also gas-filled, however there are some significant differences between the TPedge and NICE PV modules. The gas-filled TPedge modules do not have under pressure to press the interconnections together, instead the busbars are connected to the solar cells. Furthermore, adhesive pins are added to provide additional mechanical strength [51, 52]. In total, 70 gas-filled TPedge modules have been integrated into the facade of the Fraunhofer ISE building located in Germany. The first 10 modules were installed in 2013, with 60 more added in 2015. The modules face 30° south and are vertically integrated into the side of the Fraunhofer ISE building. The performance of all installed modules has been monitored and the performance ratio from 2013 up to 2017 is shown in Figure 1.5 [53]. The performance ratio is a way to quantify the efficiency of a PV plant independent of its location. The graph below shows that the performance ratio stays stable around 60% to 70% for the first 10 modules and with the 60 extra modules it remains constant between 70% and 80%. In comparison, the performance ratio of 170 grid connected PV plants in northern Germany were fond to range from 47.5% to 81%, with a mean performance ratio of 66.5% [54].

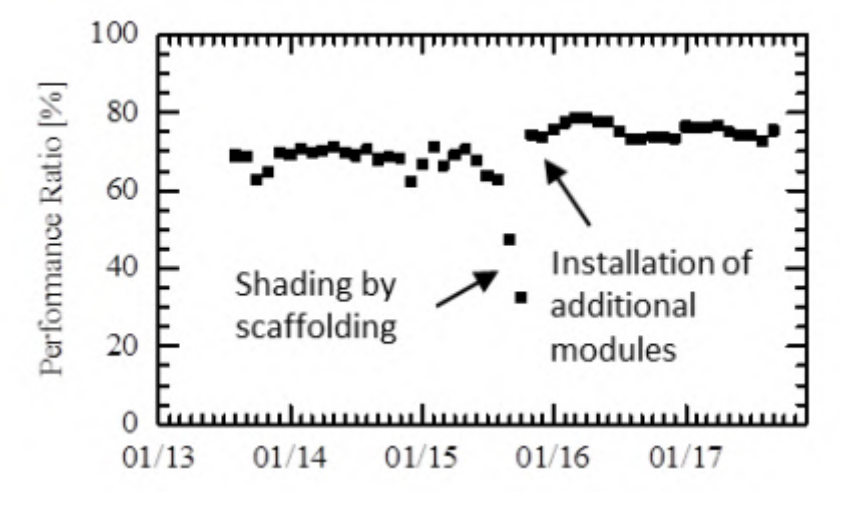


Figure 1.5: Performance ratio of TPedge building integrated PV application [53]

Biosphere Solar

Biosphere Solar is a Dutch company founded in 2021, their focus lies in creating recyclable PV modules by building further on the air-filled concepts of NICE and TPedge modules. To fix the arising issues of air-filled modules whilst maintaining the benefits of the edge sealant, Biosphere Solar is working on modules that are filled with liquid instead of gas. These liquids ideally adhere to the following properties, among other things they should have an as optimal as possible refractive index, no material

interactions, a low thermal expansion coefficient and a high transmittance. These are only a few of the most important properties required, making it a challenge to find the perfect liquid for this application.

1.5. Accelerated Ageing and Testing Methods

Accelerated ageing is a key method for evaluating the reliability of PV modules by simulating harsh environmental conditions that stress test them. This process speeds up the degradation a module typically endures over its lifetime, allowing for faster assessment of its long-term performance. To effectively assess reliability, two main steps are involved: first, applying stress through accelerated ageing techniques and second, measuring the degradation by tracking specific characteristics of the PV module under standard test conditions (STC).

Accelerated Ageing

Accelerated ageing is an industry-transcending method of testing that uses extreme temperatures, humidity, and other weathering conditions to assess the durability, weak points, and lifetime of a product. Various approaches to accelerated ageing are relevant regarding PV modules, with the most important ones compiled by the international electrotechnical commission (IEC) in their 61215 series standard [55]. This standard contains tests ranging from insulation tests to static mechanical load tests. The accelerated ageing methods highlighted in the IEC 61215 standard include UV preconditioning, thermal cycling, humidity freeze (HF) and damp heat (DH) tests. For all these tests specific requirements must be met. For instance the UV preconditioning must be carried out with a total irradiance dose of 15 kWh/m² (280-315 nm) at 60 °C. Whilst the thermal cycling should have 200 cycles, moving from -40 °C to 85 °C. Furthermore the humidity freeze test consists of 10 cycles consisting of 30 minutes at -40°C followed by 20 hours at 85°C with a relative humidity of 85%. Finally, the damp heat test makes the PV module endure 85 °C and 85% relative humidity at the same time for 1000 hours. PV modules filled with gas have already been successfully tested under damp heat accelerated ageing [56, 57]. For this thesis project the manufactured solar panels will be subjected to the humidity freeze test. This will be achieved with the use of a climate chamber to have complete control of the temperature and humidity and to ensure the temperature can reach both -40 and 85 °C and the relative humidity can reach 85%. For thoroughness and additional assurance that test requirements are met and the test will be passed. up to 30 cycles will be performed instead of the 10 required according to the IEC test.

Standard Testing Conditions

The standard testing conditions are a worldwide standard for comparing the output of solar panels where the same input parameters are adhered. The STC consist of a controlled irradiance, temperature and light spectrum. With an irradiance of 1000 W/m², a cell temperature of 25 °C and a wavelength distribution comparable to the air mass 1.5 Global (AM 1.5G) light spectrum [58]. If the STC are carefully controlled, they provide a consistent testing environment, making it possible to assess the variations over time in output values, and thereby asses the induced degradation.

Testing Methods

By testing the PV modules under a solar simulator adhering to the STC, the current and voltage can be measured. From this, the IV curve, short-circuit current density (Jsc), open-circuit voltage (Voc), fill factor (FF) and efficiency, among others, can be derived. These are all key parameters that determine the performance of a PV module and the changes in these parameters indicate the amount of degradation induced. Next to this, there are different ways to check if a PV module has degraded. For example, cell defects can be highlighted with the use of electroluminescence, abbreviated to EL. By using EL, it can be made visible what parts of a solar cell are still able to generate a current. This is done by running a reverse bias current through the solar cell, forcing all working areas of the cell to emit a very dim light, highlighting the contrast between the working and defect areas. The used setup and the precise workings of EL are explained in Chapter 4.2

1.6. Research Gap

There is plenty of research occurring in the field of photovoltaics. This is however mainly focused on making it cheaper, more reliable, more accessible and improving efficiency. Meanwhile, there is only a

handful of studies regarding recyclability and creating a closed-loop system for solar panels. Previous research in improved recyclability of solar panels includes Apollon Solar's NICE technology [41–44, 56, 57, 59–61], TPedge PV modules [51–53] and independent research in the topic [62–66].

All of the previously mentioned research focuses on innovative module architectures and their recyclability at the EOL. However, the module efficiency is lower than desired, primarily due to optical losses. This can be overcome by filling the modules with liquid instead of air or gas due to the preferred refractive index of certain liquids. This thesis will focus on the understudied liquid-filled modules and their degradation under accelerated ageing conditions. To be as comprehensive as possible multiple liquids will be selected, tested and compared to each other and the more common EVA PV modules.

1.7. Thesis Objective

This thesis project aims to improve the lifetime of liquid-filled PV modules by understanding their main degradation mechanisms and suggesting strategies to mitigate these degradation losses. This will be achieved through the following sub-goals:

- 1. Evaluating the initial performance of self-manufactured liquid-filled PV modules.
- 2. Understanding possible degradation mechanisms in liquid-filled modules after humidity freeze accelerated ageing.
- 3. Determining the relative degradation of the liquid-filled modules and comparing them with air-filled and EVA-encapsulated modules.
- 4. Suggesting strategies to mitigate degradation losses in the liquid-filled modules.

1.8. Thesis Outline

This thesis consists of the following structure: Firstly, in Chapter 2, a closer look will be taken at the liquid selection. In Chapter 3, the manufacturing of the liquid encapsulated modules is explained and shown step by step. Then, Chapter 4 explains the testing setup and elaborates on why this was the chosen testing method. Thereafter, Chapter 5 provides the resulting data, graphs and EL pictures for each tested liquid. This data will be discussed in the same chapter. Finally, in Chapter 6, the conclusions of the thesis are presented and recommendations are discussed.

Liquid Selection

To understand what properties are relevant for the liquid encapsulants, the important aspects fulfilled by EVA in a traditional PV module are studied in detail. Traditionally, the encapsulant layer has five main functions. Firstly, it should hold the module together, in the novel technology this is already achieved by a PIB edge seal. Secondly, the encapsulation should allow for as much light as possible to reach the solar cell. Next to this, the material should be electrically insulated to allow for efficient current collection. Furthermore, it should be stable during extreme temperatures, high humidity and UV exposure. Finally, the liquid should be chemically stable and, at least relatively, environmentally friendly by for example being biodegradable. In total, the liquid to be used should ensure the best performance of the PV modules whilst also considering the lifetime and sustainability. Multiple liquids will be selected for testing in this research.

The liquid selection process starts in Chapter 2.1, where the desired properties for application in liquid-filled PV modules are laid out in detail. Thereafter, in Chapter 2.2, the liquid selection process will be highlighted. Finally, in Chapter 2.3, the final selection of liquids and the proposed division for the number of modules to be tested for each module structure are explained.

2.1. Desired Properties

To assess if a liquid could be suitable for application in liquid-filled PV modules, their properties are first checked to see if they meet the essential and desired properties. The properties of a liquid will be assessed in five categories. These categories are optical, electrical, thermal, physical and chemical properties. If the liquid adheres to these properties, it means it shows potential to be suitable for application in liquid-filled modules. Finally, there is a preference for liquids that are as pure as possible. This is beneficial to the reusability of the liquid and with knowing what material interactions are happening and could be expected. In a mixture of liquids it could occur that a non-essential additive of the mixture interacts with the edge seal or the cell, meaning the liquid can be classified as non-compatible by untraceable factors.

Optical

An essential aspect of all materials present in PV modules are their optical properties. This is because the more light is able to reach the solar cell, the more current can be generated. The most important optical property is the complex refractive index (\tilde{n}), consisting of the real (n) and imaginary (k) components, with the formula: $\tilde{n} = n + ik$. The combination of real and imaginary components completely describe the refraction and absorption of light in a material. Ideally, the real part of the refractive index, n, closely aligns to that of the glass layer, which is around 1.5-1.52 [67]. When the n values of two interfaces closely align there are very low reflection losses, allowing for optimal light transmission. EVA for example has a refractive index of n = 1.48, matching that of the soda-lime glass almost perfectly. The imaginary part of the refractive index, k, is known as the extinction coefficient. The k value should ideally be as low as possible because the extinction coefficient is directly correlated to the material's absorption coefficient [68]. Lower absorption means more light is transmitted through the material.

Measuring the complex refractive index of a liquid is a challenging process, normally performed by spectral ellipsometry, which is an indirect method of measuring [69]. This method is unsuitable for measuring liquids due to two limiting factors. Unlike solid materials, liquids need a container or cuvette to be measured through spectral ellipsometry, which affects the resulting values. Furthermore, the measurement equipment not being perfectly levelled or small vibrations will mess up the results. Due to this complexity, there is currently another ongoing Master thesis project by Thomas Rijsman, which focuses on modelling the optical behaviour of liquid-filled modules. Therefore, in this thesis, the main goal regarding the optical properties is to match the n and k values of the liquid to that of soda-lime glass in the range of 300-1200 nm. The n value of soda-lime glass is between 1.50-1.52 from 300-1200 nm whilst the k value typically lies somewhere between $1*10^-7$ and $5*10^-6$ [67].

Electrical

The working principle of a solar cell essentially boils down to the current generation and collection. Because the solar cell will be completely submerged in the liquid an electrically conductive liquid would short-circuit the solar cell. In order to prevent the short-circuiting of the solar cell, it is essential for the liquid to have a high electrical resistivity, which is expressed in $\Omega*cm$. A high electrical resistivity ensures that the generated current follows the desired path, which flows through the busbars, without leaking too much current. Next to having a high electrical resistivity, it is desired for the encapsulation material to have a high dielectric strength. The dielectric strength is the maximum electric field that a material can withstand before breaking down electrically and starting to conduct electricity, which is expressed in kV/cm. The electrical resistivity of EVA is > $1*10^{15} \Omega*cm$ and the dielectric strength is > 200 kV/cm [70].

Thermal

There are several thermal properties which are relevant to the behaviour and safety of the liquids. Three of these properties are expressed in °C, these are the flash, fire and pour points. Furthermore, the thermal conductivity, heat capacity and thermal expansion are deemed relevant parameters.

The flash and fire points are considered the most essential parameters regarding safety. The flash point is defined as the lowest temperature at which the liquid gives off vapour that can be ignited. This is an essential safety requirement in both the testing and real-world application of liquid-filled modules, with the testing being the bottleneck due to the 85 °C that will be reached and maintained during the accelerated ageing tests. To be on the safe side, any liquid with a flash point below 100 °C will be excluded from this research. The fire point is the lowest temperature at which a liquid will continue to burn for at least 5 seconds after ignition. For the liquid to keep burning, ignitable vapour has to be present and therefore the flash point is always lower than the fire point. For this reason the fire point is excluded from further comparison whilst the flash point is deemed relevant.

Another important thermal property is the pour point, which is defined as the lowest temperature at which a liquid maintains its flow characteristics. It is mostly used to characterise oily liquids, whilst for liquids such as water, it is more relevant to look at the freezing point due to the material characteristics changing significantly. To ensure that the behaviour of the liquids can be assumed uniform over a wide temperature range, the pour/freezing point ideally should be no higher than -20 °C.

The thermal expansion coefficient of the liquid is relevant to ensure that not too much pressure is building up inside of the modules during the accelerated ageing. A high thermal expansion coefficient stress tests the edge seal, which in the worst case can be a cause for the module to explode. The thermal expansion is expressed in 1/K

Finally, both the thermal conductivity (W/(m²K)) and the heat capacity (KJ/(kg*K)are relevant for the amount of heat the solar cell has to endure and for how fast the module changes temperature. First, the temperature matters because solar cells generally have a negative temperature coefficient regarding efficiency, meaning that they perform worse under higher temperatures and that they operate best under colder conditions. For this reason, the cooling of solar cells to increase output efficiency is an active topic of research [71–73]. Second, these thermal properties are relevant for the testing phase because the modules need to heat up from -45 °C to 25 °C to adhere to the STC temperature necessary for the measurements performed every six humidity freeze cycles.

Physical

The physical properties, taken into account for the liquid selection, are the density and the kinematic viscosity. The density is expressed in g/cm³ and is relevant because it impacts the total weight of the PV module, which can be a significant factor for rooftop PV. The kinematic viscosity is relevant for injecting the liquid in the modules, a high viscosity can make the liquid injection process more difficult and increase the time needed, as will be discussed in 3.5. The kinematic viscosity is expressed in mm²/s, which equates to centistokes (cSt). Both of the physical properties are relevant, however they will not be the deciding factor for excluding certain liquids from the testing.

Chemical

The chemical stability of the liquid is of high importance for the prolonged functionality of liquid-filled PV modules. It is the essential property which is the most difficult to assess, this is due to it being made up of a variety of factors that can all influence the stability and there is not a single value that can be measured and compared. The most important aspect to look out for is material interactions between the liquid with both the solar cell and the PIB edge seal. These material interactions can consist of corroding the solar cell and deteriorating and weakening the edge seal. UV stability is another important factor for PV encapsulants due to their outdoor UV exposure. Furthermore, a look will be taken at the biodegradability of the liquids, since a liquid-filled module failing in the field can spill the liquid into nature. The chemical stability is assessed by researching if there is any known information on material interactions or UV degradation that may occur, if significant interactions are to be expected the liquid is excluded from testing.

2.2. Liquid Selection Process

The scope of materials to be considered could first of all be narrowed down significantly by the fact that they should be in liquid form at room temperature (25 °C) and that, for safety reasons, the flash point of the material should never be reached. Realistically the liquid will reach a temperature of 85 °C during the accelerated ageing. However, to be extra cautious, the lower limit of the flash point is set at 100 °C. This requirement for the flash point excludes liquids such as benzene, ethanol, methanol and toluene. All of which show potential in their optical constants and are liquid at room temperature. However, they are considered too dangerous to test in the lab, let alone to use in the real world.

Most materials that are in liquid form at room temperature have a refractive index (n) within the desired range of 1.4-1.6, whilst at the same time being colourless and transparent. Even though the complex refractive index is an important factor regarding the module efficiency, almost no liquids were excluded due to poor optical properties. There are a few exceptions, such as mercury for example. Which is a liquid metal and is not transparent at all due to its extremely high extinction coefficient k = 7.08 at a wavelength of 1000 nm [74].

Some liquids have previously been tested or proposed in literature under reasonably comparable applications. Silicon concentrator solar cells, which were coated with a silicone layer and submerged in deionised water, have shown a reliable performance through damp-heat and thermal cycling accelerated ageing tests [75]. Furthermore, glycerol has been the preferred liquid of choice in modules made with a partially similar novel encapsulation technique, proposed at the start of the year 2025 [63]. These modules also made use of PIB edge seal, however they varied by implementing a thin polymer based layer in between the solar cell and the glass layers for more optimal light transmission. This polymer layer is not attached to the solar cell, therefore still allowing for relatively easy separation of materials.

Besides the previously mentioned published research in this topic, some research has been internally conducted by Biosphere Solar regarding material compatibility between some liquids and the PIB edge seal. From these previously carried out tests it became apparent that paraffin oils and synthetic hydrocarbons, both of which are regularly used as cooling fluids, interacted with the PIB edge seal and started leaking out of the modules. Therefore these types of liquids where excluded from further investigation in this thesis.

For quick comparison, the most promising liquids and their main properties are listed in Table 2.1. If data could not be found for a certain property a "-" is in place and if a material does not have a certain property at all a "X" is put in place. The properties of EVA, air and demi water are also presented in

the table. EVA is relevant because it is the current industry standard encapsulant, air is relevant due to air-filled modules being the current standard for recyclable solar panels and finally demi water is relevant because it is the most abundant liquid on earth and, whilst not perfect, its properties show some potential for being suitable as liquid PV encapsulant.

2.3. Selected Liquids

After researching the possibly suitable liquids and comparing their properties, a final selection could be made. The liquids that show to be promising enough regarding safety, optical constants and material compatibility are glycerol, mono propylene glycol (MPG) and polydimethylsiloxane (PDMS). Besides the preference for liquids to be pure, several composite liquids were also considered. The main candidates considered were Mivolt DFK, Shell Diala and Midel 7131, all of which are usually used as transformer fluids. As can be seen in Table 2.1, the relevant material properties of these three liquids differ only slightly. Due to time restraints, availability of manufacturing materials, and due to the similarities in material properties of the composites, it is preferred to use only one of them. In the end, the Mivolt DFK liquid was selected to be used because it was readily available.

2.3.1. PDMS

PDMS is considered a type of silicone oil and it has the chemical formula $(CH_3)_3$ -Si-[O-Si(CH₃)₂]n-O-Si(CH₃)₃, where n defines the amount of times the [O-Si(CH₃)₂] monomer repeats [82]. The viscosity of PDMS depends on the amount of repeating monomers whilst the other parameters remain virtually the same. For the liquid injection process low viscosity liquids are preferable, thus a PDMS silicone oil was used with a viscosity of 50 cSt. PDMS is generally used as lubricant, water repellent coating and as anti-foaming agent [83]. It is safe for human consumption, with an acceptable daily intake (ADI) up to 1.5 mg/kg of bodyweight [84]. Finally, PDMS can cause problems in wastewater treatment facilities and it degrades by evaporating into CO_2 , SiO_2 and H_2O [85].

2.3.2. glycerol

Glycerol is generally obtained from triglycerides, the main part of vegetable and animal fat [86]. Most of the manufactured glycerol as a by-product from the production of biodiesel [87]. Glycerol is a colourless and odourless liquid which seems to be suitable as a liquid PV encapsulant material when looking at parameters such as refractive index, flash point and thermal conductivity, as shown in Table 2.1. The only characteristics that could cause problems are the pour point and its viscosity. With a pour point at 19 °C it indicates that it is almost frozen at room temperature, explaining the high viscosity of 1130 cSt. Furthermore, glycerol is is readily biodegradable and it is safe for human consumption [87]. It is used in several products from sectors such as foods, cosmetics and pharmaceutics. It is also often used in electronic cigarettes to create the vapor that carries the nicotine and flavours to the user [88].

The preferred IUPAC name for glycerol is propane-1,2,3-triol [89]. It consists of the chemical formula $C_3H_8O_3$ and has the following molecular structure:

$$^{
m OH}$$
 $^{
m CH}$ $^{
m CH_2}$ $^{
m OH}$

2.3.3. MPG

The preferred IUPAC name for MPG is propane-1,2-diol [89]. It consists of the chemical formula $C_3H_8O_2$ and has the following molecular structure:

$$\operatorname{CH_3}$$
 $\operatorname{CH_2}$ OH

MPG shows a close resemblance to glycerol, both in chemical structure and in use cases. Chemically the only difference lies in one oxygen molecule being replaced with a hydrogen molecule. First of

Table 2.1: Selected materials and their characteristics

Encapsulation Material	Refractive Index (n)	Pour Point (°C)	Flash Point (°C)	thermal conductivity (W/m²·K)	heat capacity (kJ/kg·K)	thermal expansion (1/K)	Density (g/cm³)	Kinematic Viscosity (cSt)/(mm²/s)	Electrical resistivity (Ω*cm)	Dielectric Constant (kV/cm)
EVA [70]	1.48	×	270	0.23	1.40	ı	0.95	•	1.0 * 10 ¹⁵	200
Air	1.00	-213	×	0.03	1.01	0.0034	0.001	1	$1.3 * 10^{16}$	30
Demi water	1.33	0	×	0.62	4.18	0.0002	0.997	0.89	1.8 * 107	59
Glycerol [76]	1.47	19	199	0.29	2.38	0.0005	1.25	1130	1.0 * 109	43
MPG [77]	1.41	-57	104	0.18	2.48	0.0006	1.04	42.1	2.3 * 107	32
PDMS [78]	1.40	-70	318	0.15	1.51	0.0010	96.0	20	1.0 * 10 ¹⁵	40
Mivolt [79]	1.46	-50	250	0.14	1.90	0.0008	0.97	75	9.0 * 108	75
Midel 7131 [80]	1.46	-56	260	0.14	1	ı	0.97	59	2.0 * 10 ¹²	75
shell Diala [81]	1.45	-45	191	0.14	2.14	0.0008	0.81	8.6	9.0 * 10 ¹⁰	78

2.4. Conclusion

all, this close resemblance allows for MPG to be manufactured from glycerol, however it is mostly produced from propylene oxide (C_3H_6O) and water (H_2O) [90]. Some common use cases for MPG are, the de-icing of air planes, as electronic cigarette fluid and as food additive [88, 91, 92]. MPG is readily biodegradable and soluble in water, making it relatively easy to clean up and dispose of.

2.3.4. Mivolt DFK

Mivolt DFK is a liquid from Mivolt, specifically made for cooling electrical systems through immersive cooling. This is a cooling method where electronic components, generally servers, are cooled by being fully submerged in a liquid. Mivolt DFK can be classified as an ester oil, making it different than the earlier tested cooling fluids which consisted of paraffin oil or synthetic hydrocarbons. With favourable values for all considered parameters, as shown in Table 2.1, the Mivolt DFK liquid seems promising as possible liquid PV encapsulant. The only downside is that the material structure of the liquid is unknown, and therefore it is difficult to exclude beforehand that material interactions will occur.

2.3.5. Reference Encapsulant Materials

Next to the selected liquids, demi water will also be tested as a liquid encapsulant. This is mainly because water is abundant and environmental friendly. However, it is assumed to degrade relatively fast due to material interactions such as corrosion. Furthermore, air-filled modules will be tested to determine if the liquid improves the total module efficiency and whether the liquid encapsulants change the induced degradation. Finally, traditional EVA modules will be tested as a reference value to compare the difference in performance degradation of the liquid-filled modules against traditional encapsulation.

2.3.6. PV Module Division

For redundancy and thoroughness reasons, it was decided that three modules per chosen liquid will be manufactured and tested. However, since PV modules containing air and EVA are already better studied, and since water seems less suitable than the other liquids, two samples will be tested for each of these three materials. This brings the total of modules to be manufactured to 18, which seems reasonable regarding both the time planning and the materials available. An overview of the number of modules that will be manufactured for each material is shown in Table 2.2.

Encapsulation Material	# of Modules
EVA	2
Air	2
Demi water	2
Glycerol	3
MPG	3
PDMS	3
Mivolt DFK	3
Total	18

Table 2.2: Number of desired modules per selected encapsulation material

2.4. Conclusion

In this chapter, the desired properties of liquids for application in liquid-filled PV modules were thoroughly examined. Starting from the essential properties that traditional EVA encapsulant fulfils, five key categories of material properties were identified: optical, electrical, thermal, physical, and chemical. The potential liquids were compared and evaluated on basis of these categories.

2.4. Conclusion

A wide range of materials was considered based on these criteria. Some aspects are preferable for ease of manufacturing and optimal performance, such as a glass-matching complex refractive index, low kinematic viscosity and high electrical resistivity. Some parameters, mainly regarding safety, were more direct reasons for exclusion, such as flash point, as well as compatibility with module components like the PIB edge seal and the solar cell. Through this process, a shortlist of four promising liquids was identified: glycerol, mono propylene glycol, polydimethylsiloxane, and Mivolt DFK. Each selected liquid has its benefits and downsides regarding the desirable properties. In addition, EVA, air, and demi water are included as reference encapsulants to compare the performance of the selected liquids.

The next steps involve the manufacturing and experimental testing of the 18 PV modules using these selected liquids. The manufacturing process is from start to finish explained in the upcoming chapter.

Manufacturing Process of Liquid-Filled Modules

Before the accelerated ageing tests can be carried out, the PV modules need to be manufactured and injected with the liquid encapsulants. In this chapter the manufacturing process will be explained step by step, all the way from the solar cell to the fully operational mini-modules. In Chapter 3.1 the used type of solar cell is explained and discussed. Hereafter the soldering process used to connect external busbars to the solar cells is explained. Then, in Chapter 3.3 the lamination processes used to laminate air-filled modules and EVA encapsulated modules are shown step by step. After initial lamination, two air-filled modules were tested on air and water tightness by water submersion, this is described in chapter 3.4. Finally, in Chapter 3.5 the liquid injection method in order to transition an air-filled to a liquid-filled module is highlighted.

3.1. Solar Cells

To ensure consistent testing conditions such that the effects of the liquid can be isolated, all modules used in this thesis should contain the same type of solar cell. Two crystalline silicon solar cell technologies were initially considered: TOPCON and IBC cells. TOPCON cells offer high efficiency and bifacial operation, making them increasingly popular in commercial applications. However, they are mechanically fragile and prone to cracking during manual processing. Preliminary tests confirmed that hand manufacturing one cell modules using TOPCON cells was difficult to accomplish without significant cell breakage, making them unsuitable for the hand-assembled modules.

IBC cells, by contrast, are more robust and easier to handle during manual assembly due to their thicker wafer size. Their rear-side contact architecture increases the active front surface area, improving light absorption and eliminating front-side shading by cell fingers. Figures 3.1a and 3.1b show the front and back of the used IBC cells respectively. Given their mechanical stability, simplified hand soldering requirements, growing industrial relevance, and their abundant availability, IBC cells were selected as the most suitable cell choice for this research. The specific solar cells used are the Maxeon gen 3 IBC solar cells, manufactured by SunPower [93].

3.2. Soldering

Normally, to connect the solar cells together and to collect the electricity generated, external wiring must be securely connected to the cell's electrical contacts. Because for this thesis single cell modules are manufactured, no cells need to be stringed together, and only external wiring must be connected. This was achieved by first soldering so called dog-bones to the two designated edges, these are the top and bottom edges of Figure 3.1b. Finally, to complete the soldering process, a busbar can be soldered onto the dog-bone. The in-between steps of soldering the busbars to the IBC solar cell are shown in Figure 3.2. The solar cell with the dog bones attached is shown in Figure 3.2a, and the fully soldered solar cell with the busbars is shown in Figure 3.2b.

3.3. Lamination

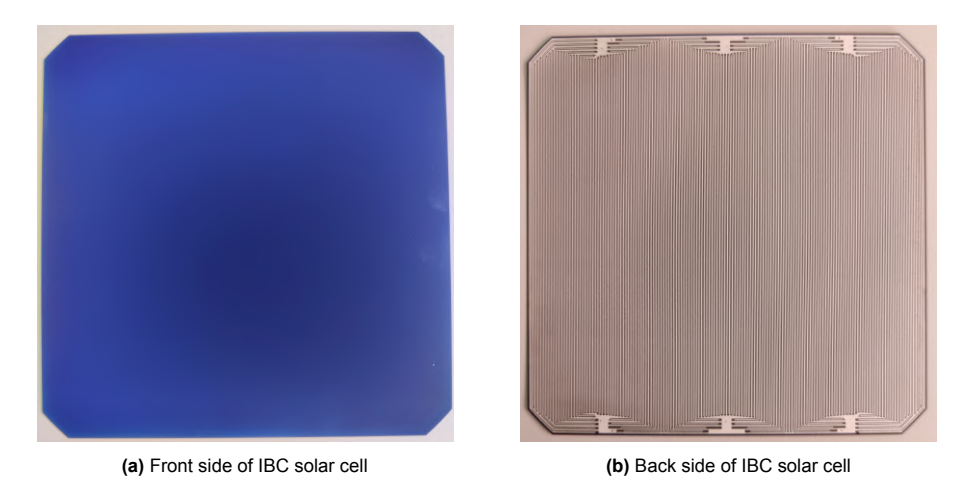
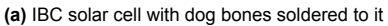
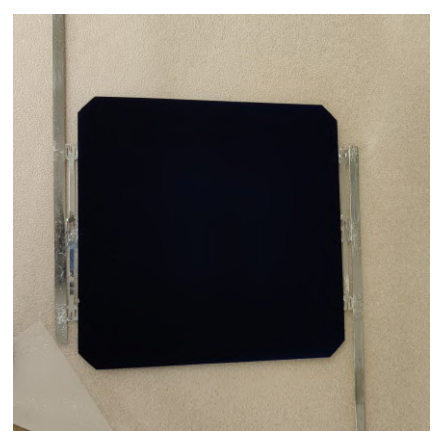


Figure 3.1: Front and back view of the selected IBC solar cells

To minimise energy losses and to maximise power output, it is crucial to ensure a mechanically strong and low-resistance connection. Furthermore, it is of importance that no harmful materials are used. Therefore, a non-toxic and low-resistivity aluminium alloy was used as soldering metal. Proper soldering technique also helps in preventing mechanical failure and in ensuring long-term stability.







(b) IBC solar cell with busbars soldered to it

Figure 3.2: Steps taken during the soldering of an IBC solar cell

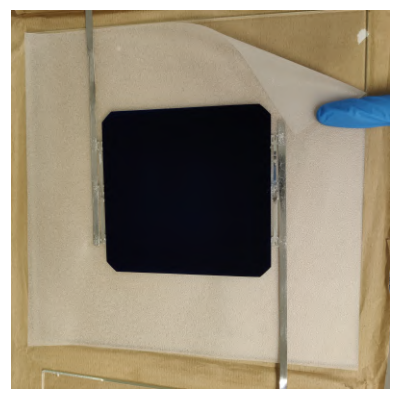
3.3. Lamination

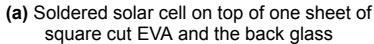
In this chapter, the lamination processes will be highlighted. Firstly, the lamination of an EVA module will be shown, whereafter the PIB edge seal lamination is explained. Both lamination methods will be compared to highlight the differences and similarities between them.

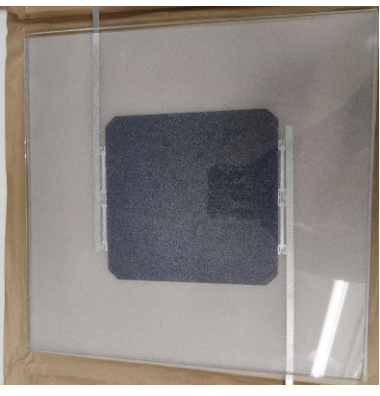
3.3.1. EVA

A traditional EVA PV module is laminated by heating up and compressing the desired stack of layers. From bottom to top this consists of the back glass, EVA layer, the solar cell, EVA layer and finally the front glass. This structure is shown in Figure 1.4a. This stack of layers is then placed inside a laminator with pressure and temperature control. The temperature control is required because the EVA structure permanently changes above a temperature of 150 °C. This change in structure, also known as crosslinking, provides the EVA with the essential mechanical and optical properties [94], changing the EVA from being opaque to transparent. To ensure direct contact between the EVA and the other materials, the stack is pressed together. This is done by first creating a vacuum and thereafter creating a pressure difference of around 900 mbar between the top and bottom of the module. After maintaining the 150 °C temperature and pressure difference of 900 mbar for 10 minutes, the chamber can be aired

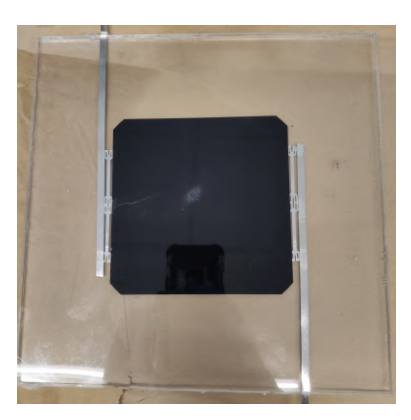
and the laminated module can be taken out of the laminator so it can cool down. In Figure 3.3c it can be seen that a small air bubble is still present in the middle of the cell after the lamination process. This irregularity is ideally not present because it indicates an imperfect adhesion of the EVA encapsulant layer with the front glass and the solar cell.







(b) Complete module consisting of glass, EVA and solar cell before lamination



(c) Complete EVA module after lamination, the EVA has become see through

Figure 3.3: Lamination process of the EVA module

3.3.2. Edge Seal

Edge seals have proven to be valuable additions for slowing down moisture ingress in EVA laminated glass-glass modules [10, 46, 48]. With desiccant filled polyisobutene (PIB) constantly being found to be the most suitable material, with some papers concluding that: "Of the materials studied, desiccant filled polyisobutylene materials demonstrate by far the best potential to keep moisture out for a 20 to 30 y lifetime." [46] .

The manufacturing process of an air-filled PV module with a PIB edge seal has more or less the same steps as that of EVA. First of all, the structure is created by placing a strip of PIB all around the edges of the back glass, with the corners partially overlapping. Then the solar cell is placed in the middle of the glass and its busbars are made sure to be in between two pieces of the PIB. Finally, the front glass is placed on top. Whereafter, the module is ready to be placed in the laminator.

The steps required for manufacturing an air-filled module are relatively the same as for an EVA module, however the main difference can be found in the lamination recipe. First of all, because of the lower melting temperature of PIB, a temperature of 90-100 °C is used for the lamination. Secondly, the pressure is also set to a lower value of between 300 and 500 mbar of pressure. This is because the air layer surrounding the solar cell gives almost no protection against the pressure, whilst an EVA layer provides some damping due to its softness. Finally, in consideration of the liquid injection, there should be enough space between the glass sheets such that a 0.8 mm needle can fit through. Two methods are used to guarantee enough space is available for the needle to fit through. First of all, a 1 mm thick spacer is placed in the corners such that the PIB can not become too compressed. And secondly, it was experimented to use two layers of PIB on top of each other. Which allowed for enough pressure to press the glass firmly to the PIB whilst still leaving enough space between the glass sheets.

3.4. Water Submersion Test

Before the modules are injected with a liquid, it is important to be certain that the lamination process works properly and that the edge seal is capable of containing the liquid. As a method of checking the water tightness of the laminated PV modules and mainly to test the PIB edge sealant, two of the manufactured modules were subjected to a complete water submersion test for 60 minutes. Two modules were chosen for this test because they were manufactured with a slightly different lamination method. The first module was laminated as described in Chapter 3.3, allowing the PIB to be compressed uniformly, whilst the other module was laminated with the use of 1 mm thick spacers in the corners to ensure enough room for the 0.8 mm needles which are required for the liquid injection. Both modules showed no signs of air leaking out or water leaking in, meaning that both modules passed the test. Be-

cause these modules are representative of all lamination methods used, it is assumed that all modules are leak resistant and can therefore be filled with the necessary liquids. The accompanying pictures of the water submersion test can be found in Appendix B.1.

3.5. Liquid Injection

The liquid injection can start after it has been ensured that the edge seals are water-tight, as shown in the previous section. First, the general liquid injection method will be discussed. Whereafter, a detailed look will be taken for each of the specific selected liquids and what difficulties arose during their liquid injection.

The method used for liquid injection, used in this thesis, starts off by manufacturing air-filled modules. Whereafter the liquid will be injected through the PIB edge seal. This works by first softening the PIB by locally heating the edge seal, which is shown in Figure 3.4a. After the PIB is softened, a needle can be pierced through. This is done in two different places, one to inject the liquid and one to allow the air to escape. In Figure 3.4b, the hole used for liquid injection can be seen in the top left, whilst the hole used to release the air can be seen in the top right. Then the liquid is injected through the needle with the use of a syringe. In Figure 3.4b, it can also be seen that the module is almost completely filled with liquid. The light blue area on the solar cell is caused by air that is in between the cell and the front glass, this air slowly moves away when the module is stored sideways. Finally, the PIB is resealed by locally reheating the PIB and using clamps to slightly compress the edge seal. This is the method of choice for this research because it is relatively straightforward and has been proven to work for similarly sized modules by Biosphere Solar. After injecting the liquid, it is checked whether the edge seal of the module is completely sealed by placing it on its side on top of a dry piece of paper for at least 60 minutes, with the liquid injection holes near the bottom. If within this time no wet spots appeared on the paper, the module was classified as properly sealed and thereby successfully manufactured.





(a) Softening the PIB with the use of a heat gun so the needle (b) The module directly after liquid injection, with the two required can pierce through



(c) The procedure of closing the module by softening the PIB with a heat gun and by applying pressure with multiple F-clamps for uniformity

holes and the needle at the top



(d) A different module shown for visualisation, with the cell completely submerged after letting it disperse. With the holes used for injection still visible on the right

Figure 3.4: Process used for liquid injection

3.5.1. Water

Water was found to be relatively easy to inject into the modules. The main reason is its low viscosity, which allows for a very low injection time. The water did not seem to give any problems by coming in contact with the edge seal. On the first try, two modules were successfully injected with water since they did not show any signs of leakage when stored upside down for over 60 minutes.

3.5.2. PDMS

The viscosity of the used polydimethylsiloxane (PDMS) was, despite being significantly higher than that of water, not a problem for the liquid injection. However, some problems were encountered with regards to PDMS injection. Due to the oiliness of the liquid, the PIB could no longer reattach to the glass after PDMS had made contact. Furthermore, the PDMS seemed to slightly soften the edge seal, which also complicated the resealing process. The combination of these two problems made it so that once some of the PDMS got stuck in between the PIB or between the PIB and the glass, it became extremely difficult to reseal the module properly. In the early phases of this project, before the failure mechanisms were completely clear, this caused the failure of several PDMS injected modules. By being extremely careful to not get PDMS residue in the holes which have to be resealed, the fail rate could be decreased, but the problem still sometimes occurred.

3.5.3. Mono Propylene Glycol

The mono propylene glycol (MPG) has around the same kinematic viscosity as the PDMS, 42.1 and 50 respectively [77, 78]. This small difference did not really affect the liquid injection. In general the MPG was straightforward to insert in the modules and it did not cause any problems.

3.5.4. Glycerol

Pure glycerol, at room temperature, was almost impossible to inject due to its high viscosity. The solution for this was to heat the glycerol before injection, which severely decreased the viscosity. During its injection process, it could very clearly be seen that the glycerol slowed down as soon as it was in the module. This is assumed to happen because it cooled down against the cold glass sheets. Therefore, in order to ease the liquid distribution in the module by keeping the viscosity low, the heat gun was used to heat both glass sheets of the module. Even though this heating of the glass clearly had some effect, the glycerol injection process took by far the longest of all tested liquids.

3.5.5. Mivolt

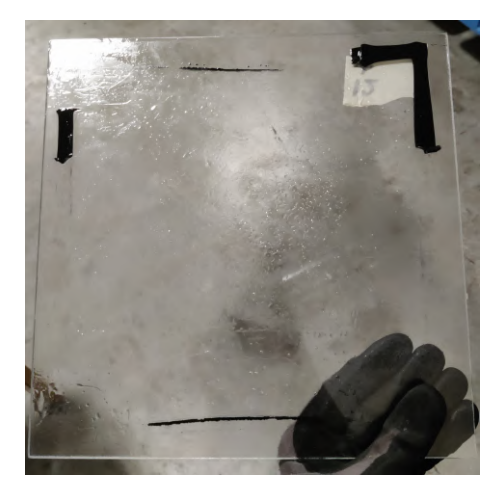
The first time Mivolt was injected in one of the modules, it seemed to work perfectly well. However, after leaving the module standing sideways for over 60 minutes, with the liquid injection holes at the top, there was only a bit of liquid left inside. When inspecting the edge seal, it could be seen that the liquid leaked out of the bottom and both sides of the module. The fact that it did not leak out of the holes used for the liquid injection, but out of seemingly sealed parts of the module. Hereafter, two more modules have been tried to fill with Mivolt. In both cases the exact same leakage problems occurred. Upon further inspection, it became apparent that the PIB was significantly softened and it could no longer stick to the glass, allowing for the PIB to be peeled off very easily, as can be seen in Figure 3.5

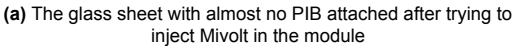
3.6. Reusability of the Modules

The main motivation for this research is to make recyclable and reusable PV modules more efficient, such that the gap between efficiency focussed and reusability focussed modules becomes smaller. Therefore, it is important to take a closer look at the ease of reusability for the manufactured minimodules. First the reasons for reusing the modules during this project are explained. Thereafter, the materials are discussed in the order they are encountered when taking apart the module. First, the liquid has to be taken out of the module, then the module gets opened and the solar cells can be removed. Finally, the PIB and the glass sheets need to be separated so they can both enter their respective recycling streams.

3.6.1. Failed Modules

During this project, several reasons for taking apart the modules and reusing them occurred. First of all, the reusing of failed modules lowers the amount of materials required and minimizes the waste







(b) The softened PIB, peeled off in one piece after injecting Mivolt in the module

Figure 3.5: Glass sheet and PIB after trying to inject Mivolt

generated for this research. For a previous experiment, some air-filled TOPCON modules were manufactured. These were taken apart and their materials reused in the manufacturing of the required modules. Other than that, sometimes the manufacturing process failed. In some instances, the gap between the glass sheets was not wide enough for the liquid injection needle to fit in between. Two of these modules were designated as air-filled modules, however, the other ones had to be taken apart and remade. Furthermore, as discussed in Chapter 3.5, the liquid injection process sometimes failed. Thereby requiring the modules to be completely remade to give the liquid injection another try. Finally, it happened on two occasions that the lamination and liquid injection all went smoothly, yet the module still had to be remade because one of the external busbars broke off. This likely occurred due to the metal being repeatedly bent, inducing material fatigue. Luckily this occurred before the accelerated ageing test, therefore it was not too severe of a setback.

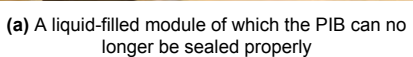
3.6.2. Liquid Encapsulant

The first step in taking the liquid-filled modules apart is to remove the liquid. In cases where the module has to be reused because the PIB failed to close after injecting the liquid, such as the module in Figure 3.6a where it is already open so the liquid could directly be drained in a controlled way. If the modules needs to be reused after resealing, it can be opened by softening the PIB edge seal by locally heating it with a heat gun such that it can be cut open. Alternatively, a hot knife can be used to combine the steps of heating and cutting in one. During this research, a hot knife was not available so the former option of locally heating with a heat gun was used. After opening the module, the liquid can be collected in a container by placing the module sideways such that the liquid drains inside the container, this process is shown in Figure 3.6b whilst the collected liquid is shown in Figure 3.6c. Finally after collecting all of the liquid it can in theory be fully reused and the current module can go to the next step of the process.

3.6.3. Solar Cells

For the continuation of the process, the two glass sheets need to be separated. This is achieved by applying heat to the whole edge seal, whereafter it can be cut open as shown in Figure 3.7a. After cutting through the edge seal on all sides, the module is separated into two glass sheets with PIB, one of which contains the cell as shown in Figure 3.7b. This allows for the solar cell to be removed. The solar cell is not suitable to be directly reused because most of the time it is either broken or contaminated with liquid, which is near to impossible to completely clean off. In some cases the cell breakage was caused by the cell sticking to the front glass due to the thin film of liquid which was in between. After the cell is taken out it gets cleaned and entered into its recycling waste stream, allowing for all materials inside to be recycled. Even though the cell can not be directly reused, the recycling is more efficient than that of EVA laminated modules due to the cell not being stuck to an EVA layer. The pib and glass sheets are left as the final two components to be separated, as shown in Figure 3.7c.





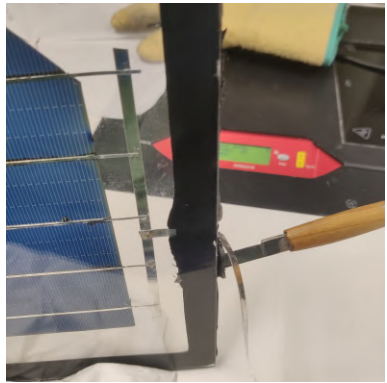


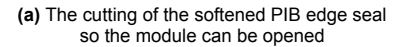
(b) The used method for draining and collecting the liquid

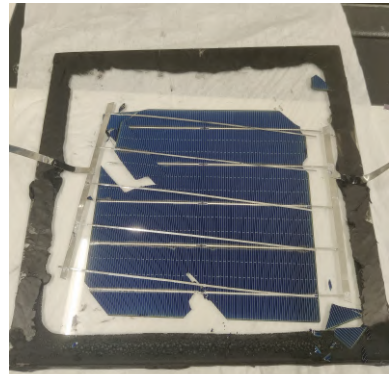


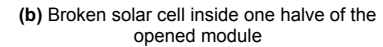
(c) The collected liquid, ready to be reused in future modules

Figure 3.6: Process of collecting the liquid for it to be reused or recycled











(c) The final part of the module that needs to be separated

Figure 3.7: Step by step process of opening the module

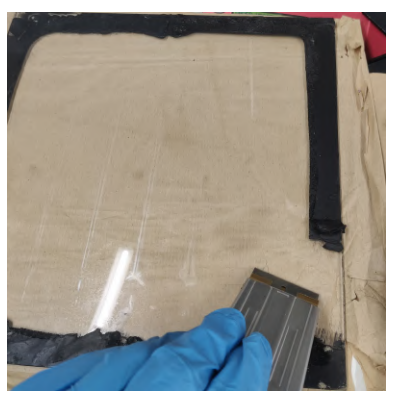
3.6.4. PIB edge seal

The final step in the separation process is to remove the PIB from both glass sheets. This is achieved by using a glass scraper to clear the PIB from the glass. The edge seal had to be scraped twice, with the first round used to remove the bulk of the material. The second time was necessary to scrape the final, smaller pieces, off the glass. This separation process is shown in Figure 3.8, with the start of the process shown in Figure 3.8a and the finalised product shown in Figure 3.8b. Due to the PIB possibly being contaminated with small pieces of solar cell, dust and liquids it can not be directly reused. This, in combination with PIB being difficult to recycle, means it is being disposed. Ideally the whole module would be recycled, however with PIB accounting for less than 1% of the weight of a full-scale module, it being the only non-recycled component still means the module is relatively recyclable.

3.6.5. Glass

The final step before the glass can successfully be reused is to clean all residue of the solar cell, liquid and PIB off the glass. This is important for the new PIB edge seal to attach directly onto the glass. Which would become unnecessarily difficult if the glass was still oily from the previous liquid that was injected. After wiping the worst residues off the glass with dry disposable cotton cloths, isopropyl alcohol is used to fully clean and degrease the glass. After the cleaning of the glass, it is completely reusable, allowing for new modules to be manufactured with them. This has successfully been achieved for this thesis project.

3.7. Conclusion 24





(a) The scraping off of the pib

(b) The separated PIB and glass sheet

Figure 3.8: Separation process of the PIB and the glass

3.7. Conclusion

In this chapter the manufacturing process the liquid-filled PV modules was highlighted and discussed. This was no easy process with multiple modules failing during manufacturing. One of the reasons for failure is the gap between the glass sheets not being wide enough for liquid injection, which was later prevented by using 1 mm spacers and a thicker sample of PIB. Another failure point is the imperfect resealing after liquid injection, this mainly occurred due to liquid seeping in the holes that should be resealed, thereby no longer allowing the PIB to easily re-attach to itself. This could not be completely prevented with the used liquid injection method, however, by taking extra caution not to contaminate the holes, the success rate could be slightly increased. Furthermore, in two cases the metal busbars broke off, after being more careful with the busbars, for example by not bending them in the same place every time, this problem no longer occurred. Finally, the Mivolt DFK liquid leaked through all sides of the module on all injection attempts. Therefore, it was concluded that Mivolt DFK and PIB are incompatible and no Mivolt-filled modules are to be tested in this thesis.

The initial aim was to manufacture 18 modules, however due to the Mivolt and PIB incompatibility this was lowered to 15 modules. Furthermore, due to 11 modules failing during manufacturing, in total 26 modules had to be attempted to be manufactured in order to successfully reach the goal of 15 fully operational modules. Due to the many failures, the reusability of the one cell modules could be demonstrated. Showing that the glass is fully reusable whilst all other components, such as the PIB and the solar cells, can be easily separated. With only the light weight PIB being non-recyclable, the modules are relatively completely and easily recycled when compared to EVA laminated modules.

4

Methodology

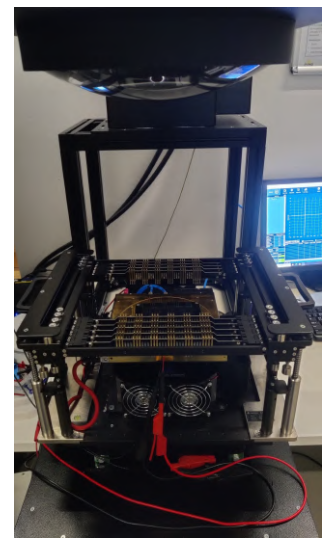
In this chapter the chosen methodology for carrying out the tests on the manufactured modules is discussed. The testing method starts by measuring the JV curves of the modules under STC conditions. This is done with the use of a solar simulator and the process is explained in detail in Chapter 4.1. Hereafter, to see whether cracks are present in the solar cells, the process of taking electroluminescence (EL) images is explained in Chapter 4.2. After taking the measurements, the humidity freeze test will induce degradation by stress testing the liquid-filled modules, the process of which is explained in Chapter 4.3. After leaving the climate chamber, the PV modules need to reach 25 °C to adhere to the STC conditions, a calculation for the time it takes the modules to reach the desired temperature is made in Chapter 4.4.

4.1. Solar Simulator

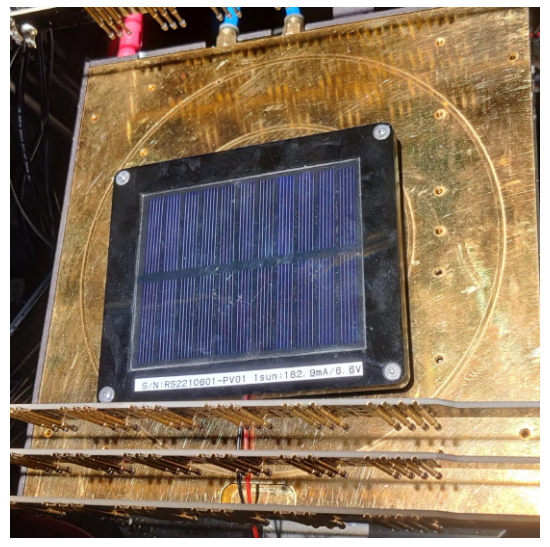
A solar simulator is the best way to consistently measure the performance of solar cells under STC. This is important so you can make sure the degradation you measure is actually occurring and not just a measurement error. For the measurements performed during this thesis, an Enlitech solar simulator is used, which is shown in Figure 4.1a. This solar simulator uses a single Xenon lamp to output the desired radiation of 1000 W/m². The lamp is turned on at least 30 minutes before starting the measurements, such that the temperature and the irradiance output can stabilise. This single lamp is capable of closely following the AM1.5G spectrum over a wide range of wavelengths (300 nm to 1700 nm). Which is achieved through precision optical filters and a unique spectral shaping approach to minimise spectral mismatch and maximise measurement accuracy [95]. The outputs of the solar simulator are measured and initially analysed with the IVS-KA6000 software and later exported to Microsoft Excel to be analysed.

The solar simulator is able to get accurate measurements of the current and voltage outputs under known levels of illumination. However, first the level of illumination needs to be calibrated, this is done with the use of a designated reference module with a known output current (182.9 mA) and voltage (6.6 V) under 1 sun illumination. The calibration is performed every time before starting the measurements and after the lamp of the solar simulator has stabilised. The reference module is shown in Figure 4.1b. Due to the reference module being a different height than the manufactured modules, a thin piece of foam was consistently used in an attempt to match the cell heights of the modules, this matching height, after the use of the thin foam is shown in Figure 4.2. For the measurements of the one cell mini modules a four-probe measurement setup was used. With the use of crocodile clamps that are attached to both the positive and negative external busbars. On both busbars one voltage and one current measurement clamp are attached, allowing for precise measurement of the output current and voltage under 1 sun of illumination.

4.1. Solar Simulator 26







(b) The reference module under the solar simulator

Figure 4.1: The solar simulator (left) and the reference module, ready for the calibration of the solar simulator (right)



Figure 4.2: Reference module (left) next to the PV module lying on top of a small piece of foam to match the cell heights

After being calibrated, the solar simulator can consistently measure the current and voltage outputs of a module, given that all other factors such as the temperature stay constant. Nonetheless, a margin of error can be expected. Whilst no information regarding the margin of error was provided by Enlitech, an error margin was found in literature. It turns out that a relative error of 1.9% was found to be the 95% confidence interval when taking efficiency measurements of crystalline silicon solar cells [96, 97]. This error margin is based on looking at all error margins of properties that can influence measurement results, including, but not limited to, the cell temperature, the effective irradiance, temperature non-uniformity and reproducibility factor. Margins of error are also found for the current (1.3%), voltage (0.6%) and the FF (1.2%). These relative margins of error only hold up for the absolute values and not for the relative changes, whilst for ease of comparison the relative changes will be looked at in the results. To switch from the absolute values to the relative values, the following formula is used:

$$Relative \ change = \frac{A - B}{B} * 100 \tag{4.1}$$

Where A is the initial value and B is the final value. Due to this calculation, the initially found margins of error are no longer valid. This formula takes the change in efficiency, divides it by the initial value and finally multiplies by 100 to get to a percentage value. For example, if a module increases its efficiency from 20 to 22 percent, this absolute increase of 2% is equivalent to a relative increase of 10%. The margin of errors have to be converted following the rules of error propagation [98]. For ease of calculation, the previous formula, Formula 4.1, can be rewritten as:

Relative change =
$$(\frac{A}{B} - 1) * 100$$
 (4.2)

Where A is still the initial value and B the final value. This makes the error propagation easier due to the number of times the error margins are multiplied or divided impacting the calculation of the final error. Due to one division happening the formula for calculating the absolute margin of error (MOE) of the relative changes is as follows:

$$MOE_{new} = \sqrt{MOE_A^2 + MOE_B^2}$$
 (4.3)

Plugging the different margins of error into this formula gives the following absolute margins of error: efficiency (2.7), current (1.8), voltage (0.8), FF (1.7). Note that these are the absolute values due to their transformation through the formula.

4.2. Electroluminescence

An alternative method of assessing whether the modules, but especially the solar cells, are degrading is by taking electroluminescence (EL) pictures. EL makes the solar cell, which can electrically be seen as a reverse diode, emit infrared light due to radiative recombination induced by a reverse current being fed through the solar cell [99]. Because the light emitted is in the infrared, the EL images are to be taken in a blacked-out room and with the use of a long exposure camera. Because only the working parts of the cell can emit light, it becomes really clear what parts of the cell are still working as intended. Cracks in the solar cell become extremely visible through EL images. Broken parts of the solar cell can be used to explain sudden drops in the performance of the modules.

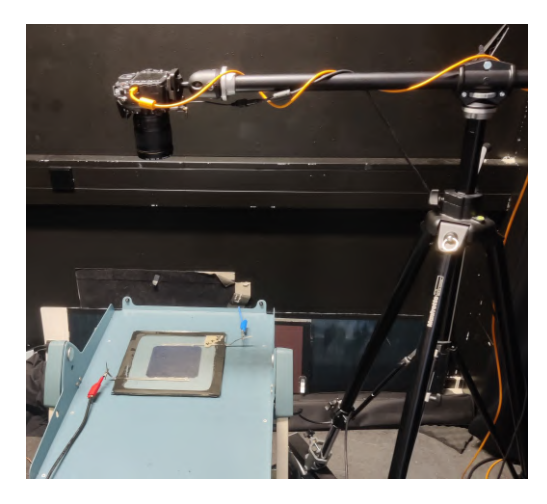


Figure 4.3: Camera setup used for obtaining EL images

The used setup is shown in Figure 4.3. It can be seen that the module, connected in reverse bias, is lying flat on the table whilst the camera is held in place right above the module. The used camera is a Nikon with the AF-S NIKKOR 28mm f/1.8G lens attached to it. The room where this took place could be completely blacked out with the use of black-out curtains and the camera could be controlled via software installed on a pc on the other side of the curtains. The power supply used to initiate the EL is a EA-PS 9200-25 power supply from Elektro-Automatik, with a range of 0-200 V and 0-25 A. Due to the IBC cells in the one cell modules emitting a lot of light, at the applied voltage of 0.7 V with a current of around 300 mA, an exposure time of only 4 seconds was required to capture the EL image.

4.3. Accelerated Ageing

As briefly discussed in Chapter 1.5, accelerated ageing is a method of testing that uses extreme conditions of temperature, humidity and other weathering conditions to assess the durability, weak points and estimated lifetime of a product. The main benefit of accelerated ageing is that it is much faster method of finding problems than real-life testing, failure mechanisms can become known within weeks rather than decades. Specific tests and test sequences are defined by the international electrotechnical commission (IEC) and are compiled in their IEC61215 and IEC61730 standards [55, 100]. Precise

control of both temperature and humidity is essential in order to adhere to the requirements stated in these standards. To achieve this an ESPEC PL-3J climate chamber is used. This climate chamber has temperature control over a range from -40 to +100 °C and humidity control from 20 to 98% relative humidity. Allowing for very precise control for adhering to the IEC standards. Furthermore, within its total inside volume of 408 litres, the climate chamber has room for several racks on which the samples can be placed to allow for a free flow of air around the modules such that they follow the set temperature as best as possible. Due to 6 modules fitting on one rack and three racks being available, there is enough room to test all 15 modules at the same time.

There are several accelerated ageing tests, all targeting specific types of degradation [101]. Thermal cycling is used to induce open circuit failures by switching between 85 °C and -40 °C, with one cycle taking 4-6 hours. The damp heat test focuses on accelerating moisture penetration in the module in order to induce corrosion which normally builds up over a longer period. Furthermore, the humidity freeze test is designed to allow moisture to penetrate the encapsulant during the first step of 85 °C combined with 85% relative humidity. Whereafter, the temperature drops to -40 °C, allowing for the moisture to freeze and expand.

4.3.1. Humidity Freeze

Due to its humidity requirements and temperature changes, the humidity freeze test can be seen as a combination of the thermal cycling and damp heat tests, making it a more thorough test. This is backed up by the fact that, modules fail damp heat and thermal cycling tests around 9% and 5% respectively, whilst the B1 sequence, with 20 humidity freeze cycles as main degradation factor, has a failure rate of just above 40% [102]. Whilst the IEC has not set a threshold for module failure, generally more than 5% of power degradation is considered as test failure [102]. Because conducting all tests not being an option due to time constraints, and with humidity freeze being the most thorough testing method, it was decided that using the humidity freeze test would be the most suitable option.

A schematic of one complete cycle of the humidity freeze test is shown in Figure 4.4. A test cycle starts at 25 °C, from where it should increase to 85 °C with a maximum temperature rate change of 100 °C per hour. Whilst at 85 °C, the relative humidity should be set to 85% with a maximum error margin of 5%. The samples endure this 85 °C and 85% humidity for a minimum of 20 hours, whereafter no humidity control is present and the temperature drops all the way to -40 °C. Again, there is a maximum rate of temperature change so as not to induce thermal shock. Once the temperature of -40 °C has been reached, it should dwell for a minimum time of 30 minutes. Whereafter the temperature should increase again allowing for the cycle to restart.

The humidity freeze test is for classically laminated PV modules a test for the adhesion and strength of the encapsulant. However in liquid-filled modules this test becomes extra interesting because of the moisture ingress combined with the effects of expansion and shrinkage of the liquid inside of the module. Following the IEC testing guidelines, and more specifically the B1 testing sequence, 20 cycles of the humidity freeze test need to be performed. In order to pass the test, the PV modules must retain at least 95% of their initial performance. For this thesis up to 30 cycles will be performed to thoroughly test the liquid-filled modules.

4.4. Cell Temperature Calculation

When the mini modules are taken out of the climate chamber, after enduring six cycles of the humidity-freeze test, the climate chamber has just heated up from -40 °C to 25 °C. The modules however, are unlikely to have heated up to 25 °C already. For accurate results of the current and voltage values from the solar simulator, it is of utmost importance that the STC conditions are adhered to, meaning that the solar cell should be 25 °C. It is challenging to measure whether this is the case because the solar cell is submerged in a liquid, which in turn is contained within two glass sheets. To be aware of how the different liquids inside this layered structure affect the change in temperature of the solar cell, a thermal calculation has been made in Python. This Python script can be found in Appendix A.

4.4.1. Used Equations

In order to calculate the cell temperature at a given time, a thermal calculation is performed. For this calculation, the thickness, area, thermal conductivity, heat capacity and density are used. With

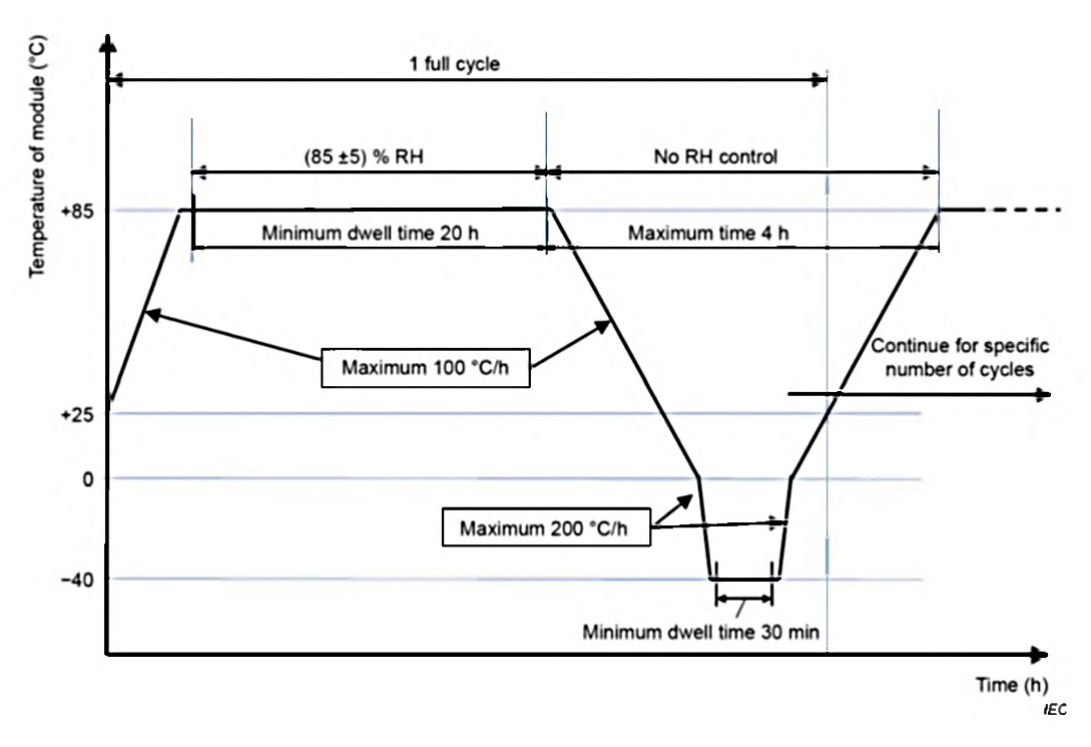


Figure 4.4: Time diagram for one cycle of the humidity freeze test

these parameters, the thermal balance of every individual layer can be simulated by calculating the conductive and convective heat transfer at every time step. Note that the radiative heat transfer was excluded due to it severely complicating the calculation whilst it is expected to have the least influence on the temperature. For calculating the conductive heat transfer, Fourier's law is used.

$$Q_{conductive} = \frac{k * A * (T_1 - T_2)}{L}$$
(4.4)

Where Q is the heat transferred through conduction (W), k is the thermal conductivity of the material $(W/(m^*K))$, A is the surface area (m^2) , T1 is the temperature (K) of one of the materials, whilst T2 is the other materials temperature (K), and finally, L is the material thickness (m). The conductive heat transfer is calculated from the solar cell to the liquid, from the liquid to the glass, and from the glass to the air. This is calculated at every time step, which is 1 minute. Because convective heat transfer works mainly through a fluid moving away the heat, this was only calculated for the glass to air interface. The formula for convective heat transfer is also known as Newton's law of cooling and is:

$$Q_{convective} = h * A * (T_{surface} - T_{ambient})$$
(4.5)

Here, Q is the heat transferred through convection (W), h is the convective heat transfer coefficient of air (W/(m^2*k)), A is the surface area (m^2), $T_{surface}$ is the temperature of the surface and $T_{ambient}$ is the temperature of the ambient air, which is set at 25 °C. By adding up the conductive and convective heat transfer of the glass the total heat transfer is given. Through these formulas, the calculated temperature can reach infinitely close to the ambient temperature, but never really reach it. Therefore, the threshold to reach was set at 24.8 °C.

4.4.2. Required Heating Time

The time required for heating up the modules from -40 °C to 25 °C was found to be 118-145 minutes, depending on the encapsulation material used. The time and cell temperature are plotted in Figure 4.5. These calculated times align with the IEC standard of letting the modules rest for 2-4 hours before

measuring the IV curve. Therefore, it is decided to leave at least 2 hours between the measuring of the PV modules under the solar simulator and the end of a humidity freeze cycle.

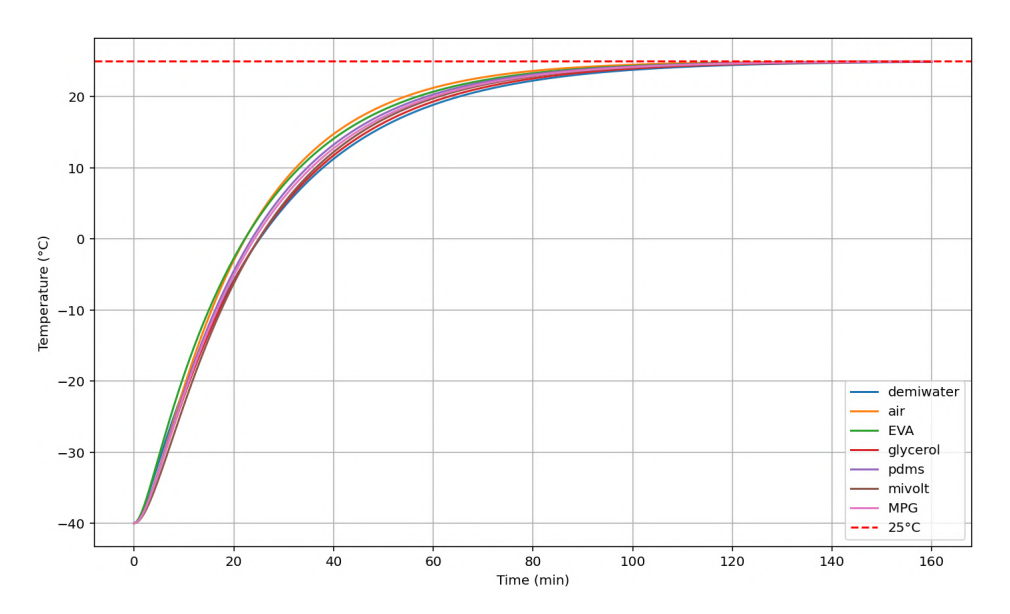


Figure 4.5: Cell temperature dependent on different encapsulants plotted over time

Measurement Results and Discussion

In this chapter, the obtained measurement results are presented and discussed. In all of the sections, a closer look will be taken at changes in terms of module efficiency and electrical performance. This chapter starts with the air-filled versions of all modules and their performance compared to when the same modules are liquid-filled, this will be discussed in Chapter 5.1. This will highlight the effects of injecting the different liquids compared to EVA lamination. Then, in Chapter 5.3, the results at the end of the 30 humidity freeze cycles will be presented and discussed per encapsulation material. Hereafter, the degradation for every six cycles will be discussed in Chapter 5.2. Finally, in Chapter 5.4 the degradation mechanisms will be assessed with the use of electroluminescence images and visual inspection.

5.1. Air-Filled to Liquid-Filled Modules

In this section, the performance of the manufactured modules will be compared before (air-filled) and after liquid injection (liquid-filled). This is done to quantify which encapsulation material has the largest increase in performance. First, the results of the initial air-filled modules will be presented in Chapter 5.1.1. Hereafter, the results of the liquid-filled modules will be presented and the relative changes in efficiency per material will be discussed in Chapter 5.1.2. Then, the variations in current density, open-circuit voltage and fill factor between the initial air-filled and the liquid-filled modules will be discussed in Chapter 5.1.3.

5.1.1. Air-Filled Modules

Only the air-filled modules which are successfully injected with liquid will be discussed because they tell the complete story from air-filled to liquid-filled modules. This entails there are 15 air-filled modules, consisting of the air-filled module structure as shown in Figure 1.4b. Furthermore, there are two modules laminated with EVA, of which the solar cells have been sandwiched in between two glass sheets to simulate an air-filled module for this measurement.

Even though the cell types, soldering methods, glass types, glass thickness and module structures are all the same, the efficiency values of the air-filled modules still vary from 20.78% to 22.27%, with an average efficiency of 21.68%. These variations in efficiency can come from differences in cell quality, or manufacturing variances such as soldering quality. In Figure 5.1, the measured efficiency per module is plotted in the bar graph with the dashed orange line showing the average value. Modules number 1 and 2 are the modules which are measured as the earlier described simulated air-filled modules whilst modules number 3-15 are all laminated air-filled modules following the earlier mentioned structure from Figure 1.4b.

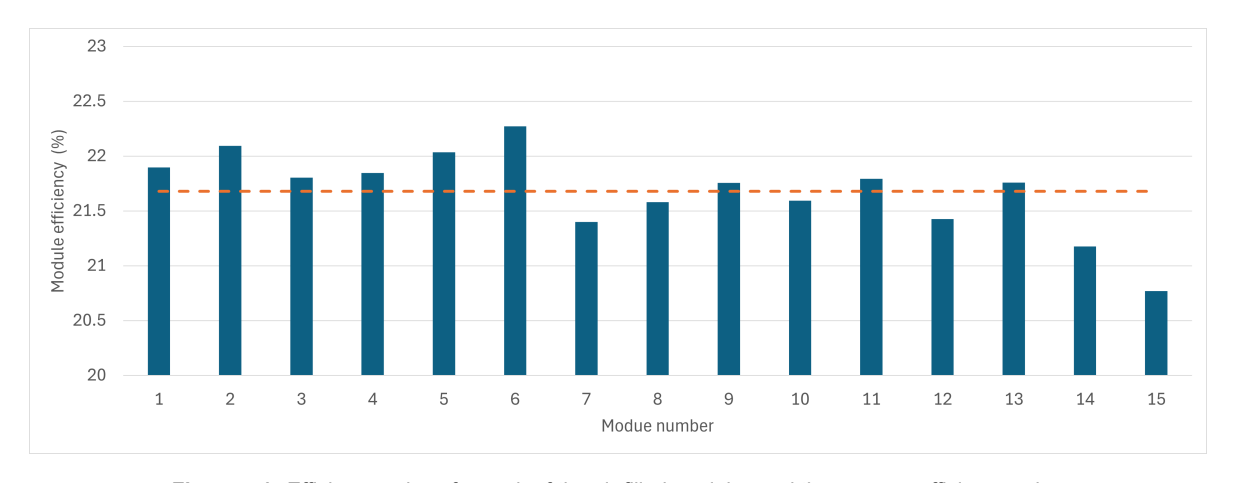


Figure 5.1: Efficiency values for each of the air-filled modules and the average efficiency value

5.1.2. Air- to Liquid-Filled Efficiency

In the previous section the baseline efficiencies are shown, measured before injecting liquid in the modules. The data of the air-filled modules was taken in order to have a baseline value to compare against the performance of the liquid-filled modules. In this section, the performance of the liquids is assessed in terms of changes in module efficiency between the air- and liquid-filled modules. In Figure 5.2, the measured efficiencies of all 15 air-filled modules from the previous section are plotted next to the newly measured liquid-filled modules. Furthermore, as discussed during the methodology in Chapter 4.1, error bars of 1.9% are present since that was found to be the 95% confidence interval when taking efficiency measurements of crystalline silicon solar cells [96, 97]. A large overlap between the error bars of the air-filled an liquid-filled bars of a module indicate that the change is not significant, whilst a small or even no overlap indicate that the change is likely significant.

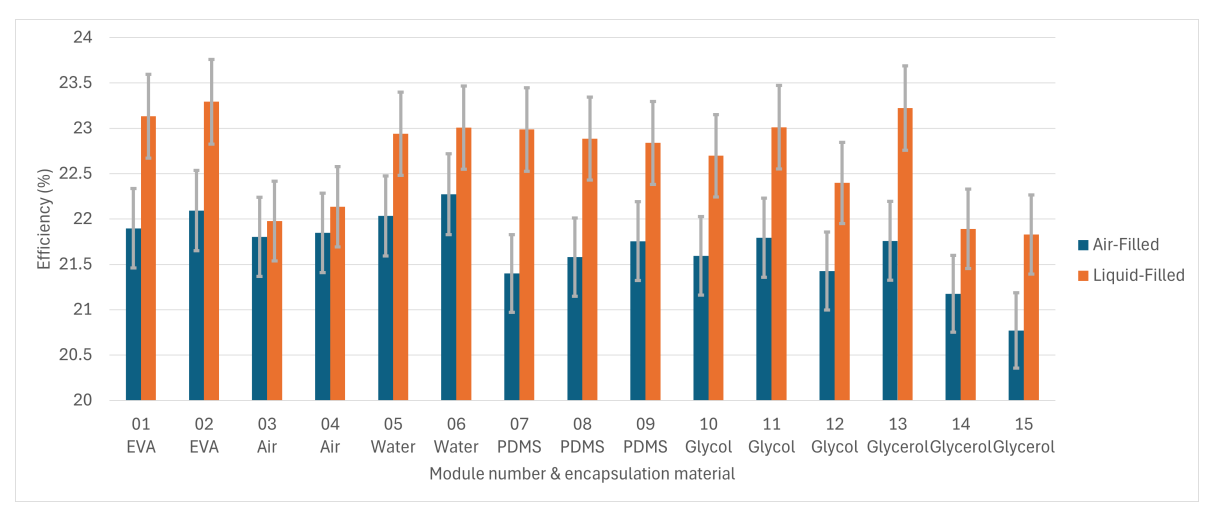


Figure 5.2: Measured efficiencies for each of the air-filled and the liquid-filled versions of the modules

From Figure 5.2 it might initially seem that the performance of the two glycerol-filled modules (sample 14 and 15) is slightly worse than that of the air-filled modules (sample 3 and 4). The glycerol modules had respective efficiencies of 21.9% and 21.8% and air-filled module numbers 3 and 4 measured efficiencies of 22.0% and 22.1%, respectively. However, for a fair and more useful comparison between the performance of the liquids it makes more sense to look at the relative increase in module efficiency instead of the absolute efficiency values. More precisely at the relative change in performance, which is explained in Chapter 4.1 and of which the formula is shown in Equation 4.1.

In Figure 5.3 the relative changes in efficiency between the air-filled and liquid-filled modules are shown for all 15 samples. Because these are the relative changes in efficiency, the 1.9% relative error bars

are no longer valid. Instead, the absolute error bar of 2.7% will be used, this was calculated in Chapter 4.1. To allow for direct comparison between the different encapsulants, the average change in module efficiency per encapsulant material is plotted in Figure 5.4, together with the absolute error bar of 2.7%.

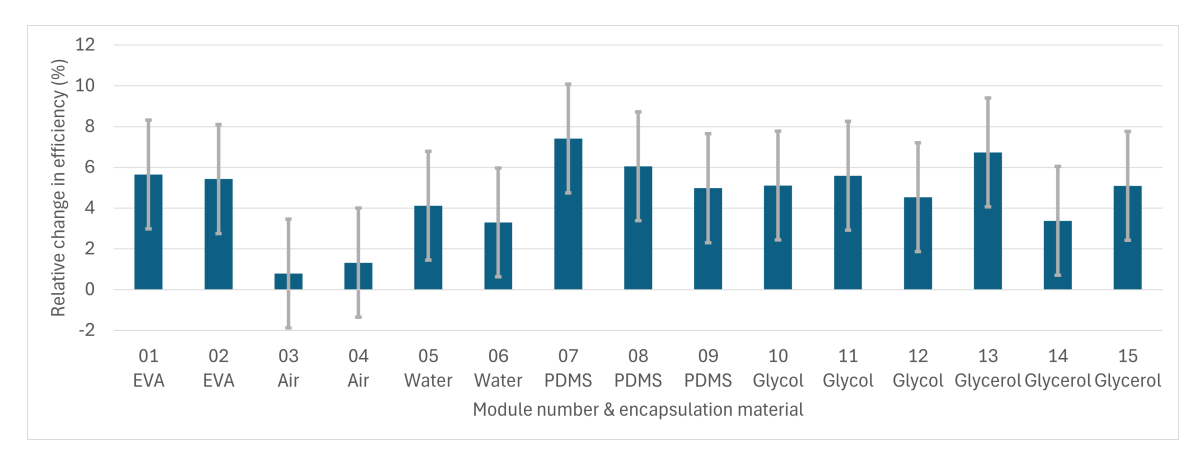


Figure 5.3: Relative change in module efficiency between the air-filled and liquid-filled modules

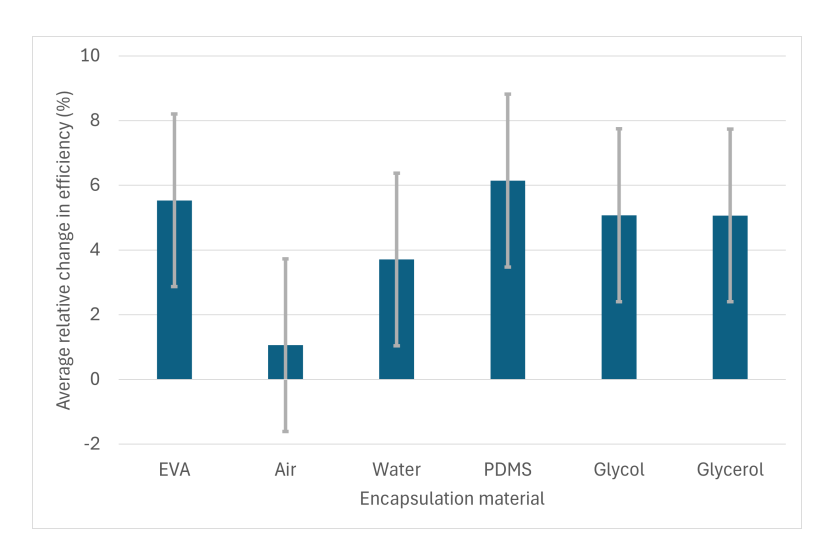


Figure 5.4: Average change in module efficiency between the air-filled and liquid-filled modules per liquid

EVA

The EVA laminated modules showed a relative increase in module efficiency of 5.6% for sample 1 and 5.4% for sample 2. This brings the average relative increase from air-filled to EVA encapsulation to 5.5%. This increase in efficiency can be completely attributed to the real refractive index of EVA (1.48) significantly more closely aligning to that of the glass (1.5) when compared to the module encapsulated with air (1.0) [67, 70]. Due to these closely aligned real refractive indices, the reflection of light is minimised and thereby more light is transmitted through to the solar cell. The average increase of 5.5% from the EVA laminated modules will be the baseline value to which the liquid-filled modules are compared.

Air

Since no adjustments are made between the first and second measurements of the two air-filled modules, they should return similar efficiencies between both measurements. Nonetheless, air-filled module 3 increased by 0.8% and module 4 increased by 1.3%. This increase, of on average 1.05%, should in theory not occur, however due to the severe overlap of the error bars in Figure 5.2, in combination with the value of 1.05 lying comfortably within the absolute error margin of 2.7, the changes in module efficiency of both air-filled modules can be regarded as non significant.

Water

The two water filled modules showed an increase in module efficiency of 4.1% and 3.3%, amounting to an average relative increase of 3.7%. This increase being far more than 2.7, shows that replacing the air with water does significantly improve the module efficiency, however it increases with almost 2% less than EVA laminated modules. This can be explained by the refractive index (n) of water being 1.33, whilst being more closely aligned to the refractive index of glass when compared to air, it is still quite far off.

PDMS

Module number 7, injected with polydimethylsiloxane (PDMS), has the highest efficiency increase of all modules, with a relative increase of 7.4%. The other two PDMS filled modules, number 8 and 9, also show a substantial increase of 6.1% and 5.0%. Bringing the average increase in efficiency to 6.2%, meaning that using PDMS as encapsulant shows a higher relative increase in efficiency than EVA. PDMS (1.40) has a lower refractive index (n) than EVA (1.48). therefore the PDMS encapsulated module is expected to show less of an increase in efficiency, whilst in reality the PDMS shows a larger increase in module efficiency when compared to EVA.

MPG

Of the liquids used for encapsulation, mono propylene glycol (MPG) showed the most consistent increase in efficiency over its three samples. With 5.1%, 5.6% and 4.5% for module 10, 11 and 12 respectively, bringing the average increase in module efficiency, resulting from adding MPG to 5.1%. This improvement is only 0.45% lower than the increase shown when using EVA as encapsulation material. MPG has a refractive index of 1.41 whilst EVA is more closely aligned to the glass with a refractive index of 1.48. Thus it is to be expected that the MPG modules show a severe increase, but less than the EVA laminated modules. The MPG increases with 5.1% on average whilst the PDMS increases with 6.1% on average, even though they have almost the same refractive index. The difference in efficiency gain, could come from the high electrical resistivity from PDMS, thereby leaking less generated current.

Glycerol

The final three modules, number 13-15, were encapsulated with glycerol. Number 13 showed the second biggest improvement in module efficiency with an increase of 6.7%. Furthermore, the other two glycerol modules showed an increase of 5.1% and 3.4%. On average the glycerol as an encapsulant showed an average increase in module efficiency of 5.1%. This average efficiency improvement is the same as for MPG and a little bit lower than for EVA laminated modules.

5.1.3. Current, Voltage and Fill Factor

The module efficiency is the main metric regarding the performance of a PV module. However the efficiency directly correlates with the open-circuit voltage (Voc), the short-circuit current (Jsc) and the fill factor (FF). Thus, to get a better understanding of the underlying causes for the change in module efficiency, the changes in Voc, Jsc and FF will be compared.

Current

The relative change in short-circuit current density (Jsc) between being air-filled and liquid-filled is plotted, for each of the modules, in Figure 5.5. The error bars show the maximum to be expected absolute error regarding the current change, which was found to be 1.8% [96, 97].

By looking at the changes in Jsc per encapsulation method, it becomes clear that the EVA encapsulated modules again perform the best, with an average increase of 4.8%, closely followed by the PDMS modules with 4.5%. As 3rd best, the MPG modules with an average increase of 4.4%. The worst performing two liquid encapsulation methods are water and glycerol with 3.3% and 3.2% increases respectively. Finally, as expected, the air-filled modules showed the lowest increase of all with an average 1.3%. This entails that, just like for their efficiency, the air-filled modules fall within the absolute error margin of 1.8% whilst all other encapsulants do show a significant increase.

When looking at the average over all the modules, the increase in short-circuit current is a little bit lower

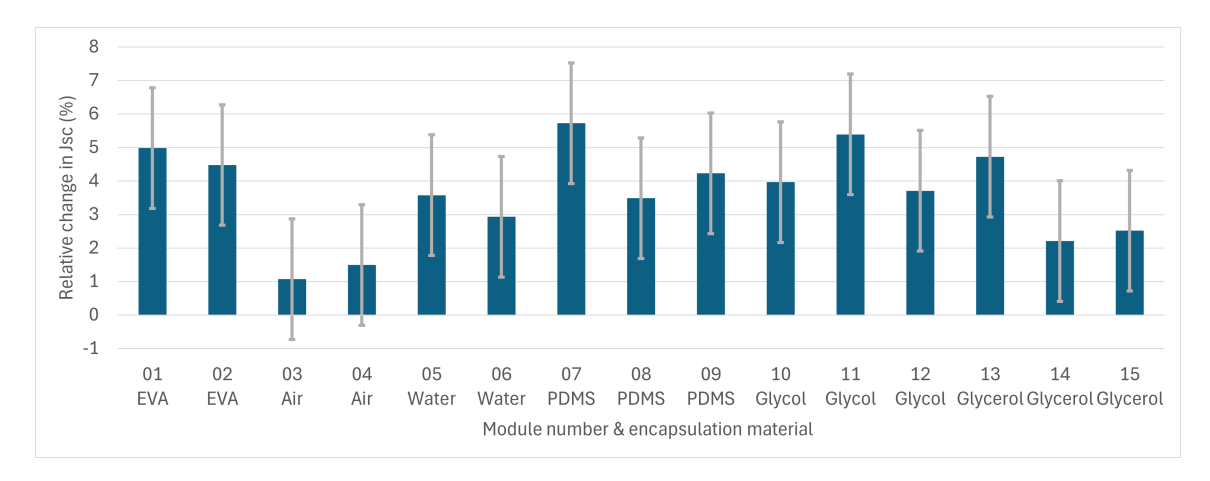


Figure 5.5: Relative change in Jsc between the air-filled and liquid-filled modules

than the increase in module efficiency, with 3.6% and 4.6% respectively. On first look, the modules with a high increase in Jsc seem to also perform the highest regarding the module efficiency as shown in Figure 5.3. The more optimal refractive index of all of the liquids compared to air means more light gets transmitted through the layers to the solar cell. Since the generated current is directly correlated to the amount of transmitted light, their short-circuit current density all increases. The expected order of improvement regarding the current is the same as the order of the refractive index. However, in reality the glycerol seems to underperform when compared to theory.

Voltage

In Figure 5.6 the change in open-circuit voltage between the air-filled and fully encapsulated modules is plotted. Regarding the Voc measurements an absolute error margin of 0.8% can be assumed, as was calculated in Chapter 4.1 [96, 97].

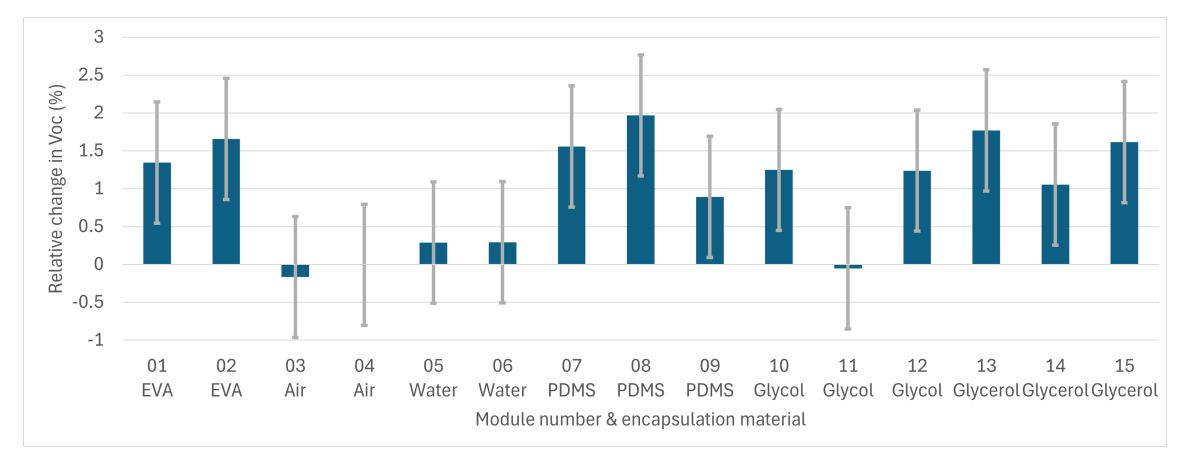


Figure 5.6: Relative change in Voc between the air-filled and liquid-filled modules

From Figure 5.6, it can be seen that the Voc does not significantly change for the air-filled and water-filled modules. Furthermore, for one of the MPG modules, the Voc also shows an insignificant change. When looking at the average changes in Voc per encapsulation type, it was found that the EVA, together with the PDMS and glycerol filled modules, showed the biggest change with an increase of 1.5%. Even though two MPG modules show an increase of around 1.2%, the MPG has an average increase of 0.8% due to the Voc of the third module staying almost constant. Finally, the Voc of both the water-and air-filled modules show an insignificant change of 0.3% and -0.1% respectively. The insignificant change in Voc of the air-filled modules is to be expected, since no adjustments are made between the two different measurements. The Voc of the water encapsulated modules changing insignificantly can be explained due to the suboptimal electrical resistivity of water, which lowers the positive effect of

increased light transmission.

Fill Factor

The final parameter to be viewed more closely is the fill factor. The change regarding the fill factor, between the air-filled and liquid-filled modules is plotted in Figure 5.7. The absolute error margin of the FF, was found in Chapter 4.1 to be 1.7% [96, 97].

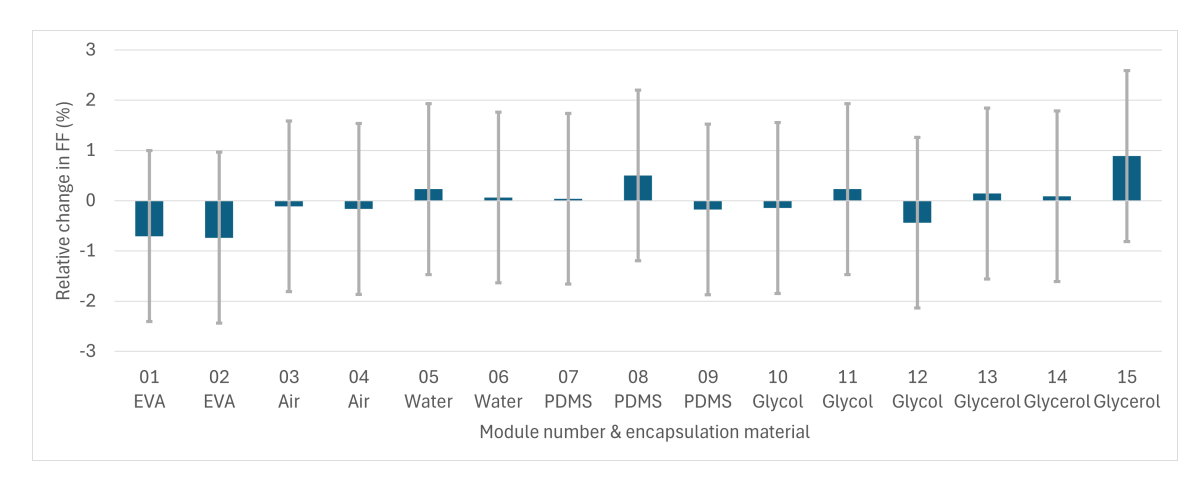


Figure 5.7: Relative change in fill factor between the air-filled and liquid-filled modules

For the fill factor no clear, consistent changes are found. All of the changes are insignificant and stay well within the absolute error margin of 1.7%, with none of the changes exceeding 0.9%. Furthermore no patterns can be noticed per encapsulation material, implying that the encapsulant method does not impact the fill factor.

5.1.4. Discussion

From the presented results, it becomes clear that the choice of encapsulation material has a significant effect on the performance of the PV modules. The PDMS-filled modules showed the highest average increase in module efficiency of 6.2%, which is even higher than the 5.5% increase found for the EVA laminated modules. This is interesting, since EVA has a higher refractive index (1.48) than PDMS (1.40), and therefore would theoretically allow for better light transmission. One possible explanation is that PDMS might provide better electrical insulation or surface passivation, thereby reducing current losses.

The MPG and glycerol filled modules both showed an average increase of 5.1%, which is only slightly lower than that of EVA. This suggests that these liquids also offer good performance improvement potential. The lowest increase in module efficiency came from the water-filled modules, which had an average increase of 3.7%. Whilst water has a refractive index of 1.33, which is much closer to that of glass than air, the efficiency gain was still limited. This can be attributed to water having the worst refractive index for optimal light transmission and therefore not transmitting as much light as the other encapsulants. Furthermore, it may be explained by water's relatively low electrical resistivity, which could introduce leakage currents or increased surface recombination, limiting the small but positive effect from the improved light transmission over air-filled modules.

When looking at the change in short-circuit current density (Jsc), all liquid encapsulated modules showed a noticeable improvement compared to the air-filled modules. The best performing ones in terms of Jsc were EVA and PDMS, followed closely by MPG. This is consistent with the theory that replacing air (n = 1.0) with a material of higher refractive index leads to less light reflection at the glass interface, allowing more light to reach the solar cells and increasing the generated current. Glycerol underperformed slightly in terms of Jsc, which does not fully align with its optical properties, and may be related to its electrical behaviour or its high viscosity which does not uniformly distribute the liquid.

The open-circuit voltage (Voc) showed small increases for most encapsulants, with EVA, PDMS, and glycerol all reaching around 1.5% average increase. These changes are relatively minor but consistent

across materials with good insulating properties. Water showed almost no change in Voc, which is in line with expectations as no additional passivation or electrical benefit is expected.

Finally, the fill factor (FF) did not show any significant or consistent changes between air-filled and liquid-filled modules. All relative changes stayed within the 1.2% margin of error, indicating that the encapsulant has no meaningful effect on FF under the tested conditions.

In summary, replacing air with the tested encapsulation materials resulted in improved module efficiency, with PDMS showing the highest overall gain. Followed by EVA, which in turn was closely followed by both glycol and glycerol, showing that all three of these liquids are competitive with EVA regarding electrical performance. The improvement is mainly driven by increased current due to better light transmission, although small improvements in voltage may also play a role. The results highlight the importance of both optical and electrical properties of the encapsulant when aiming to improve PV module performance.

5.2. Degradation Every 6 Humidity Freeze Cycles

In the previous section, Chapter 5.3, the initial module performances were discussed. In this section, the degradation results from the humidity freeze testing will be presented and discussed. To quantify whether an encapsulant is performing well they should be compared to the currently used methods, EVA encapsulated and air-filled modules. Therefore, for all performance parameters (efficiency, Jsc, Voc and FF), EVA and air-filled results will be discussed first, whereafter the liquid-filled modules are discussed and compared.

5.2.1. Early Failures

After the modules were manufactured, they are ready to start the humidity freeze testing. Just over half of the modules showed signs of failure within the first 6 cycles, all of which occurred due to leakages through the PIB edge seal. These leakages most significantly happened at the resealed liquid-injection points, whilst in some cases also occurring at the busbar exit points of the module. The leakages happened in both of the water-filled, two of the PDMS, two of the MPG, and two of the glycerol-filled modules. With some of the modules it was extremely clear that liquid had leaked out of the module, such as for PDMS-filled module 9, which is shown in Figure 5.8 after six humidity freeze cycles. Here it can clearly be seen that the desired amount of liquid is no longer present within the module. For other modules however, the leakage had to be detected through closely looking for liquid outside of the edge seal or by comparing the initial visual inspection images with the 6 cycle visual inspection image. To double check whether all suspected leaking modules were in fact leaking, their weight after six cycles was compared to their initial weight before starting the humidity freeze test. From this it became clear that all modules that, through visual inspection, seemed to be leaking had in fact lost weight, indicating that some of the liquid has leaked out of the modules.



Figure 5.8: visual inspection of module 9, initially encapsulated with PDMS, after six humidity freeze cycles

In total 8 out of the initial 15 modules showed signs of early leakage. Because a leaking module can no longer uniformly encapsulate the solar cell and because it is extra vulnerable to moisture ingress, all modules which are leaking are removed from the test. This exclusion leaves a total of 7 of the manufactured modules to be tested for the full planned 30 cycles of humidity freeze testing. This consists of he following amount of modules per encapsulant type: 2 EVA, 2 air, 1 PDMS, 1 MPG and 1 glycerol. Even though, preferably, water-filled modules and more modules per liquid are tested, the test was continued due to at least one module per liquid still being intact.

5.2.2. Efficiency

First of all, the main performance indicator will be compared, the module efficiency. The measured module efficiency for every 6 humidity freeze cycles is plotted in Figure 5.9. Where the light-red area is the region in which the 10 cycle module degradation is over 5% and the module can be classified as a failure.

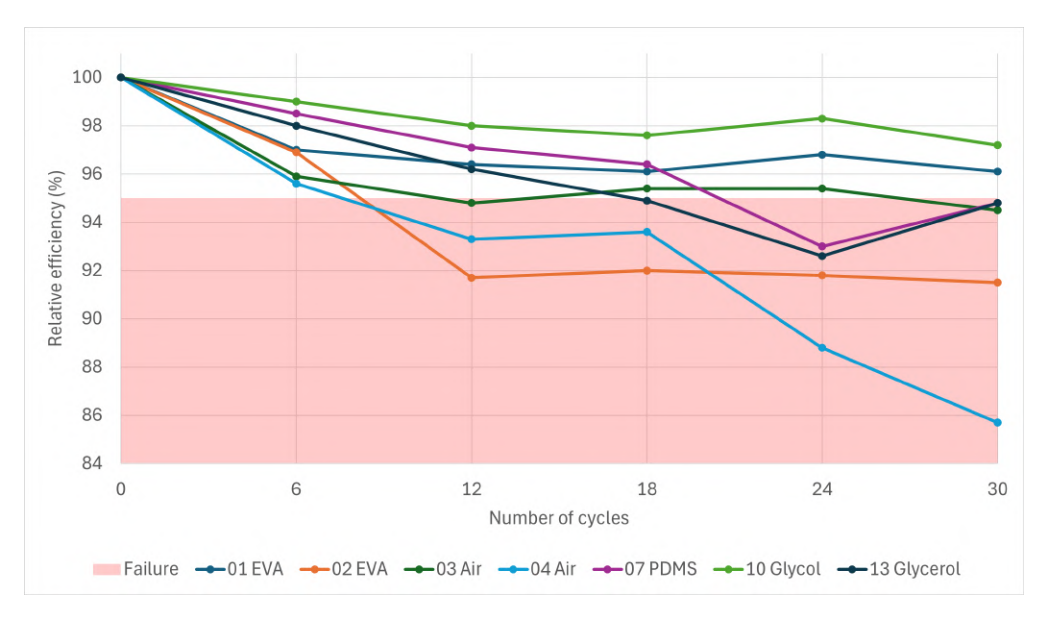


Figure 5.9: Relative change in module efficiency from 0 to 30 humidity freeze cycles

Both EVA laminated modules (sample 1 and 2) lost around 3% of module efficiency within the first 6 cycles, with only the air-filled modules showing an even worse degradation. This amount of degradation is not entirely surprising when considering that around 40% of modules normal fail the B1 testing sequence, which includes 20 humidity freeze cycles as main degradation factor [102]. EVA (1) lost only 0.6% efficiency more in the following 6 cycles. Its efficiency degradation stayed relatively constant from 12-30 cycles. The other EVA laminated module (sample 2) decreased significantly from cycle 6 to cycle 12, from 96.9% to 91.7% of relative module efficiency. After this significant drop its efficiency stayed more or less stable. The reason for the difference in relative degradation between the two EVA encapsulated modules is explained through visual inspection of the modules, which will be discussed in Chapter 5.4.

The two air-filled modules had the biggest decrease in module efficiency after the first 6 cycles, with air (3) losing 4.1% and air (4) losing 4.4% of relative efficiency compared to their initial module efficiency. This is significantly higher degradation than the value of 0.3% which was found in earlier research [56]. The high difference in degradation makes more sense in the context of the other degradation values found in this research due to the modules being similar to each other. Furthermore, the severe degradation of the air-filled modules can mainly be attributed to the fact that in both modules, the PIB got flattened and the solar cells cracked, as will further be discussed in Chapter 5.4. Air-filled sample 3 decreased by 1% in the next 6 cycles, whereafter the degradation stabilised over the final 18 cycles. Air-filled sample 4 also decreased up to cycle 12, all the way down to 93.3% of its initial efficiency. However, this sample did not stabilise. In fact, it decreased by almost 8% over the final 12 cycles, from 93.6% after cycle 18 to 85.7% after cycle 30.

The PDMS and glycerol encapsulated modules followed very similar patterns and both ended up retaining 94.8% of their initial module efficiency. Within the first 18 cycles they both show a consistent, almost linear pattern in efficiency degradation. The only difference between them is that glycerol (13) degrades more than PDMS (7) within those 18 cycles. After 24 cycles, both of them have a significant drop in relative efficiency. However, it seems to increase again in the final 6 cycles, leading up to the total of 30 cycles. This sudden drop and rise are not to be expected and might have to be written off as a measurement error.

5.2.3. Jsc

The measured short-circuit current density (Jsc) of all the modules is plotted in Figure 5.10 for every 6 cycles of the humidity freeze test.

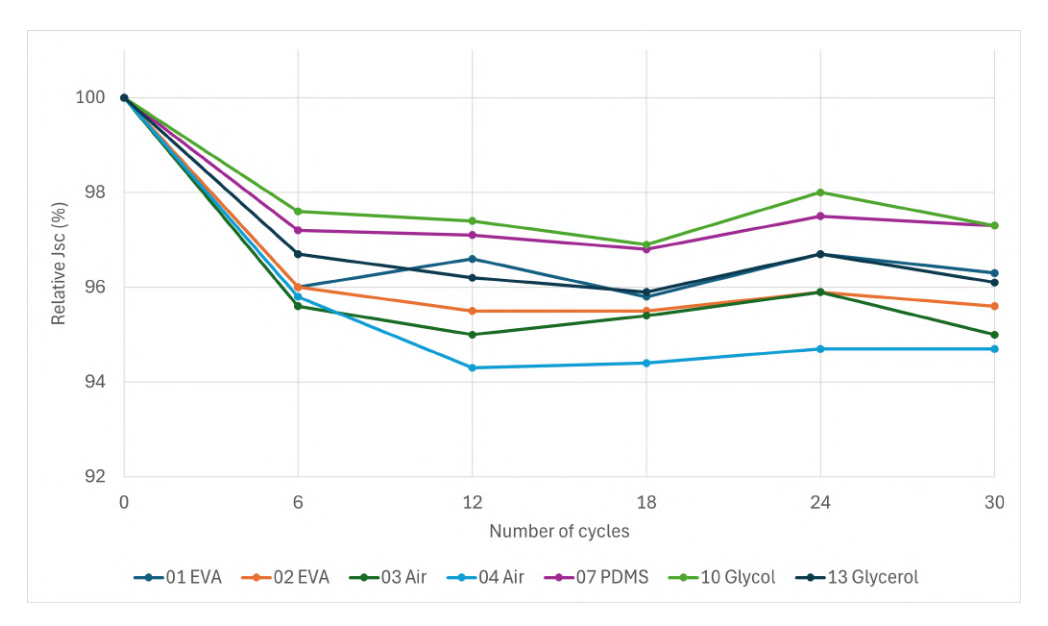


Figure 5.10: Relative change in short-circuit current from 0 to 30 humidity freeze cycles

All of the modules follow the same trend, no matter their encapsulation material. They all drop most significantly within the first 6 cycles, whilst up to 12 cycles, all but one (EVA 1) of the modules keep decreasing, but with a smaller jump. The initial cycles inducing the largest current degradation can be explained due to initial small defects being exposed due to the severe temperature changes. After 12 cycles they all stabilise, only to show a one-off increase after 24 cycles. Even though the trend is the same as for the efficiency degradation, the amount of degradation is not the same.

5.2.4. Voc

The measured open-circuit voltage (Voc) of all the modules is plotted in Figure 5.11 for every 6 cycles of the humidity freeze test.

For the Voc, the same thing holds as for the Jsc, all modules show more or less the same trend in their measurements. With one-off peaks occurring at 6 and 18 cycles, which probably should be written off as calibration or measurement errors, due to all samples experiencing the same amount of change at the same moments.

5.2.5. Fill Factor

As a final parameter to be looked into, the Fill Factor (FF) is taken into account. The FF of all the modules is plotted in Figure 5.12 for every 6 cycles of the humidity freeze test.

Three of the samples had some variations per measurement, but no big permanent changes, these are EVA (1), air (3) and MPG (10). Sample 2, laminated with EVA had a 4% drop in its FF from 6 to 12 cycles, whereafter it stayed stable. Indicating some degradation occurred between its 6th and 12th cycle. Sample 4, which is air-filled, showed a small initial decrease within 6 cycles, whereafter it stayed

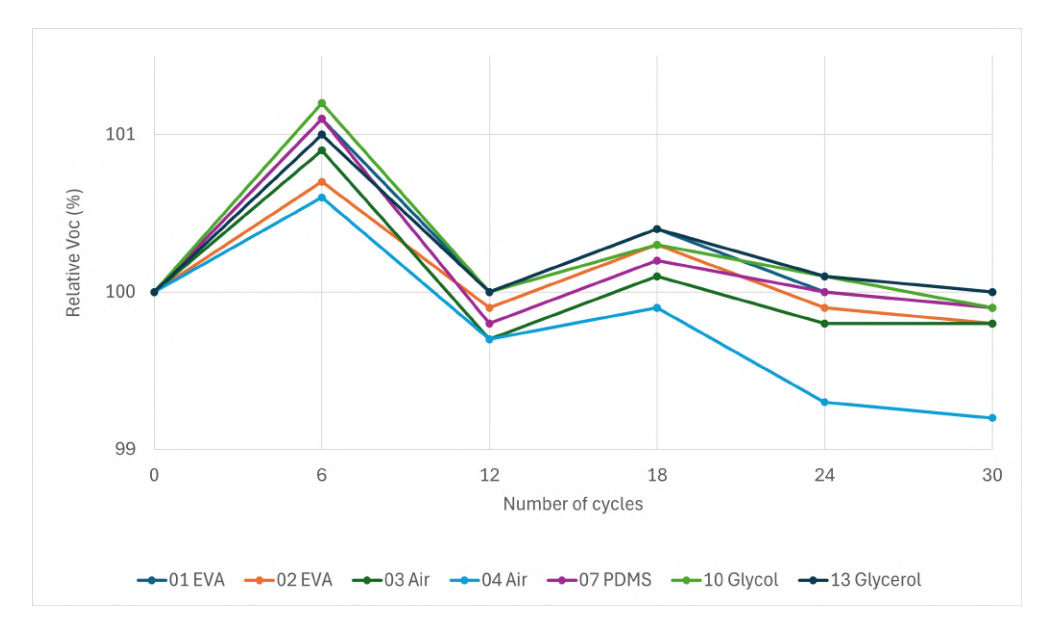


Figure 5.11: Relative change in open-circuit voltage from 0 to 30 humidity freeze cycles

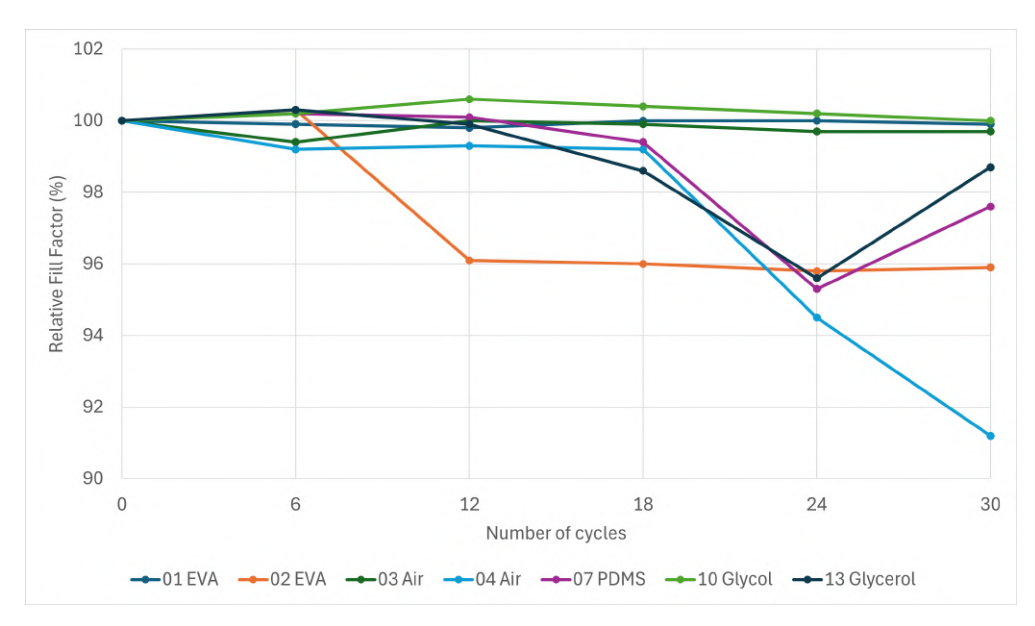


Figure 5.12: Relative change in fill factor from 0 to 30 humidity freeze cycles

stable up to 18 cycles. From 18 to 24 and from 24 to 30 cycles, air (4) showed two very significant decreases regarding its Fill Factor. Finally, the PDMS (7) and glycerol (13) encapsulated modules, both had a significant decrease in their FF after 24 cycles, which increased again within the final 6 cycles. For the glycerol (13) module this increase was all the way back to the FF at 18 cycles, for the PDMS (7) module this decrease was however not completely restored. Nevertheless, the decrease in fill factor after 24 cycles is odd because it occurred to only two of the modules instead of all of them.

5.3. 30 Humidity Freeze Cycles

After looking at the changes in degradation for every six cycles of humidity freeze, it is time to look at the final results obtained after 30 humidity freeze cycles. The same key parameters are looked at, efficiency, Jsc, Voc and FF. The results from the PDMS, MPG and glycerol filled modules will be compared against that of the EVA and air-filled modules.

In Table 5.1, the performance of the key parameters is shown for all 7 modules after 30 cycles of humidity freeze testing. The four key parameters which will be investigated are the efficiency, Voc, Jsc and FF. Furthermore, to visualise where a result stands compared to the other modules, a colour scale from green, yellow and red is used. The colour scale is different for each of the parameters, however in all cases, yellow indicates a relatively average performance, red indicates a negative outlier whilst green is reserved for the top results.

Encapsulant (sample number)	Efficiency	Jsc	Voc	FF
EVA (1)	96.1	96.3	99.9	99.9
EVA (2)	91.5	95.6	99.8	95.9
Air (3)	94.5	95.0	99.8	99.7
Air (4)	85.7	94.7	99.2	91.2
PDMS (7)	94.8	97.3	99.9	97.6
MPG (10)	97.2	97.3	99.9	100
Glycerol (13)	94.8	96.1	100	98.7
Average result	93.5	96.0	99.8	97.5

Table 5.1: Relative performance in efficiency, short-circuit current density (Jsc), open-circuit voltage (Voc) and fill factor (FF) after 30 cycles of humidity freeze testing

5.3.1. Efficiency

The least amount of degradation, regarding module efficiency, was achieved by the MPG-encapsulated module (sample 10) at 97.2%, indicating minimal optical or electrical losses and excellent compatibility with the photovoltaic material. This was closely followed by EVA (sample 1) with 96.1%, demonstrating that industrial grade EVA can still deliver excellent performance when processing is optimal. Both PDMS (sample 7) and glycerol (sample 13) showed identical efficiencies of 94.8%, suggesting their potential as alternative encapsulants with some, but limited degradation. Sample 3, which is air-filled, maintained a comparable efficiency of 94.5%. Furthermore, the other EVA module (sample 2) retained only 91.5% of its initial module efficiency, likely due to variations in lamination quality or degradation pathways. Finally, one of the Air-filled modules (sample 4) performed by far the worst with 85.7% of its initial performance.

5.3.2. Short-Circuit Current Density (Jsc)

In terms of Jsc, MPG (10) and PDMS (07) shared the top spot by maintaining 97.3% of their initial current. EVA (1) followed closely with 96.3%. Glycerol (13) and EVA (2) showed slightly lower values at 96.1% and 95.6%, respectively. Finally, the two air-filled modules (3 and 4) had the worst performance regarding Jsc by only retaining 95.0% and 94.7% respectively.

5.3.3. Open-Circuit Voltage (Voc)

Most modules showed barely any reduction regarding their Voc. Glycerol (13) perfectly maintained its original Voc of 100%, while MPG (10), EVA (1), and PDMS (7) followed closely by retaining 99.9% of its Voc. EVA (2) and air (3) were slightly lower, but still showed virtually no degradation at 99.8%. Only one sample had a significant drop in its Voc, this was one of the air-filled modules (sample 4), with drop to 99.2% compared to its initial Voc.

5.3.4. Fill Factor (FF)

The fill factor displayed more variance across encapsulants. Some encapsulants showed reasonably no change in FF, whilst others reached almost 9% decrease compared to initial value. MPG (10) was the top performer with a perfect 100.0% FF. Very closely followed by EVA (1) and Air (3) at 99.9%, indicating minimal resistive losses. Glycerol (13) and PDMS (7) showed some decrease but still performed strongly with 98.7% and 97.6%, respectively. EVA (2), however, dropped to 95.9%, which may point to some serious degradation occurring. The lowest FF was again observed in air (4) at 91.2%, hinting at some serious connection problems.

5.3.5. Overall Performance

This analysis shows that MPG is one of the top two encapsulants for all considered degradation parameters, thereby clearly outperforming all other encapsulants. With EVA (1) being the overall 2nd best sample behind the MPG. Furthermore, PDMS (7) and glycerol (13) also offer competitive stability. In contrast, air-encapsulated samples consistently underperform in the considered parameters.

5.4. Electroluminescence and Visual Inspection

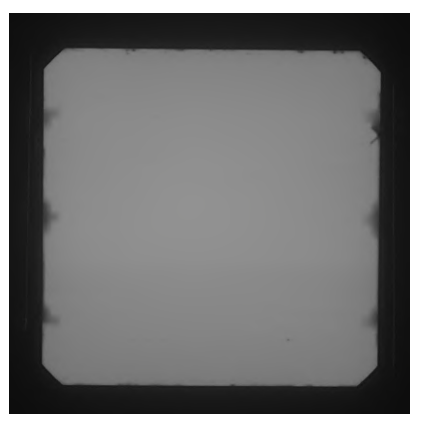
As a final method to try and explain why a module's performance is decreasing, electroluminescence and visual inspection will be used. After every 6 cycles of humidity freeze testing an electroluminescence image was taken. Allowing for small cracks and defects in the cell to become visible. Furthermore, every 6 cycles a visual inspection was performed to check for leakages and other defects.

5.4.1. Electroluminescence (EL)

In some of the samples, it became clear through the EL images that some small cracks were present. One example of this is seen in Figure 5.13a, where the EL image of sample 2 (EVA) is shown, before enduring any humidity freeze cycles. Furthermore, the EL image of the same sample after 30 humidity freeze cycles is shown in Figure 5.13b.







(b) Electroluminescence image of sample 2 (EVA) after 30 cycles of humidity freeze test

Figure 5.13: Electroluminescence images of sample 2 (EVA) before any accelerated ageing and after 30 humidity freeze cycles

In Figure 5.13a, a small crack is visible in the top right, originating from the solder contact point. This phenomenon occurred in several of the samples, likely due to a too thick layer of solder being applied. By comparing Figure 5.13a to Figure 5.13b, it becomes clear that the already existing crack did not propagate and that no new cracks, hotspots or other cell defects occurred. For both of the EVA laminated modules and for all three modules containing PDMS, MPG or glycerol, the initial EL image looked virtually identical as the EL image taken after the full 30 cycles of humidity freeze. All of their EL images, taken every 6 cycles, can be found in Appendix B.2.

In the other two out of the seven samples, a change in existing cracks between 0 and 30 cycles could be seen, however. This was only the case for both of the air-filled modules (samples 3 and 4). In Figure 5.14 the EL images of air-filled sample 3 are shown at 0, 6 and 30 humidity freeze cycles.

In Figure 5.14a, only very minor cracks seem to be present such as on the bottom left solder contact point. However, within the first 6 humidity freeze cycles, several new cracks occurred in the bottom middle of the cell as can be seen in Figure 5.14b. These cracks only slightly propagated when comparing the EL image at 6 cycles to Figure 5.14c. Furthermore, the light dark, horizontal stripe, that has appeared near the bottom, indicates that the cell finger is no longer fully connected and therefore can no longer collect current. This explains air-filled sample 3 having a worse efficiency and current degradation than all other tested encapsulants after 6 cycles, as shown in Figures 5.9 and 5.10.

Due to more changes occurring in the EL images of air-filled sample 4, the EL images of every 6 cycles are shown in Figure 5.15. Again, in the initial EL image, no prolific cracks or defects are present. But

before starting humidity freeze tests

after 30 cycles of the humidity freeze test

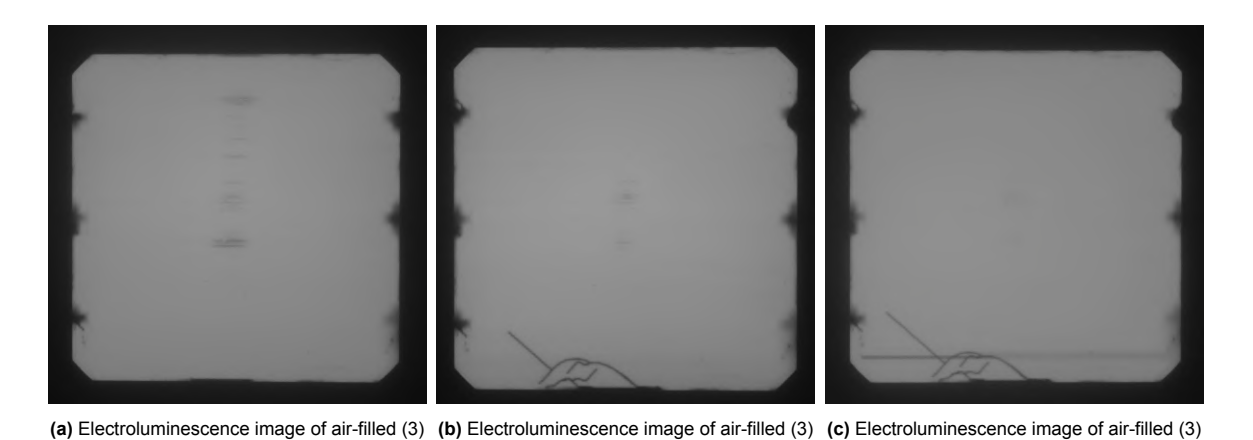


Figure 5.14: EL images of air-filled sample 3 at different moments during the process

after 6 cycles of the humidity freeze test

just like air-filled sample 3, within the first 6 cycles severe cracks occurred in the bottom of the solar cell. Just like for air-filled sample 3, this explains the worst degradation after 6 humidity freeze cycles of all encapsulants. Furthermore, a smaller crack also occurred at the top right solder point contact. This time however, the cracks were so severe that within a total of 12 cycles multiple fingers of the cell can no longer collect current and therefore showed up as darker lines in Figure 5.15c. After 24 cycles these darker lines stopped emitting light altogether, as can be seen in Figure 5.15e. Furthermore, another defect can be seen in the top right of the solar cell. These degradations coincide with the significant drop in efficiency, Voc and FF at 24 cycles, as discussed in Chapter 5.2. It is interesting to note that the Jsc stays stable from 18 to 24 cycles whilst all other key parameters decrease.

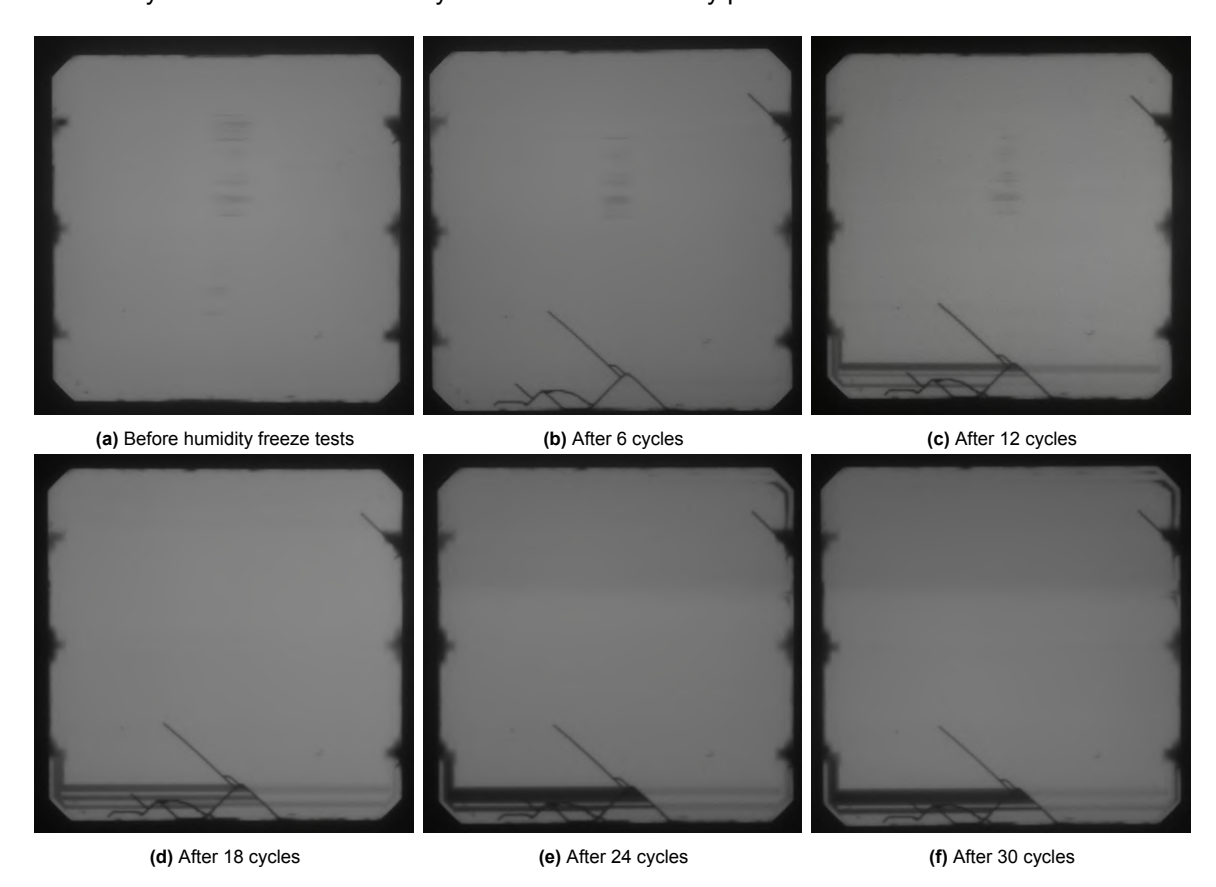


Figure 5.15: EL images of air-filled (4) after every six cycles of humidity freeze testing

5.4.2. Visual Inspection

Just like the EL images, a visual inspection can help identify what degradation mechanisms are occurring and why they are happening. Every 6 cycles of humidity freeze test, all seven samples were visually inspected to check for discolouration, material interactions, and intactness of the PIB edge seal and solar cell. Initially, none of the samples showed any defects or signs of leakages. Otherwise, they would have been re-manufactured before entering the climate chamber.

In both of the EVA laminated modules, the first signs of moisture ingress started appearing within the initial 6 cycles. With both modules showing creep happening at the edges. Furthermore, small air bubbles started forming close to the bus bars of both EVA laminated modules. Both of these degradations occurred within the first 6 cycles, however they did not seem to significantly continue over the following humidity freeze cycles. Next to these two forms of degradation, EVA (sample 2) showed severe discolouration regarding the solder used to connect the cell to the busbars. This started within the first 6 cycles but kept worsening all the way till 30 cycles. EVA (sample 2) showed only a slight discolouration which became noticeable after 18 cycles. The busbars after 30 cycles are shown in Figure 5.16, with the slight discolouration of EVA (1) being shown in Figure 5.16a and the discolouration of EVA (2) being shown in Figure 5.16b and 5.16c. The degradation on the busbars directly impacts the resistance, and thereby the efficiency and FF of the module, which correlates with the decreases in efficiency and FF from Figures 5.9 and 5.12. This form of degradation is known to occur in EVA encapsulated modules, it does however seem that the severity at which it occurs in this experiment is extreme, especially for EVA sample 2 [16, 18].

Finally, by trying to look through the EVA, it became clear that the EVA layer in both modules seemed to have become a bit more hazy after 30 cycles, whilst it was completely see through directly after lamination. This lowers the transmission through the encapsulant and thereby the generated Jsc and efficiency.



(a) The busbar of EVA (1) with the most degradation, showing only very slight discolouration



(b) Left busbar of EVA (2) with severe discolouration and small air



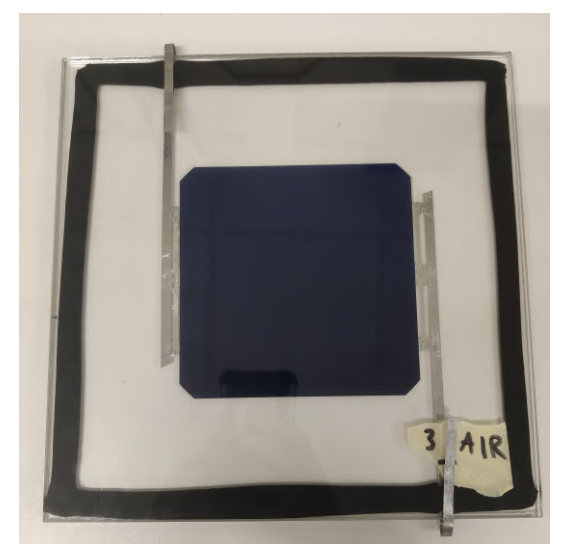
(c) Right busbar of EVA (2) with severe discolouration and adjacent air hubbles

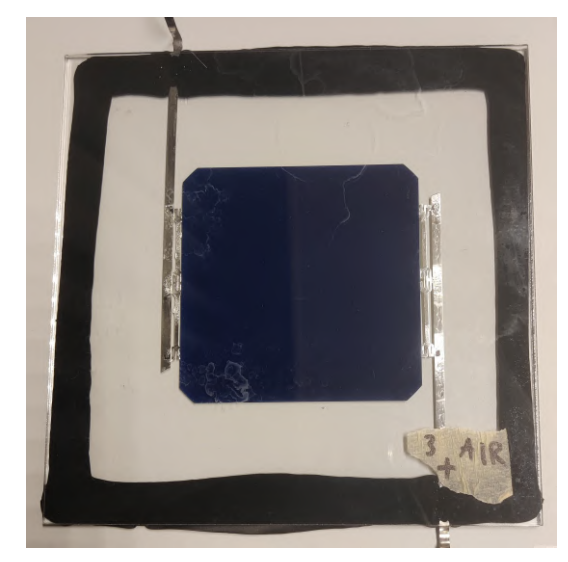
Figure 5.16: Discoloured busbars in the EVA modules after 30 humidity freeze cycles

The air-filled modules (sample 3 & 4) had their own series of problems, which also started within the first 6 cycles. In Figure 5.17, air-filled sample 3 is shown before entering the climate chamber (5.17a) and after 6 cycles of humidity freeze test (5.17b). By seeing these images next to each other, it becomes clear that the PIB has significantly widened within the first 6 cycles. This same phenomena was observed in air-filled sample 4, possibly explaining the cell cracks which were revealed through EL.

Air-filled sample 3 showed no extra visual changes. Sample 4 on the other hand, broke down severely between 18 and 24 humidity freeze cycles. To be more precise, the PIB edge seal completely failed by both delaminating and tearing open around the busbar connections. After 18 cycles no indications

5.5. conclusion 45





(a) Initial visual inspection before starting humidity freeze tests

(b) Visual inspection after 6 cycles of humidity freeze

Figure 5.17: Visual inspection of air-filled module 3 at 0 and 6 cycles

of edge seal degradation were present other than the widening, and thereby thinning of the PIB. The top side of air-filled sample 4 after 24 cycles is shown in Figure 5.18. The black parts are the places where the PIB is still making contact with the glass and the lighter grey parts are the places where it is delaminating. Furthermore, on the left side of the figure, it can be seen that the PIB is torn apart. These phenomena are occurring all around the edges of this air-filled sample, however this side is highlighted due to it having the most severe defects.



Figure 5.18: Visual inspection of air-filled module 4 at 24 cycles

Regarding the visual inspection of the PDMS and MPG filled modules, no variations were noticed between the initial modules and after 30 cycles. Finally, for the glycerol-filled module, the only noticeable change was that liquid was seemingly leaking out through the PIB edge seal. However, this was kept to such a low quantity that after 18 cycles the module lost 1 gram of weight and after 30 cycles it lost 3 grams, likely due to the relatively high viscosity of the liquid.

5.5. conclusion

From this chapter, it can be concluded that PDMS, MPG, and glycerol are competitive with EVA when it comes to initial module efficiency, as well as Jsc and Voc. Both air-filled and water-filled modules underperform in optical and electrical performance. They are therefore less suited when aiming for high module efficiency at the start of a PV module's life. After being subjected to the initial six humidity freeze cycles, the PIB edge seal failed for 8 out of the 15 initial modules. The failures occurring near the liquid injection points, highlights the vulnerability left from resealing the edge seal after liquid injection.

The remaining seven modules stayed intact for the full 30 cycles of the humidity freeze test and they provided valuable insights into their long-term stability. From all encapsulants, MPG stood out as the most stable, achieving top results in all four key parameters and outperforming the EVA samples. EVA (sample 1) also maintained strong performance, demonstrating that when properly processed, EVA

5.5. conclusion 46

remains a reliable standard. Glycerol and PDMS encapsulants showed consistent and acceptable degradation trends, remaining competitive with EVA but not quite reaching the performance of MPG.

Across all modules, the early humidity freeze cycles had the greatest impact on degradation, particularly in Jsc and efficiency, while later cycles contributed more subtle changes. The exception being, that in modules where structural failures occurred, such as air (sample 4), significant jumps in degradation were induced. In conclusion, these results suggest that MPG shows the strongest potential as an alternative encapsulant.

6

Conclusion

In this thesis, the performance and reliability of liquid-filled photovoltaic (PV) modules were investigated. This was done by selecting suitable liquids, manufacturing the modules, subjecting them to humidity freeze accelerated ageing conditions, measuring their electrical performance, and comparing them to air-filled and ethylene vinyl acetate (EVA)-laminated modules. In this chapter, the final conclusions will be drawn. Following this, recommendations for future work and improvements regarding liquid-filled PV modules will be given.

6.1. Conclusion

The liquids tested as encapsulant in liquid-filled modules were selected by inspecting their optical, thermal, chemical, electrical and physical properties. From this, polydimethylsiloxane (PDMS), mono propylene glycol (MPG) and glycerol emerged as suitable liquids, mainly due to their favourable optical and electrical properties, and their compatibility with the polyisobutene (PIB) edge seal.

During the manufacturing and testing of the liquid-filled PV modules, one main failure point became apparent, the PIB edge seal. Several modules revealed leakages within the first six cycles of humidity freeze testing, with almost all of the failures occurring at the liquid injection points, sometimes accompanied by minor leakages occurring at the busbars. This implies that due to the resealing of the PIB, which is required after liquid-injection, the PIB is more prone to failure. Through visual inspections and electroluminescence (EL) images, it became clear that the air-filled modules are prone to cell breakage, likely induced by the flattening of the PIB edge seal.

The module failures were a good opportunity to take apart the modules and reuse their materials. This proved that the liquid encapsulant can be collected after cutting open the edge seal, that the solar cell can be separated from the other materials and finally, that the glass sheets can be fully reused after being thoroughly cleaned. This proves the ease of disassembly and the reusability potential of liquid-filled PV modules due to the lack of solid encapsulant layers such as EVA.

From evaluating the initial performance of the self-manufactured liquid-filled PV modules before and after liquid injection, it became clear that adding a liquid encapsulant shows a significant improvement in efficiency, short-circuit current and open-circuit voltage over air-filled modules. This holds for all three tested liquids, PDMS, MPG and glycerol. When comparing the increase in module efficiency of the liquid-filled modules to the increase in module efficiency of an EVA laminated module, the PDMS (6.2%) outperforms the EVA (5.6%), whilst both MPG and glycerol show a slightly smaller increase in module efficiency of 5.1%. This shows that, as expected when looking at the refractive index (n), the initial efficiency performance of all three liquid encapsulants is relatively close to that of EVA, which is the current encapsulation standard.

In total, 7 modules stayed intact after 6 cycles, and were able to be subjected to 30 cycles of humidity freeze. The module division is as follows: 2 EVA, 2 air, 1 PDMS, 1 MPG and 1 glycerol. However, one of the two EVA encapsulated modules showed severe degradation, whilst the degradation of the other EVA

6.2. Recommendations 48

module seems to be more aligned with literature. Therefore, the degradation of the best-performing EVA module is used as a benchmark for the liquid-filled modules. Just like EVA, the degradation results between the two air-filled modules differed significantly. Due to severe breakage in one of the two modules, the best-performing air-filled module is taken as the representative module, even though it also experienced cell breakage. The relative degradation in module efficiency after 30 humidity freeze cycles for both the PDMS (5.2%) and the glycerol (5.2%) is comparable to that of the best-performing air-filled module (5.5%) but slightly worse than that of the best-performing EVA laminated module (3.9%). Furthermore, the module filled with MPG outperformed all other tested encapsulants by degrading only 2.8% compared to its initial module efficiency.

None of the degradation mechanisms found in air- and liquid-filled modules are comparable to those occurring in the EVA laminated modules. With the three degradation mechanisms present in the EVA laminated modules being: delamination through the forming of air bubbles, corrosion due to moisture ingress, and a slight reduction in transparency of the encapsulant. These degradation mechanisms indicate a good resilience to mechanical failure but a higher sensitivity to moisture-related and optical degradation, which are less prevalent in the liquid-filled modules.

The findings of this thesis show that PV modules filled with MPG, PDMS or glycerol are promising candidates to compete with the efficiency and long-term stability of EVA modules, both in initial performance and in electrical degradation after 30 humidity freeze cycles. It also showed the ease of disassembly of liquid-filled modules. The tested liquids did not show any visual degradation, in contrast to the EVA and air-filled modules. However, MPG and glycerol did show comparable electrical degradation to EVA. MPG emerges as the strongest candidate for further development due to its superior stability under humidity freeze induced stress conditions in combination with its initial efficiency being comparable to that of EVA laminated modules. However, the early-stage failures of liquid-filled PV modules have to be eliminated and prevented for the technology to become scalable.

6.2. Recommendations

Future research is suggested to focus on developing alternative liquid injection methods that preserve the integrity of the PIB edge seal, such that the PIB will not be compromised after the lamination process. Additional work should explore the scaling of the module size, since for this thesis, only one-cell modules were tested. Furthermore, compatibility with various solar cell technologies and the scalability of manufacturing processes can be researched. Finally, a broader range of testing methods can be used to induce degradation. For example, mechanical strength or ultraviolet (UV) light tests can be conducted to simulate long-term UV exposure as typically experienced outdoors.

Realising improved reliability for the edge seal and continued testing under different conditions will be critical in optimising the next generation of circular, liquid-filled PV modules for large-scale application.

- [1] United Nations. Paris Agreement. URL: https://treaties.un.org/pages/ViewDetails.aspx?src=TREATY&mtdsg_no=XXVII-7-d&chapter=27&clang=_en (visited on 06/24/2025).
- [2] Global Solar Council. *global-solar-council-announces-2-TW-milestone-achieved-for-solar*. Nov. 2024. URL: http://www.globalsolarcouncil.org/news/global-solar-council-announce s-2-terawatt-milestone-achieved-for-solar/ (visited on 12/10/2024).
- [3] IRENA. Renewable capacity statistics 2015. URL: https://www.irena.org/Publications/2015/Jun/Renewable-Energy-Capacity-Statistics-2015.
- [4] IRENA. Renewable capacity statistics 2025. URL: https://www.irena.org/Publications/2025/Mar/Renewable-capacity-statistics-2025.
- [5] Lazard. en. URL: https://www.lazard.com/research-insights/levelized-cost-of-energyplus/.
- [6] IRENA. World Energy Transitions Outlook 2024: 1.5°C Pathway. 2024. URL: https://www.irena.org/Publications/2024/Nov/World-Energy-Transitions-Outlook-2024.
- [7] IRENA. World Energy Transitions Outlook 2022: 1.5°C Pathway. Mar. 2022. URL: https://www.irena.org/Publications/2022/Mar/World-Energy-Transitions-Outlook-2022.
- [8] ITRPV. International Technology Roadmap for Photovoltaic (ITRPV) vdma.org VDMA. 2024. URL: https://www.vdma.org/international-technology-roadmap-photovoltaic.
- [9] Clean Energy Reviews. 2022. URL: https://www.cleanenergyreviews.info/blog/solar-panel-components-construction (visited on 12/10/2024).
- [10] M. Kempe. "Encapsulant Materials for PV Modules". en. In: Photovoltaic Solar Energy. Ed. by Angèle Reinders et al. 1st ed. Wiley, Dec. 2016, pp. 478–490. ISBN: 9781118927465. DOI: 10.1002/9781118927496.ch43. URL: https://onlinelibrary.wiley.com/doi/10.1002/9781118927496.ch43.
- [11] Gernot Oreski et al. "Properties and degradation behaviour of polyolefin encapsulants for photovoltaic modules". In: *Progress in Photovoltaics: Research and Applications* 28.12 (Dec. 2020), pp. 1277–1288. URL: https://onlinelibrary.wiley.com/doi/full/10.1002/pip.3323.
- [12] A. Wallace. Copeland, Otis D. Black, and A. B. Garrett. "The Photovoltaic Effect." en. In: *Chemical Reviews* 31.1 (Aug. 1942), pp. 177–226. ISSN: 0009-2665, 1520-6890. DOI: 10.1021/cr60098a004. URL: https://pubs.acs.org/doi/abs/10.1021/cr60098a004.
- [13] P. Hülsmann and G.M. Wallner. "Permeation of water vapour through polyethylene terephthalate (PET) films for back-sheets of photovoltaic modules". en. In: *Polymer Testing* 58 (Apr. 2017), pp. 153–158. ISSN: 01429418. DOI: 10.1016/j.polymertesting.2016.11.028. URL: https://linkinghub.elsevier.com/retrieve/pii/S0142941816305396.
- [14] Michael Schütze, Dietrich Wieser, and Roman Bender. *Corrosion resistance of aluminium and aluminium alloys*. John Wiley & Sons, 2010.
- [15] A. Virtuani et al. "35 years of photovoltaics: Analysis of the TISO-10-kW solar plant, lessons learnt in safety and performance—Part 1". en. In: *Progress in Photovoltaics: Research and Applications* 27.4 (Apr. 2019), pp. 328–339. ISSN: 1062-7995, 1099-159X. DOI: 10.1002/pip. 3104. URL: https://onlinelibrary.wiley.com/doi/10.1002/pip.3104.
- [16] M. Aghaei et al. "Review of degradation and failure phenomena in photovoltaic modules". en. In: Renewable and Sustainable Energy Reviews 159 (May 2022), p. 112160. ISSN: 13640321. DOI: 10.1016/j.rser.2022.112160. URL: https://linkinghub.elsevier.com/retrieve/pii/S1364032122000880.

[17] M. Waqar Akram et al. "Failures of Photovoltaic modules and their Detection: A Review". In: Applied Energy 313 (May 2022), p. 118822. ISSN: 0306-2619. DOI: 10.1016/j.apenergy.2022. 118822. URL: https://www.sciencedirect.com/science/article/pii/S0306261922002677.

- [18] Dirk C. Jordan et al. "Photovoltaic failure and degradation modes". en. In: *Progress in Photovoltaics: Research and Applications* 25.4 (Apr. 2017), pp. 318–326. ISSN: 1062-7995, 1099-159X. DOI: 10.1002/pip.2866. URL: https://onlinelibrary.wiley.com/doi/10.1002/pip.2866.
- [19] M. Köntges et al. Performance and reliability of photovoltaic systems: subtask 3.2: Review of failures of photovoltaic modules: IEA PVPS task 13: external final report IEA-PVPS. en. IEA, 2014, 1 Online—Ressource (140 Seiten, 9, 33 MB). DOI: 10.2314/GBV:856979287. URL: https: //www.tib.eu/suchen/id/TIBKAT:856979287/.
- [20] M. Waqar Akram et al. "Failures of Photovoltaic modules and their Detection: A Review". In: Applied Energy 313 (May 2022), p. 118822. ISSN: 0306-2619. DOI: 10.1016/j.apenergy.2022. 118822. URL: https://www.sciencedirect.com/science/article/pii/S0306261922002677.
- [21] A. Mellit, G. M. Tina, and S. A. Kalogirou. "Fault detection and diagnosis methods for photovoltaic systems: A review". In: *Renewable and Sustainable Energy Reviews* 91 (Aug. 2018), pp. 1–17. ISSN: 1364-0321. DOI: 10.1016/j.rser.2018.03.062. URL: https://www.sciencedirect.com/science/article/pii/S1364032118301370.
- [22] Juan Lopez-Garcia, Alberto Pozza, and Tony Sample. "Long-term soiling of silicon PV modules in a moderate subtropical climate". In: Solar Energy 130 (2016), pp. 174–183. ISSN: 0038-092X. DOI: https://doi.org/10.1016/j.solener.2016.02.025. URL: https://www. sciencedirect.com/science/article/pii/S0038092X16001213.
- [23] David C. Miller et al. "Degradation in photovoltaic encapsulant transmittance: Results of the first PVQAT TG5 artificial weathering study". en. In: *Progress in Photovoltaics: Research and Applications* 27.5 (May 2019), pp. 391–409. ISSN: 1062-7995, 1099-159X. DOI: 10.1002/pip. 3103. URL: https://onlinelibrary.wiley.com/doi/10.1002/pip.3103.
- [24] U. Weber et al. "Acetic Acid Production, Migration and Corrosion Effects in Ethylene-Vinyl-Acetate (EVA) Based PV Modules". en. In: 27th European Photovoltaic Solar Energy Conference and Exhibition; 2992-2995 (2012), 4 pages, 2730 kb. DOI: 10.4229/27THEUPVSEC2012-4C0.9.4. URL: https://userarea.eupvsec.org/proceedings/27th-EU-PVSEC/4C0.9.4/.
- [25] G. Oreski et al. "Acetic acid permeation through photovoltaic backsheets: Influence of the composition on the permeation rate". en. In: *Polymer Testing* 60 (July 2017), pp. 374–380. ISSN: 01429418. DOI: 10.1016/j.polymertesting.2017.04.025. URL: https://linkinghub.elsevier.com/retrieve/pii/S014294181730209X.
- [26] M. Köntges, S. Kajari-Schröder, and I. Kunze. "Crack Statistic for Wafer-Based Silicon Solar Cell Modules in the Field Measured by UV Fluorescence". In: *IEEE Journal of Photovoltaics* 3.1 (2013), pp. 95–101. DOI: 10.1109/JPH0T0V.2012.2208941.
- [27] David M. Wilt et al. "Metal Matrix Composite Solar Cell Metallization". en. In: E3S Web of Conferences 16 (2017), p. 03001. ISSN: 2267-1242. DOI: 10.1051/e3sconf/20171603001. URL: https://www.e3s-conferences.org/articles/e3sconf/abs/2017/04/e3sconf_espc2017_03001/e3sconf_espc2017_03001.html.
- [28] Tadashi Saitoh et al. "Overview of light degradation research on crystalline silicon solar cells". en. In: Progress in Photovoltaics: Research and Applications 8.5 (Sept. 2000), pp. 537–547. ISSN: 1062-7995, 1099-159X. DOI: 10.1002/1099-159X(200009/10)8:5<537::AID-PIP349>3.0. C0;2-W. URL: https://onlinelibrary.wiley.com/doi/10.1002/1099-159X(200009/10)8:5%3C537::AID-PIP349%3E3.0.C0;2-W.
- [29] S. Pingel et al. "Potential Induced Degradation of solar cells and panels". In: 2010 35th IEEE Photovoltaic Specialists Conference. June 2010, pp. 002817-002822. DOI: 10.1109/PVSC. 2010.5616823. URL: https://ieeexplore.ieee.org/document/5616823.
- [30] Neelkanth Dhere et al. "High-voltage bias testing of PV modules in the hot and humid climate without inducing irreversible instantaneous degradation". In: 2012 38th IEEE Photovoltaic Specialists Conference. June 2012, pp. 002445–002448. DOI: 10.1109/PVSC.2012.6318090. URL: https://ieeexplore.ieee.org/document/6318090/?arnumber=6318090.

[31] P. Hacke et al. "System voltage potential-induced degradation mechanisms in PV modules and methods for test". In: 2011 37th IEEE Photovoltaic Specialists Conference. 2011, pp. 000814–000820. DOI: 10.1109/PVSC.2011.6186079. URL: https://ieeexplore.ieee.org/document/6186079.

- [32] M.A. Quintana et al. "Commonly observed degradation in field-aged photovoltaic modules". In: Conference Record of the Twenty-Ninth IEEE Photovoltaic Specialists Conference, 2002. 2002, pp. 1436–1439. DOI: 10.1109/PVSC.2002.1190879.
- [33] Maoyi Chang et al. "The reliability investigation of PV junction box based on 1GW worldwide field database". In: 2015 IEEE 42nd Photovoltaic Specialist Conference (PVSC). June 2015, pp. 1–4. DOI: 10.1109/PVSC.2015.7356130. URL: https://ieeexplore.ieee.org/document/7356130.
- [34] M. Köntges et al. Assessment of photovoltaic module failures in the field: International Energy Agency Photovoltaic Power Systems Programme: IEA PVPS Task 13, Subtask 3: report IEA-PVPS T13-09:2017. eng. Paris: International Energy Agency, 2017. ISBN: 9783906042541.
- [35] Patrick J. M. Isherwood. "Reshaping the Module: The Path to Comprehensive Photovoltaic Panel Recycling". en. In: *Sustainability* 14.3 (Jan. 2022), p. 1676. DOI: 10.3390/su14031676. URL: https://www.mdpi.com/2071-1050/14/3/1676.
- [36] Xinhai Xu et al. "Nondestructive silicon wafer recovery by a novel method of solvothermal swelling coupled with thermal decomposition". In: *Chemical Engineering Journal* 418 (2021), p. 129457. DOI: 10.1016/j.cej.2021.129457. URL: https://www.sciencedirect.com/science/article/pii/S1385894721010445.
- [37] Maurianne Flore Azeumo et al. "Photovoltaic module recycling, a physical and a chemical recovery process". In: Solar Energy Materials and Solar Cells 193 (May 2019), pp. 314–319. DOI: 10.1016/j.solmat.2019.01.035. URL: https://www.sciencedirect.com/science/article/pii/S0927024819300510.
- [38] Flavia Carla dos Santos Martins Padoan et al. "Material Flux through an Innovative Recycling Process Treating Different Types of End-of-Life Photovoltaic Panels: Demonstration at Pilot Scale". en. In: *Energies* 14.17 (Jan. 2021), p. 5534. DOI: 10.3390/en14175534. URL: https://www.mdpi.com/1996-1073/14/17/5534.
- [39] Meng Tao et al. "Major challenges and opportunities in silicon solar module recycling". en. In: *Progress in Photovoltaics: Research and Applications* 28.10 (2020), pp. 1077–1088. DOI: 10.1002/pip.3316. URL: https://onlinelibrary.wiley.com/doi/abs/10.1002/pip.3316.
- [40] Nadka Tz Dintcheva, Elisabetta Morici, and Claudio Colletti. "Encapsulant Materials and Their Adoption in Photovoltaic Modules: A Brief Review". en. In: *Sustainability* 15.12 (2023), p. 9453. DOI: 10.3390/su15129453. URL: https://www.mdpi.com/2071-1050/15/12/9453.
- [41] R. Einhaus. "ECOSOLAR Factory: 40% plus Eco Efficiency gains in the Photovoltaic value chain with minimized resource and energy consumption by closed loop systems". In: *of the 32nd EU-PVSEC*. 2016.
- [42] R. Einhaus et al. "Recycling and Reuse potential of NICE PV-Modules". In: 2018 IEEE 7th World Conference on Photovoltaic Energy Conversion (WCPEC) (A Joint Conference of 45th IEEE PVSC, 28th PVSEC & 34th EU PVSEC). 2018, pp. 561–564. DOI: 10.1109/PVSC.2018.85483 07.
- [43] R. Einhaus et al. "New industrial solar cell encapsulation (NICE) technology for PV module fabrication at drastically reduced costs". en. In: ResearchGate. Jan. 2004. URL: https://www.researchgate.net/publication/236150007_New_industrial_solar_cell_encapsulation_NICE_technology_for_PV_module_fabrication_at_drastically_reduced_costs.
- [44] J. Dupuis et al. "NICE module technology From the concept to mass production: A 10 years review". In: 2012 38th IEEE Photovoltaic Specialists Conference. 2012, pp. 003183–003186. DOI: 10.1109/PVSC.2012.6318254.
- [45] Helioseal PVS 101. Adco Solar. URL: https://www.yumpu.com/en/document/view/9749801/heliosealtm-pvs-101-adco.

[46] Michael D Kempe et al. "Evaluation and modeling of edge-seal materials for photovoltaic applications". In: 2010 35th IEEE Photovoltaic Specialists Conference. IEEE. 2010, pp. 000256–000261.

- [47] Michael D Kempe, Arrelaine A Dameron, and Matthew O Reese. "Evaluation of moisture ingress from the perimeter of photovoltaic modules". In: *Progress in Photovoltaics: Research and Applications* 22.11 (2014), pp. 1159–1171.
- [48] Michael D Kempe et al. "Modeling moisture ingress through polyisobutylene-based edge-seals". In: *Progress in Photovoltaics: Research and Applications* 23.5 (2015), pp. 570–581.
- [49] Melikenur Genç and Abdülkerim Gök. "Evaluating the Impact of Edge-Seal on the Performance of Double-Glass Solar Photovoltaic Modules". In: *Gazi University Journal of Science Part A: Engineering and Innovation* 11.4 (2024), pp. 676–689.
- [50] R. Couderc et al. "Encapsulant for glass-glass PV modules for minimum optical losses: gas or EVA?" In: *Energy Procedia* 124 (Sept. 2017), pp. 470–477. DOI: 10.1016/j.egypro.2017.09. 283.
- [51] Max Mittag et al. TPedge: glass-glass photovoltaic module for BiPV-applications. May 2016.
- [52] Max Mittag et al. *TPedge: qualification of a gas-filled, encapsulation-free glass-glass photo-voltaic module.* Aug. 2015. DOI: 10.4229/EUPVSEC20152015-1C0.11.4.
- [53] Max Mittag, Ulrich Eitner, and Tobias Neff. *TPedge: Progress on Cost-efficient and Durable Edge-sealed PV Modules*. Sept. 2017. DOI: 10.4229/EUPVSEC20172017-1C0.1.4.
- [54] B Decker and U Jahn. "Performance of 170 grid connected PV plants in northern Germany—analysis of yields and optimization potentials". In: Solar Energy 59.4-6 (1997), pp. 127–133.
- [55] IEC61215-2. Terrestrial photovoltaic (PV) modules Design qualification and type approval Part 2: Test procedures. International Standard. IEC, 2021.
- [56] J. Dupuis et al. "IEC certification and extended ageing test of NICE modules". In: 25th EU PVSEC (2010), pp. 4148–4151.
- [57] F. Madon et al. "Results from extended degradation and outdoor tests of NICE modules". In: 30th Eur. Photovolt. Sol. Energy Conf. Exhib. 2015, pp. 2534–2537.
- [58] TS IEC. IEC61836 solar photovoltaic energy systems-terms, definitions and symbols'. 2016.
- [59] D. Reinwand et al. "Lab-scale manufacturing of medium-sized N.I.C.E.TM modules with high-efficiency bifacial silicon heterojunction solar cells". In: *AIP Conference Proceedings* 2156.1 (Sept. 2019), p. 020009. DOI: 10.1063/1.5125874. URL: https://doi.org/10.1063/1.5125874.
- [60] D. Reinwand et al. "All Copper NICE Modules". In: 2018 IEEE 7th World Conference on Photovoltaic Energy Conversion (WCPEC) (A Joint Conference of 45th IEEE PVSC, 28th PVSEC & 34th EU PVSEC). 2018, pp. 0628–0631. DOI: 10.1109/PVSC.2018.8547749.
- [61] D. Kray et al. "N.I.C.E.-Wire: Next Generation Robust Eco-Friendly Bifacial PV Modules With High Efficiency". In: *IEEE Journal of Photovoltaics* 12.1 (2022), pp. 38–44. DOI: 10.1109/JPHOTOV.2021.3124168.
- [62] M. Aghaei et al. "Review of degradation and failure phenomena in photovoltaic modules". en. In: Renewable and Sustainable Energy Reviews 159 (May 2022), p. 112160. ISSN: 13640321. DOI: 10.1016/j.rser.2022.112160. URL: https://linkinghub.elsevier.com/retrieve/pii/S1364032122000880.
- [63] Antoine Perelman et al. "Innovative Design-for-Recycling for Critical Material-Free Interconnection of PV Modules". In: *Progress in Photovoltaics: Research and Applications* (2025).
- [64] Sam Ellis et al. "Demonstration of non-lamination encapsulation techniques for thin film solar modules". In: 2020 47th IEEE Photovoltaic Specialists Conference (PVSC). IEEE. 2020, pp. 1924–1926.
- [65] David L. Young et al. "Towards Polymer-Free, Femto-Second Laser-Welded Glass/Glass Solar Modules". In: IEEE Journal of Photovoltaics 14.3 (2024), pp. 497–502. DOI: 10.1109/JPH0T0V. 2024.3364823.

[66] Zhanbin Shi et al. "Design of High Recycling Efficiency Solar Panels Based on Edge Sealing". In: 2024 6th Asia Energy and Electrical Engineering Symposium (AEEES). IEEE. 2024, pp. 841–848.

- [67] M Rubin. "Optical properties of soda lime silica glasses". In: Solar energy materials 12.4 (1985), pp. 275–288.
- [68] Christiana Honsberg and Stuart Bowden. *Absorption Coefficient* | *PVEducation*. URL: https://www.pveducation.org/pvcdrom/pn-junctions/absorption-coefficient.
- [69] Philipp Löper et al. "Complex refractive index spectra of CH3NH3Pbl3 perovskite thin films determined by spectroscopic ellipsometry and spectrophotometry". In: *The journal of physical chemistry letters* 6.1 (2015), pp. 66–71.
- [70] EVA photocap 15580P. Specialized Technology Resources (STR). 2015. URL: https://cdn.enfsolar.com/Product/pdf/EVA/5950c92d74b0e.pdf.
- [71] Potuganti Prudhvi and Ponnapalli Chaitanya Sai. "Efficiency improvement of solar PV panels using active cooling". In: 2012 11th International Conference on Environment and Electrical Engineering. IEEE. 2012, pp. 1093–1097.
- [72] Kemal Bilen and İsmail Erdoğan. "Effects of cooling on performance of photovoltaic/thermal (PV/T) solar panels: A comprehensive review". In: *Solar Energy* 262 (2023), p. 111829.
- [73] HG Teo, PS Lee, and MNA Hawlader. "An active cooling system for photovoltaic modules". In: applied energy 90.1 (2012), pp. 309–315.
- [74] Takashi Inagaki, ET Arakawa, and MW Williams. "Optical properties of liquid mercury". In: *Physical review B* 23.10 (1981).
- [75] Xinyue Han et al. "Reliability assessment of silicone coated silicon concentrator solar cells by accelerated aging tests for immersing in de-ionized water". In: *Solar Energy* 85.11 (2011), pp. 2781–2788.
- [76] Glycerol. Version 6.10. Sigma-Aldrich. 2025. URL: https://www.sigmaaldrich.com/NL/en/sds/sigma/g5516?userType=anonymous.
- [77] Glycol (1-2 propanediol). Version 6.8. Sigma-Aldrich. 2023. URL: https://www.sigmaaldrich.com/NL/en/sds/sial/398039?userType=anonymous.
- [78] Xiameter PMX-200 Silicone fluid 50 cst. DOW. URL: https://www.dow.com/en-us/pdp.xiameter-pmx-200-silicone-fluid-50-cst.01013181z.html#overview.
- [79] Mivolt DFK. Mivolt. URL: https://www.mivolt.com/products/mivolt-dfk/.
- [80] MIDEL 7131. MIDEL. URL: https://static.mimaterials.com/midel/documents/technical/MIDEL_7131_UK.pdf.
- [81] Shell Diala s4ZX-I. SHELL. URL: https://www.shell.com/business-customers/lubricants-for-business/sector-expertise/power-industry/wind-power/windeurope-electric-city/_jcr_content/root/main/section/simple_2118681472/text.multi.stream/1726581 236629/30ce6e8d9d69ebdcb19c946c00e1644ec7507965/shell-diala-s4-zx-i-tds.pdf.
- [82] James E Mark, Harry R Allcock, and Robert West. *Inorganic polymers*. Oxford University Press, 2005.
- [83] Georgi Gochev, Vamseekhrishna Ulaganathan, and Reinhard Miller. "Foams". In: *Ullmann's Encyclopedia of Industrial Chemistry* (2000), pp. 1–31.
- [84] Joint FAO/WHO Expert Committee on Food Additives. Meeting and World Health Organization. Evaluation of certain food additives and contaminants: sixty-eighth report of the Joint FAO/WHO Expert Committee on Food Additives. Vol. 68. World Health Organization, 2007.
- [85] E. Griessbach and R. Lehmann. "Degradation of polydimethylsiloxane fluids in the environment a review". In: Chemosphere 38.6 (1999), pp. 1461–1468.
- [86] Albert L Lehninger. Lehninger Principles of Biochemistry: David L. Nelson, Michael M. Cox. Recording for the Blind & Dyslexic New York, 2004.
- [87] Ralf Christoph et al. "Glycerol". In: Ullmann's encyclopedia of industrial chemistry (2000).

[88] Amitava Dasgupta and Kimberly Klein. *Antioxidants in food, vitamins and supplements: prevention and treatment of disease.* Academic Press, 2014.

- [89] Henri A Favre and Warren H Powell. *Nomenclature of organic chemistry: IUPAC recommendations and preferred names 2013.* Royal Society of Chemistry, 2013.
- [90] Abid A Memon et al. "Thermal decomposition of propylene oxide with different activation energy and Reynolds number in a multicomponent tubular reactor containing a cooling jacket". In: *Scientific Reports* 12.1 (2022), p. 4169.
- [91] Angela R Bielefeldt et al. "Biodegradation of propylene glycol and associated hydrodynamic effects in sand". In: *Water Research* 36.7 (2002), pp. 1707–1714.
- [92] Alton E Martin and Frank H Murphy. "Glycols, propylene glycols". In: *Kirk-Othmer Encyclopedia of Chemical Technology* (2000).
- [93] David D Smith et al. "SunPower's Maxeon Gen III solar cell: High efficiency and energy yield". In: 2013 IEEE 39th Photovoltaic Specialists Conference (PVSC). IEEE. 2013, pp. 0908–0913.
- [94] Baloji Adothu et al. "Effect of Curing Temperature on Properties of Ethylene Vinyl Acetate (EVA) Used for Crystalline Silicon Solar Module Encapsulation". In: 36th European Photovoltaic Solar Energy Conference and Exhibition. Vol. 1204. 2020, p. 07.
- [95] Enlitech. en-US. URL: https://enlitechnology.com/product-category/scientific-rese arch-measuring-instruments/solar-simulator/.
- [96] Daniela Dirnberger and Ulli Kräling. "Uncertainty in PV module measurement—Part I: Calibration of crystalline and thin-film modules". In: IEEE Journal of Photovoltaics 3.3 (2013), pp. 1016–1026.
- [97] Keith Emery. Uncertainty analysis of certified photovoltaic measurements at the national renewable energy laboratory. Tech. rep. National Renewable Energy Lab.(NREL), Golden, CO (United States), 2009.
- [98] Joel Tellinghuisen. "Statistical error propagation". In: *The Journal of Physical Chemistry A* 105.15 (2001), pp. 3917–3921.
- [99] Takashi Fuyuki et al. "Photographic surveying of minority carrier diffusion length in polycrystalline silicon solar cells by electroluminescence". In: *Applied Physics Letters* 86.26 (2005).
- [100] IEC61730-1. Photovoltaic (PV) module safety qualification Part 2: Requirements for testing. International Standard. IEC, 2023.
- [101] John H Wohlgemuth. "Reliability testing of PV modules". In: *Proceedings of 1994 IEEE 1st World Conference on Photovoltaic Energy Conversion-WCPEC (A Joint Conference of PVSC, PVSEC and PSEC)*. Vol. 1. IEEE. 1994, pp. 889–892.
- [102] Paul Gebhardt et al. "Statistical analysis of 12 years of standardized accelerated aging in photovoltaic module certification tests". In: Progress in Photovoltaics: Research and Applications 29.12 (2021), pp. 1252–1261.



Code

In this appendix, the code used during this project can be found. The only code made for this project was for the time it takes to reach the STC temperature of 25 °C after finishing the accelerated ageing tests with a temperature of -40 °C.

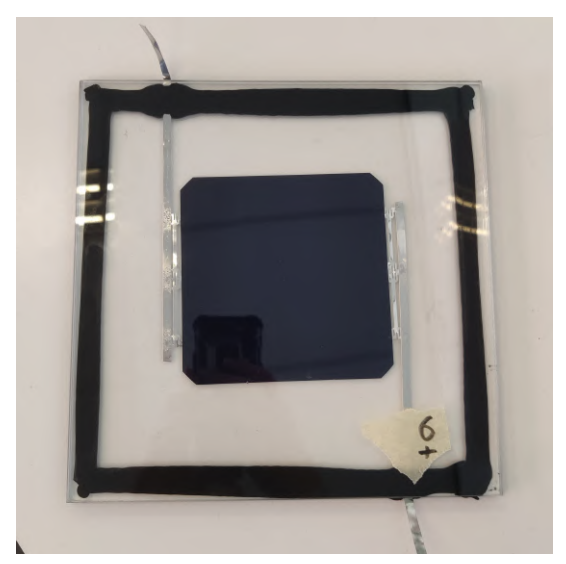
```
2 Created on Mon Mar 10 10:56:15 2025
4 @author: Sebastian
5 ""
7 import numpy as np
8 import matplotlib.pyplot as plt
9 from scipy.integrate import odeint
10
11 # Heat transfer function
def cooling_system(temp, t, k_solarcell, k_liquid, k_glass, h_liquid, h_air, A, L_solarcell,
      L_liquid, L_glass, m_solarcell, m_liquid, m_glass, c_solarcell, c_liquid, c_glass,
      solarcell_temp, liquid_temp, glass_temp = temp # Unpack temperatures
13
14
      # Conduction + Convection between solarcell and liquid
15
      Q_solarcell_liquid = (k_solarcell * A * (solarcell_temp - liquid_temp)) / L_solarcell
16
17 #
       Q_solarcell_liquid_conv = h_liquid * A * (solarcell_temp - liquid_temp)
       Q_solarcell_liquid_total = Q_solarcell_liquid + Q_solarcell_liquid_conv
18 #
19
      # Conduction + Convection between liquid and glass
20
       Q\_liquid\_glass = (k\_liquid * A * (liquid\_temp - glass\_temp)) / L\_liquid 
21
       Q_liquid_glass_conv = h_liquid * A * (liquid_temp - glass_temp)
22 #
       Q_liquid_glass_total = Q_liquid_glass + Q_liquid_glass_conv
24
25
      # Convection from glass to ambient air
      Q_glass_ambient = (k_glass * A * (glass_temp - roomtemp)) / L_glass
26
      Q_glass_ambient_conv = h_air * A * (glass_temp - roomtemp)
27
            Q\_glass\_ambient\_total = Q\_glass\_ambient + Q\_glass\_ambient\_conv  
28
29
30
      # Temperature change in each layer
      dsolarcell_temp = - Q_solarcell_liquid / (m_solarcell * c_solarcell)
      dliquid_temp = (Q_solarcell_liquid - Q_liquid_glass) / (m_liquid * c_liquid)
32
      dglass_temp = (Q_liquid_glass - Q_glass_ambient_total) / (m_glass * c_glass)
33
      return [dsolarcell_temp, dliquid_temp, dglass_temp]
35
37 # Constants
              = 0.0625 # Surface area (m^2)
39 L_solarcell = 0.0001 # Thickness of the solarcell (m)
40 L_{liquid} = 0.0005 \# Thickness of liquid (m)
              = 0.004 # Thickness of the glass layer (m)
41 L_glass
42 init_temp = [-40, -40, -40] # Initial temperatures (°C)
43 roomtemp = 25 # Ambient temperature (°C)
```

```
44
 45 # Convection coefficients
 46 h_air = 6 # W/m^2K (natural convection for air)
 47 h_liquid = 20 # W/m<sup>2</sup>K (moderate convection in liquid)
 48
 49 # Material properties
 50 liquids = {
                'demiwater': [0.624, 4187, 997],
'air': [0.026, 1003, 1.293],
 51
 52
               'eva':
                                              [0.23, 1400, 949],
 53
               'glycerol': [0.29, 2380, 1251],
'pdms': [0.15, 1510, 960],
 54
 55
               'Mivolt':
                                              [0.14, 1902, 968],
 56
                                              [0.18, 1800, 1041]
               'mpg':
 57
 58 }
 60 # Solarcell and glass properties
 solarcell = [130, 677, 2330] # [thermal conductivity, heat capacity, density]
glass = [1.8, 900, 2470] # [thermal conductivity[W/m*K], heat capacity[J/kg*K], density[
               kg/m^3]]
 63
 64 k_solarcell, c_solarcell, rho_solarcell = solarcell
 65 k_glass, c_glass, rho_glass = glass
 66
 67 # Mass calculations
 68 m_solarcell = rho_solarcell * A * L_solarcell
 69 m_glass = rho_glass * A * L_glass
 71 # Time range
 72 times = np.linspace(0, 120, 241)
 74 # Plot setup
 75 plt.figure(figsize=(10, 6))
 77 for liquid_name, liquid_properties in liquids.items():
               k_liquid, c_liquid, rho_liquid = liquid_properties
               m_liquid = rho_liquid * L_liquid * A
 79
 80
               # Solve ODE
               \texttt{temps} = \texttt{odeint(cooling\_system, init\_temp, times, args=(k\_solarcell, k\_liquid, k\_glass, args=(k\_solarcell, k\_glass, args=(k\_
 82
                        h_liquid, h_air, A, L_solarcell, L_liquid, L_glass, m_solarcell, m_liquid, m_glass,
                         c_solarcell, c_liquid, c_glass, roomtemp))
 83
 84
               # Extract and plot
               liquid_temps = temps[:, 1]
 85
               plt.plot(times, liquid_temps, label=f'{liquid_name}')
 86
               # Find time when liquid reaches 25°C
 88
 89
               target_temp = 25
               liquid_index = np.abs(liquid_temps - target_temp).argmin()
 90
               liquid_time_at_target = times[liquid_index]
 91
               93
 94 # Plot enhancements
 95 plt.axhline(y=25, color='red', linestyle='--', label='25°C')
 96 plt.xlabel('Time<sub>□</sub>(min)')
 plt.ylabel('Temperature<sub>□</sub>(°C)')
 98 plt.title('Cooling_{\sqcup}of_{\sqcup}Encapsulant_{\sqcup}Layer_{\sqcup}with_{\sqcup}Different_{\sqcup}Liquids')
 99 plt.legend()
100 plt.grid(True)
101 plt.tight_layout()
102 plt.show()
```

B

Figures

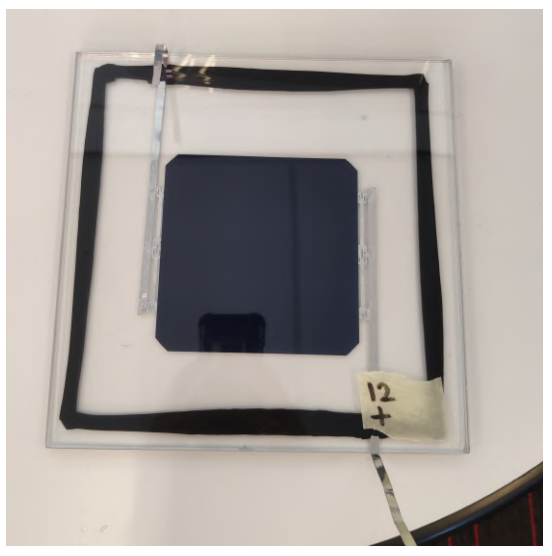
B.1. Water Submersion Test



(a) air-filled Module 6 before being submerged in water



(c) air-filled Module 6 submerged in water



(b) air-filled Module 12 before being submerged in water



(d) air-filled Module 12 submerged in water



(e) air-filled Module 6 after being submerged in water



(f) air-filled Module 6 after being submerged in water

Figure B.1: Water submersion test

B.2. All Electroluminescence Images

In this section of the appendix all of the electroluminescence (EL) images of the manufactured modules that entered the climate chamber will be shown. First module number 1 is shown with EL images every 6 cycles, then module 2, etc.

EL images module 1 EVA

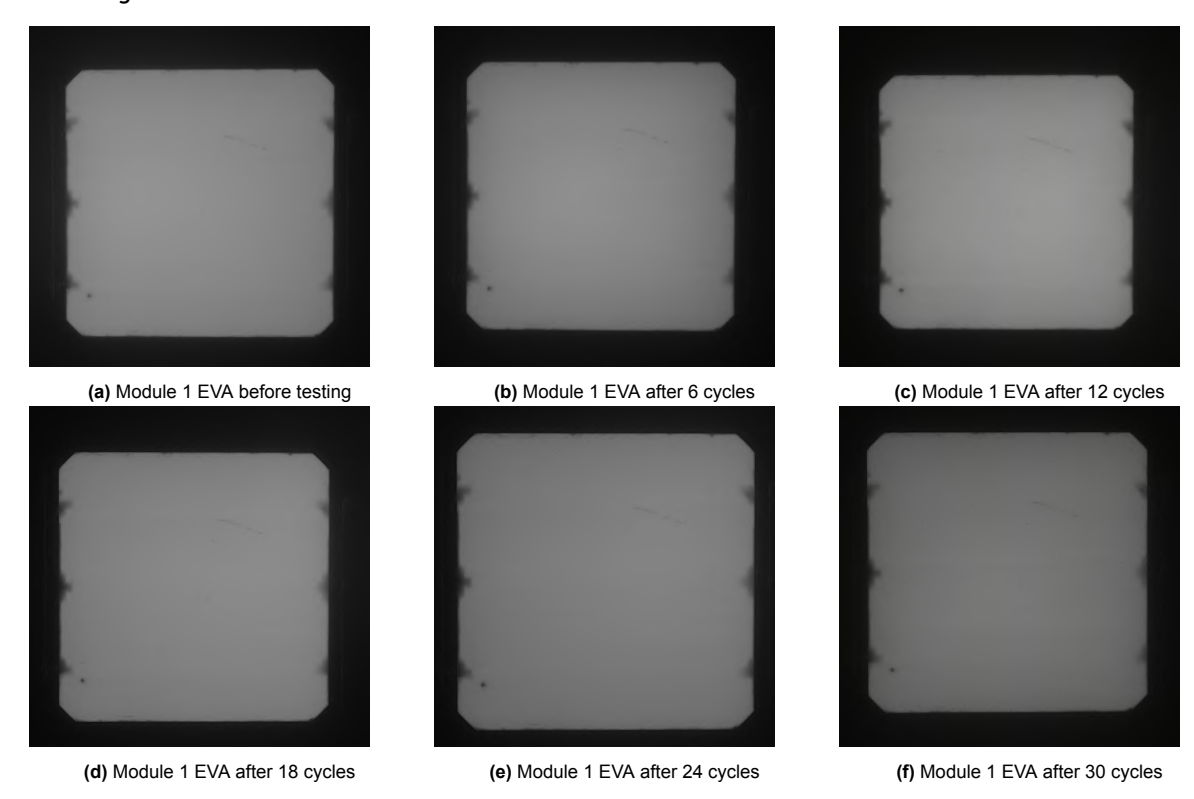


Figure B.2: EL images of module 1, laminated with EVA

EL images module 2 EVA

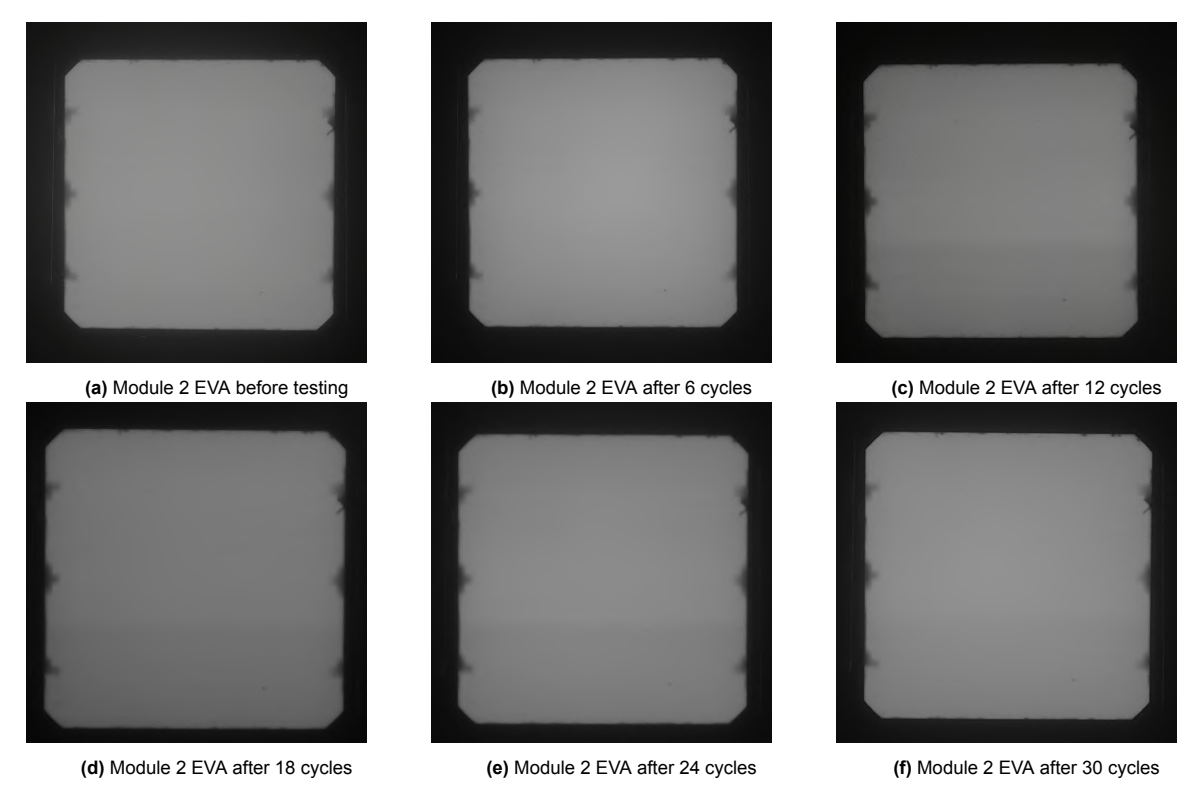


Figure B.3: EL images of module 2, laminated with EVA

EL images module 3 air

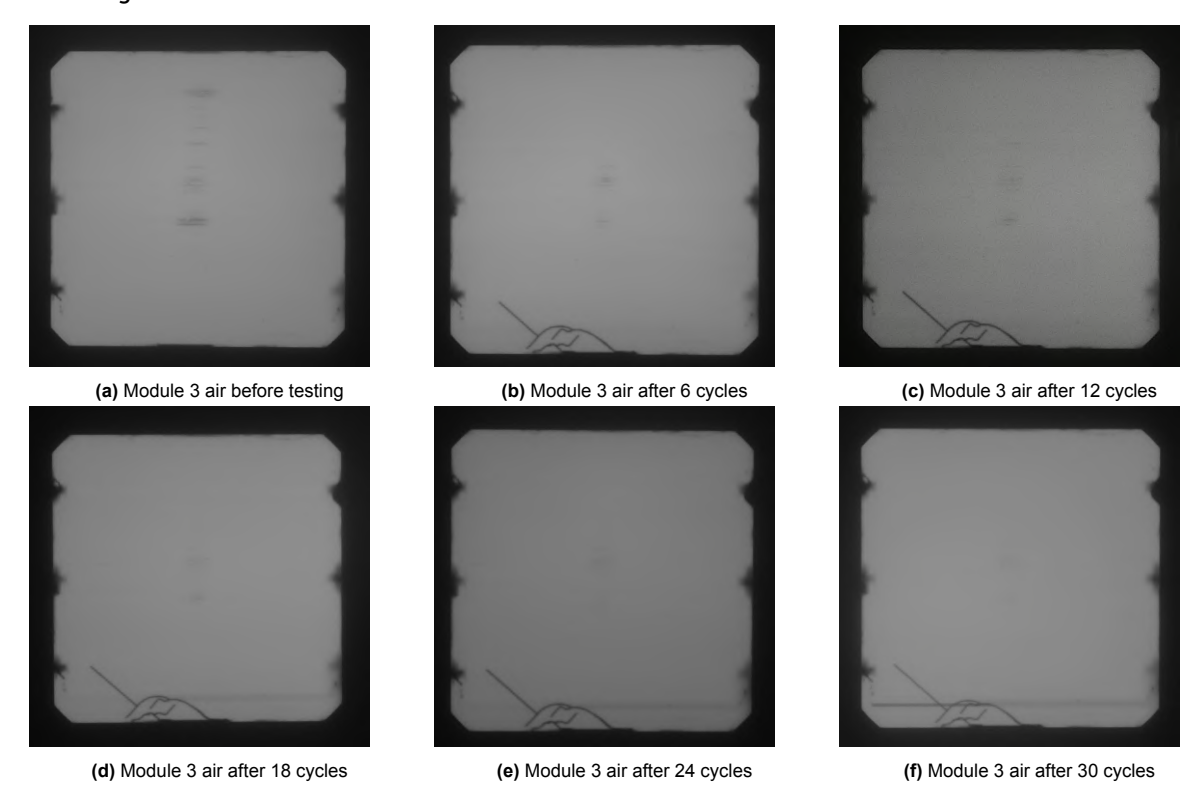


Figure B.4: EL images of module 3, air-filled

EL images module 4 air

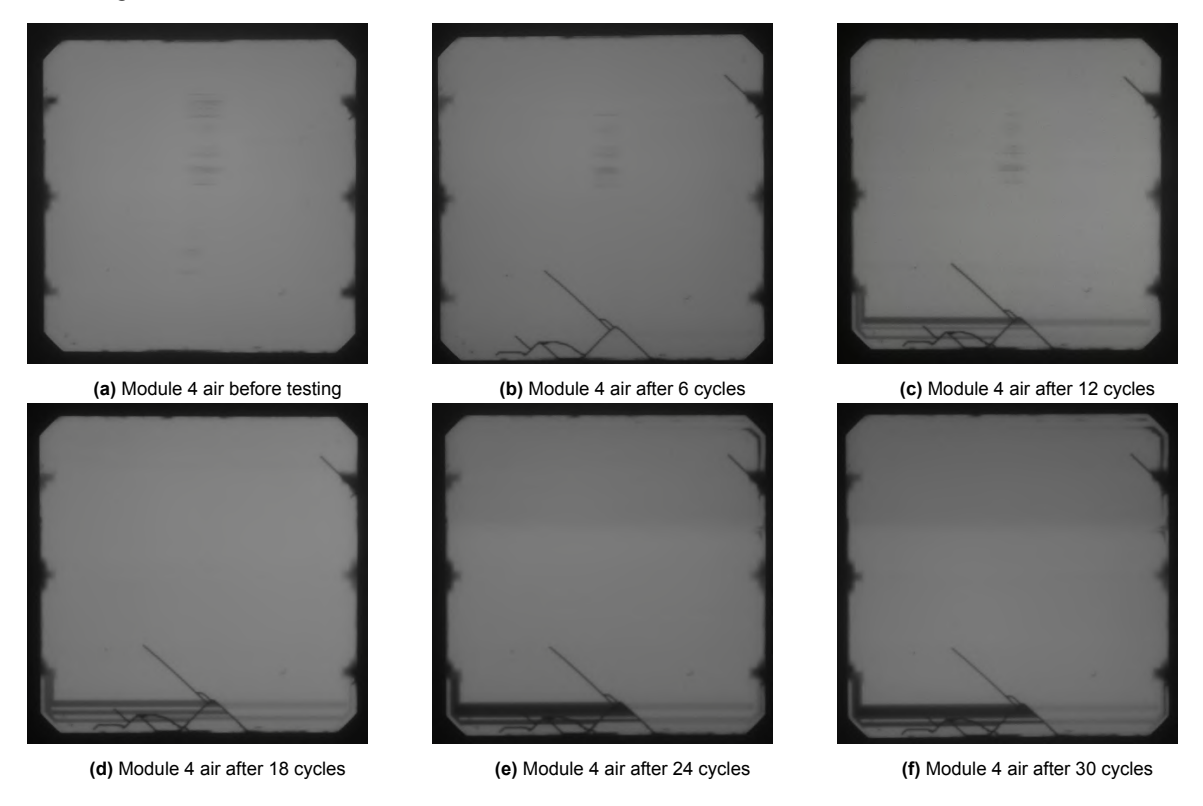


Figure B.5: EL images of module 4, air-filled

EL images module 7 PDMS

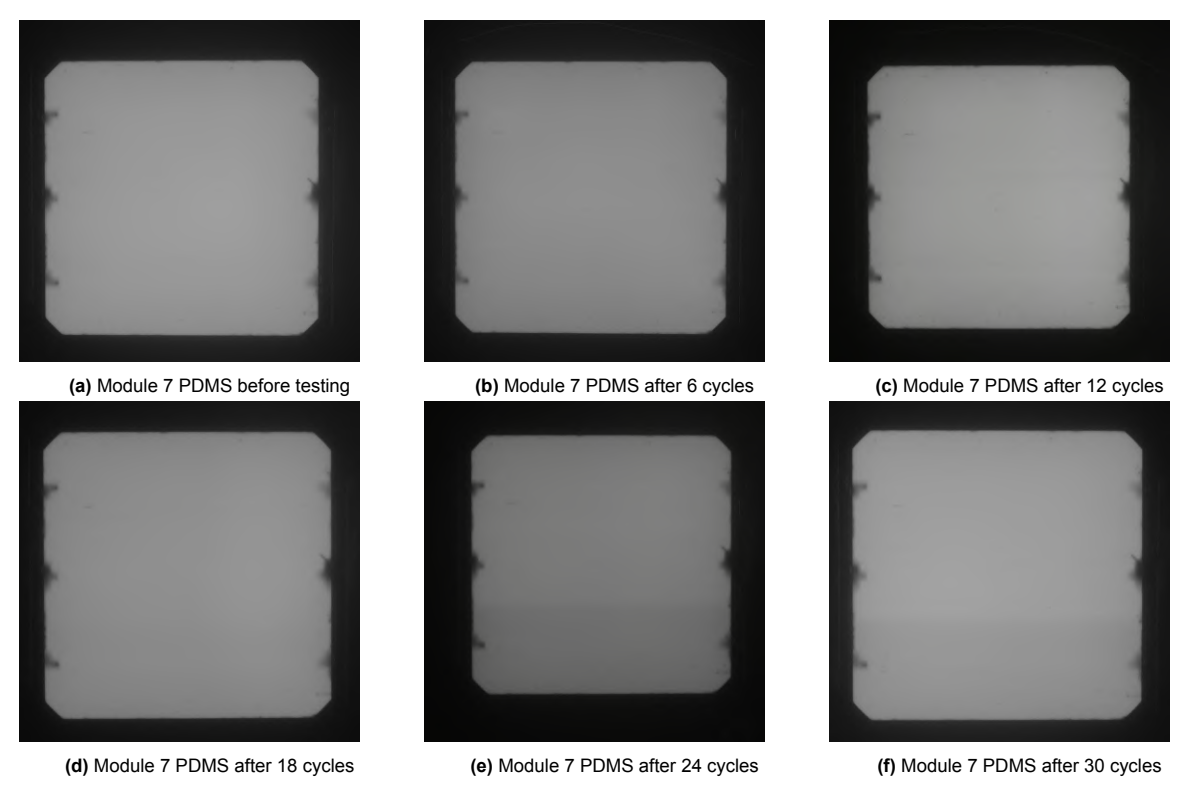


Figure B.6: EL images of module 7, encapsulated with PDMS

EL images module 10 glycol

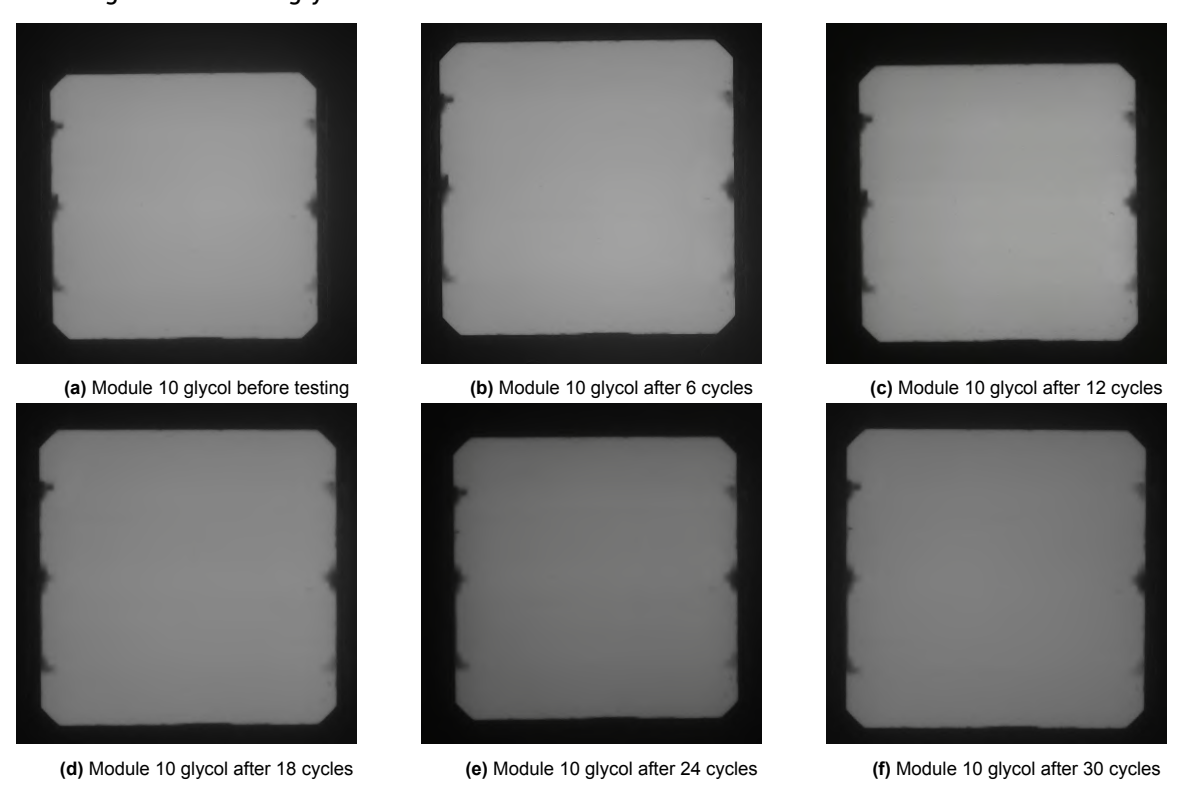


Figure B.7: EL images of module 10, encapsulated with glycol

EL images module 13 glycerol

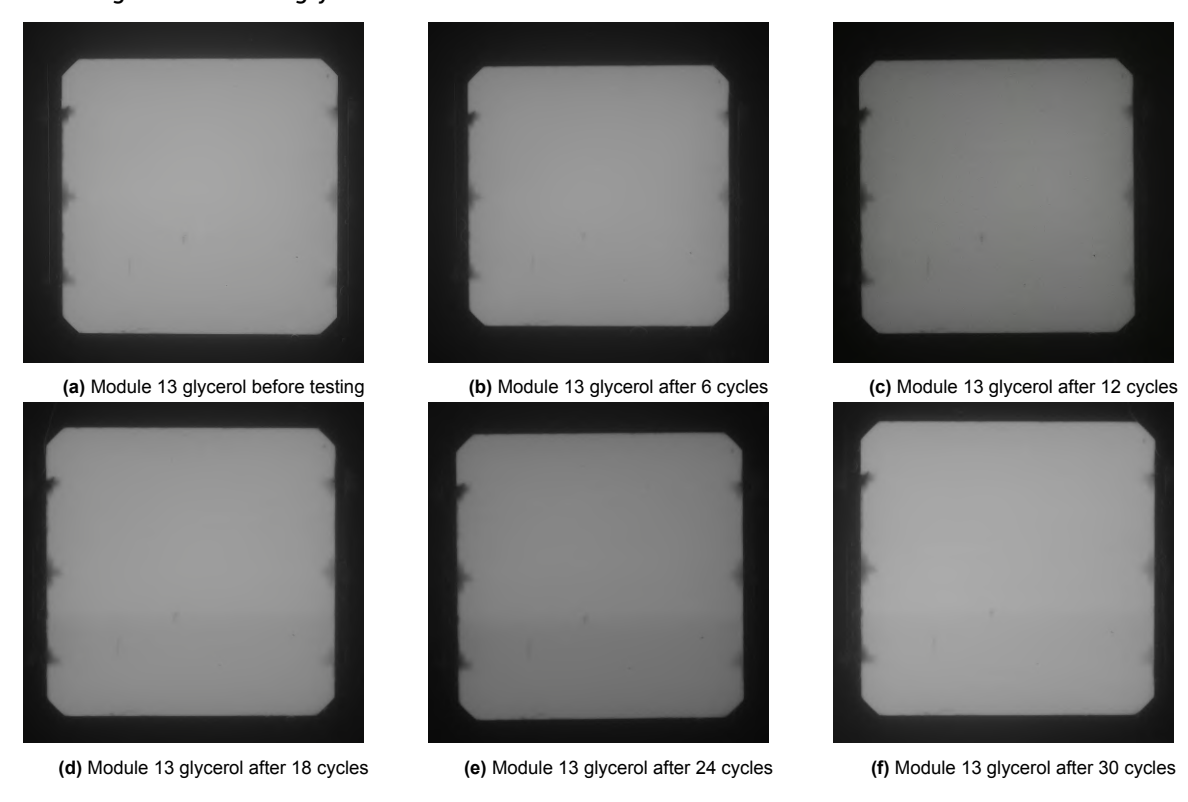


Figure B.8: EL images of module 13, encapsulated with glycerol